VIRTUAL ANTHROPOLOGY? RELIABILITY OF THREE-DIMENSIONAL PHOTOGRAMMETRY AS A FORENSIC ANTHROPOLOGY MEASUREMENT AND DOCUMENTATION TECHNIQUE

Rita Kemunto OMARI

A thesis submitted in fulfilment of the requirements for the degree of Master of Forensic Science (Professional Practice and Research)

in

The School of Veterinary and Life Sciences

Murdoch University

Supervisors:

Brendan Chapman

John Coumbaros

Cahill Hunt

Semester 2, 2019

MURDOCH
UNIVERSITY
PERTH, WESTERN AUSTRALIA

DECLARATION

I declare that this manuscript does not contain any material submitted previously for the award of any other degree or diploma at any university or other tertiary institution. Furthermore, to the best of my knowledge, it does not contain any material previously published or written by another individual, except where due references has been made in the text. Finally, I declare that all reported experimentations performed in this research were carried out by myself, except that any contribution by others, with whom I have worked is explicitly acknowledged.

Signed: OMARI, Rita Kemunto

Dated: 02/12/2019

ACKNOWLEDGEMENTS

Firstly, I would like to thank my primary supervisor, Brendan Chapman, for picking up my supervisorship amidst a lot of confusion, and for working with me constantly, patiently and tirelessly so that I can pull through this project. Words cannot suffice to express my gratitude. To my secondary supervisor, Cahill Hunt, thank you for having being so hands-on throughout my project, for proof-reading my work and being a sounding board for my ideas; for being a text away day and night to answer my incessant and sometimes silly questions. And finally from my list of supervisors, I'd like to thank Dr. John Coumbaros, who although did not work directly with me until the close of my project, still went through my work and gave such amazing feedback. I can without a doubt say I had the best team of supervisors there ever was!

To Prof James Speers, thank you for constantly being an email away and for checking up on my progress. Thank you for being ever ready to help out in any way that would make the load of the project lighter.

To the following from the Anatomy Department: Dr. Natalie Warburton, thank you so very much for accommodating me in your space and for allowing me to use your computer; to Dr. Joe Hong and Lance Boston, thank you for giving me material for my project and for being there to answer my questions and especially to Dr. Joe, thank you for showing me how use one of the software I needed for my project and for constantly checking up on me and giving me ideas on how to go about my project.

To the Animal Hospital, particularly the Diagnostic Imaging Department and specifically Joanne Cruden and Sierra Westbury, thank you for helping me out with the CT scan part of my project; and for accepting to consult with me at such a short notice when I needed it.

To Rex and Agatha, thank you for helping me out with my project. It was a lot of work that required you to sacrifice a significant amount of time on your end; I am forever indebted.

Finally, I'd like to thank my friends and family, especially my parents for their constant words of encouragement, prayers and votes of confidence. I would not have made it thus far without you all!

Table of Contents

Part One

LITERATURE REVIEW

VIRTUAL ANTHROPOLOGY? RELIABILITY OF THREE-DIMENSIONAL PHOTOGRAMMETRY AS A FORENSIC ANTHROPOLOGY MEASUREMENT AND DOCUMENTATION TECHNIQUE

ABSTRACT

Establishing the identity of unknown remains is a vital role of forensic anthropology. While establishing identity is generally straightforward due to conventional methods of identification like DNA analysis, sometimes these methods are not applicable in the case of remains that are heavily skeletonized, severely decomposed or severely charred. In such instances, a forensic anthropologist will be called upon.

The role of the forensic anthropologist is to aid in the identification of remains when conventional methods such as DNA and fingerprinting are not applicable. They may also be required to collaborate with other experts like forensic odontologists in order to attain a positive identification. A number of methods are available to the anthropologist that can aid in achieving identification: comparative radiography, nonimaged records, craniofacial superimposition, dental comparison and craniofacial reconstruction. All the methods except nonimaged records require imaging, either in two dimensions or three dimensions.

Three-dimensional imaging is quickly becoming a vital tool for reconstruction, comparison, and analysis in forensic science. It has found applications in road accident reconstruction, facial reconstruction, comparison of patterned injuries to the injury-inflicting instruments, and anthropometry. The main three-dimensional imaging methods utilized in the forensic field are photogrammetry, laser scanning and radiological scanning (computed tomography (CT) and magnetic resonance imaging (MRI)), with forensic three-dimensional/computer aided design (3D/CAD)-supported photogrammetry being the method that is primarily used due to its low cost, rapid results, does not need expertise to operate, has no radiation risks and, above all, the record is permanent. Regardless of this, CT and MRI are more established methods and are widely used in a variety of industries

The purpose of this paper is to compare and contrast the three-dimensional imaging methods currently employed in forensic science on the basis of reliability, reproducibility, and accuracy; with an ultimate aim of validating photogrammetry as an analytical and documentation method of forensic science.

TABLE OF CONTENTS

LIST OF FIGURES

LIST OF TABLES

LIST OF ABBREVIATIONS

SWGANTH	Scientific Working Group for Forensic Anthropology
EFA	Elliptical Fourier Analysis
2D	Two-dimensional
3D	Three-dimensional
CAD	Computer Aided Design
CRP	Close-Range Photogrammetry
FPHG	Forensic 3D/CAD supported photogrammetry
CT	Computed Tomography
MRI	Magnetic Resonance Imaging

INTRODUCTION

Among the principal functions of Forensic Science is the identification of human remains, and while it is generally straightforward a problem arises when there is destruction or fragmentation of the body (Harris & Lee, 2019). The traditional identification methods include dental records examination, radiography, DNA analysis (Gupta, 2015) and fingerprints (Harris & Lee, 2019). In the case of fingerprints and dental identification, there have to be antemortem records to be used in comparison to the postmortem records (Harris & Lee, 2019), which is not always possible. When the remains are skeletal or extensively decomposed (Ubelaker, Shamlou & Kunkle, 2018) traditional identification methods are not always applicable due to various factors, such as lack of proper information or condition of the remains (Gupta, 2015). Therefore, other techniques such as craniofacial superimposition and facial approximation can be utilised (Ubelaker et al., 2018). A positive identification will be required however, not only for any legal reasons that may arise, but also to provide closure to the affected family (Gupta, 2015).

Forensic facial reconstruction is an important tool that can be utilized in facial recognition of the skull and ultimately, lead to positive identification of the remains (Gupta, 2015). The first step towards identification taken by the forensic anthropologist is building a biological profile or osteobiography. This is achieved by determining the age, stature, race, sex, pathologies and other measurable anomalies of the remains (Cattaneo, 2007). The forensic anthropologist makes these determinations on the biological profile by employing principles of skeletal growth, development, degeneration and variation (Tersigni-Tarrant & Shirley, 2013). The recovery of information from the remains and the documentation of the findings must be carried out in a manner that meets the demands stipulated by legal process (Ubelaker et al., 2018). Additionally, it is critical that the techniques utilized meet the Daubert[1] standard, as falling short of this, the identification will be inadmissible in court (Rogers & Allard, 2004; *Daubert v. Merrell Dow Pharmaceuticals, Inc.*, 1993).

The first step after recovery of skeletal remains would be to document them in their original, undisturbed state for mapping and scene reconstruction purposes (Edelman & Aalders, 2018).The method of documentation often used is photography; however, because there is often loss of information when visualizing three-dimensional (3D) evidence on a two-dimensional (2D) photograph (Koller, Ebert, Martinez & Sieberth, 2019), photogrammetry is now increasingly used (Edelman & Aalders, 2018). The procedure of documentation is standardized and includes written documentation of statements. Photogrammetry involves image measurements from a series of overlapping photographs of an object from different angles (Luhmann, Robson, Kyle & Boehm, 2013). It is a technique that allows 3D documentation of objects, scenes and persons (Koller et al., 2019) in order to obtain a model of the objects or scenes (Edelman & Aalders, 2018), particularly when a detailed 3D reconstruction is necessary (Thali, Braun, Brueschweiler & Dirnhofer, 2003a). The reconstruction is in digital or graphical form (Luhmann et al., 2013) and can be virtually evaluated on the computer using a three-dimensional/computer aided design (3D/CAD) program (Thali et al., 2003a). Some of the instances photogrammetry has been applied in include generation of traffic accident reports, comparison of patterned injuries, comparison of bite wounds (Brüschweiler, Braun, Dirnhofer & Thali, 2003), crime scene and aircraft crash

[1] All subsequent references to the Daubert standard/criteria will be in relation to the case "*Daubert v. Merrell Dow Pharmaceuticals, Inc.*, 1993".

reconstruction and recording, bullet trajectory reconstruction (Luhmann et al., 2013) and archaeological excavation (Pexa et al., 2018).

The greatest advantage of photogrammetry is the fact that it does not alter the scene in any way, yet it documents the scene in its entirety. The resultant model enables a virtual return to the scene for more observation or scene measurements, even after the scene has been cleared, making it a valuable analytical tool in forensic science (Edelman & Aalders, 2018). It also allows for the evaluation of a documented injury which at the time of evaluation no longer exists, for instance, if the deceased was buried or the wound already healed. Additionally, photogrammetry allows evidence to be presented in a way that can be understood by lay people such as jury members without confusing issues (Thali et al., 2003a).

Advances in digital camera technology and computers over the past few years have paved the way for many new applications that can be utilized by untrained personnel using any type of digital camera, be it metric, non-calibrated or in a smartphone (Edelman & Aalders, 2018). This makes it easier for first responders to quickly document a scene before it is altered, especially if it is exposed to weather elements.

There are several methods a forensic anthropologist can use in carrying out a facial reconstruction. Traditionally, manual techniques in which clay or plasticine was modelled directly onto the skull were used. There was a high degree of artistic freedom involved, hence the reconstructions were not adequate for forensic use. Forensic reconstructions had to be restricted to the information provided from the investigation and, even then, the sculptures were complicated and needed time. With the rise of computer-aided facial reconstruction the process has been sped up (Buzug, 2007).

This literature review will assess the current literature on facial reconstruction in virtual space, and compare it to other 3D imaging techniques such as computed tomography (CT) scans and magnetic resonance imaging (MRI) scans.

DISCUSSION

Introduction to Forensic Anthropology

"To limit the definition of forensic anthropology to the process of identification from the skeleton is outdated and inappropriate" (Randolph-Quinney, Mallett & Black, 2009, p20). Forensic anthropology is a subdiscipline of physical and biological anthropology (Tersigni-Tarrant & Shirley, 2013), whose primary aim is positive scientific identification of human remains recovered in a medicolegal context (Ubelaker, Shamlou and Kunkle, 2018). It is more elaborately defined as:

> …that branch of physical anthropology which, for forensic purposes, deals with the identification of more or less skeletonized remains known to be, or suspected of being human. Beyond the elimination of nonhuman elements, the identification process undertakes to provide opinions regarding sex, age, race, stature, and such other characteristics of each individual involved as may lead to his or her recognition. (Stewart, 1979, ix)

Forensic anthropologists study traits of the skeleton (Ubelaker et al., 2018), and use their knowledge of skeletal variation to facilitate identification of unknown decedents by law enforcement, and to provide information regarding the circumstances of death where possible (Tersigni-Tarrant & Shirley, 2013). In order for an identification to be considered scientifically positive, evidence must be found that is sufficiently unique to the individual and can be compared to available antemortem data from that individual (Ubelaker et al., 2018). The comparison should be carried out in a systematic manner (SWGANTH, 2010, obtained from "Anthropology Subcommittee", 2019)[2].

[2] All subsequent SWGANTH in-text citations have been obtained from ("Anthropology Subcommittee", 2019).

Snow (Snow, 1982) outlined a series of questions that a forensic anthropologist should use as a guide during the process of identification of skeletal remains: (i) are the remains human? (ii) how many individuals are represented by the remains? (iii) when did the death occur? (iv) what is the decedent's: sex, race, age, stature/body weight/physique? (otherwise referred to as "biological profile") (v) does the skeleton exhibit any anatomical anomalies? (vi) what was the cause of death? (vii) what was the manner of death?. Proper recovery, documentation, and assessment of the biological profile of remains are essential factors in achieving a positive identification, and must be carried out in a manner that meets the demands of the legal process (Ubelaker et al., 2018).

Building a Biological Profile

A basic biological profile (osteobiography) is constructed from the skeletal tissues (Dirkmaat, Cabo, Ousley & Symes, 2008). The key elements that define the basic biological profile are chronological age at death, ancestry, sex and stature; and assessment of these elements aids victim identification not only by reducing the list of potential matches, but also helps them compare to missing person reports (Dirkmaat et al., 2008; Schmitt, Cunha & Pinheiro, 2010; Dirkmaat, 2012; Klales & Kenyhercz, 2014). Pathologies, healed trauma, and anomalies can also be assessed as part of the biological profile (Cattaneo, 2007; Dirkmaat et al., 2008; Schmitt et al., 2010).

In recent times, there is an increasing focus in forensic anthropology to develop methods of biological profile estimation that are scientifically valid and reliable, and meet the Daubert standard (Klales & Kenyhercz, 2014).

Ancestry Classification

According to the Scientific Working Group for Forensic Anthropology (SWGANTH), ancestry refers to the geographic region and/or ancestral origin of a population group (SWGANTH, 2013). On the other hand, Hefner (2003) defines ancestry as “ancestry is used to denote large groups of individuals who share similar morphologies in cranial form, likely the result of shared environmental constraints over great periods of time”. It is the most controversial of all the elements of the biological profile (Schmitt et al., 2010; Blau & Briggs, 2011; Klales & Kenyhercz, 2014; Sierp & Henneberg, 2015), as some critics argue that biological races do not exist (Schmitt et al., 2010; Tersigni-Tarrant & Shirley, 2013). Additionally, not only are many of the craniofacial differences used in identification difficult to quantify (Sholts, Walker, Kuzminsky, Miller & Wärmländer, 2011), there is also considerable overlap of the traits that characterize different groups so that it is difficult to classify an individual into a particular ancestry (Schmitt et al., 2010).

Traditional assessment of ancestry relies more on experience of the observer (Sholts et al., 2011; Dirkmaat, 2012) rather than understanding of the distribution of traits among humans and, as such, this method is deemed unscientific (Dirkmaat, 2012). The appropriate techniques for assessing ancestry should be objectively applied and methods documented to enable replication and verification (SWGANTH, 2013).

Determination of ancestry involves using either morphological, metric, or a combination of data to classify an individual into one of three major groups: White (Caucasoid), Black (Negroid) or Asian (Mongoloid) (Reichs, 1998; Schmitt et al., 2010). There are a total of six geographical races however, hence in addition to the three main groups, there are: Melanesian/Australian (Australoid), American Indian and Polynesian (Gill, 1998).

The skull is the most useful part of the skeleton in determining ancestry (Wheat, 2009; Parsons, 2017). In the instance that the skull is not recovered, select postcranial remains such as long bone lengths and trunk height may be used to estimate ancestry, although the study of this method is not as robust as using the cranium (Tersigni-Tarrant & Shirley, 2013).

There are two methods primarily used in forensic anthropology to assess the ancestry of a skull: metric and nonmetric analyses (Wheat, 2009; Dirkmaat, 2012; Parsons, 2017). A third method, dental morphology, is being developed and is gaining more visibility (Pilloud, Hefner, Hanihara & Hayashi, 2014).

Metric Analysis

Metric analysis involves use of precise instruments to take defined measurements of skeletal elements followed by a statistical analysis of these measurements (Dirkmaat, 2012; Parsons, 2017). The most popular metric method is the software-based Fordisc 3.0 (Wheat, 2009; Dirkmaat, 2012), which determines ancestry through discriminant function analysis of cranial measurements (Elliott & Collard, 2009; Dirkmaat, 2012; Tersigni-Tarrant & Shirley, 2013). Fordisc furnishes forensic anthropology with quantifiable statistical analysis, which is essential in order to meet the increasing demands of evidential standards (Dirkmaat et al., 2008; Parsons, 2017). Fordisc can also be used to estimate sex and stature (Tersigni-Tarrant & Shirley, 2013).

Nonmetric Analysis

Nonmetric analysis relies on the visual examination of skulls based on the differences in skull structure between ancestral groups (Wheat, 2009). However, it has not been scientifically standardized like metric analysis, but is still preferred because nonmetric observations can still be made from fragmented remains and are easy to collect (Dirkmaat, 2012

More specifically, nonmetric analysis involves visually inspecting the cranium and mandible for morphological variation (nonmetric or morphoscopic traits) (Hefner, 2009) (Figures 1 and 2).

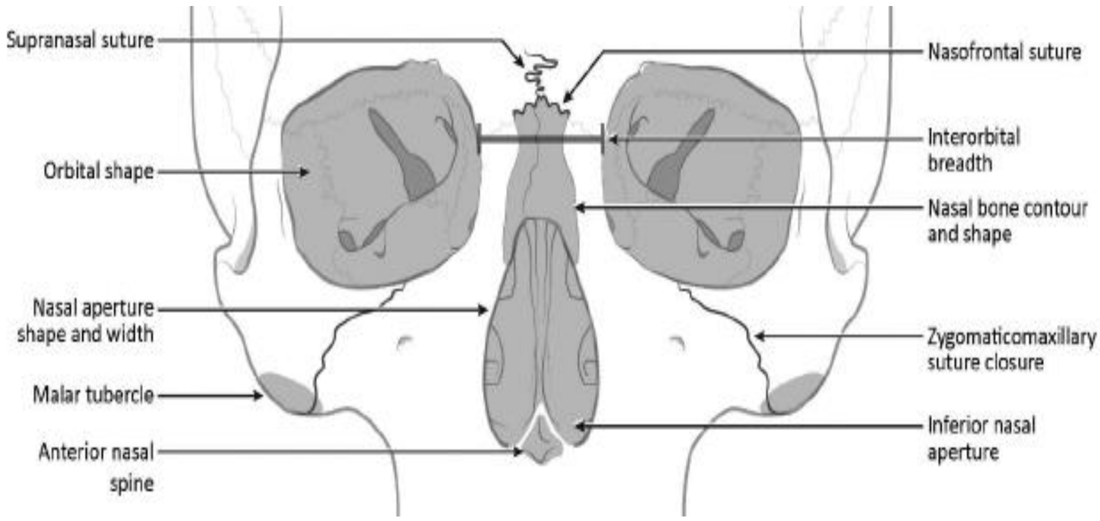

Figure 1. Anterior view of cranium demonstrating approximate location of nonmetric traits [Image adapted from Macromorphoscopics Software Version 1.61 User Manual ("MMS Software – Macromorphoscopic Data", n.d.)]

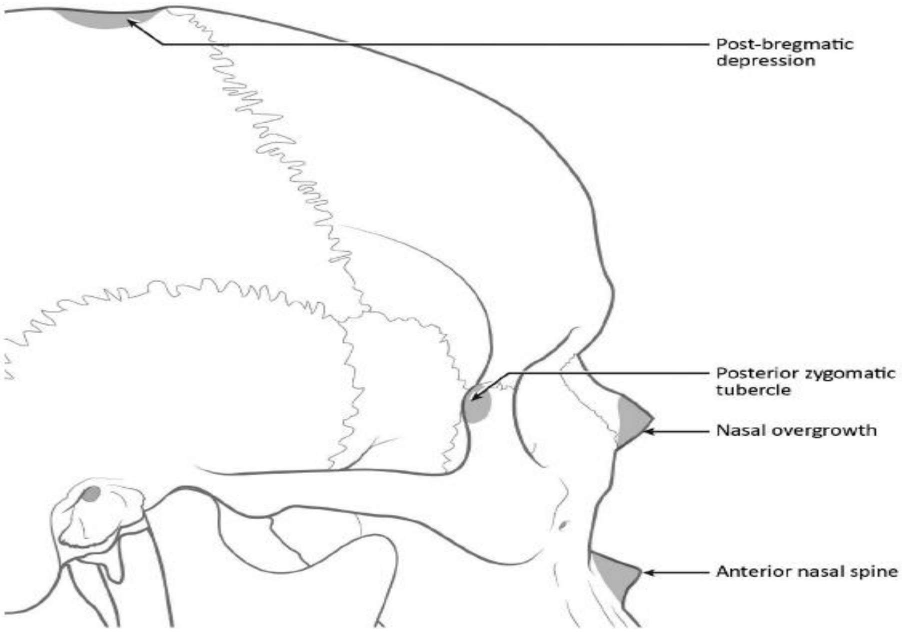

Figure 2. Lateral view of cranium demonstrating approximate location of nonmetric traits [Image adapted from Macromorphoscopics Software Version 1.61 User Manual ("MMS Software – Macromorphoscopic Data", n.d.)]

Some of the most valuable craniofacial features utilised in ancestral estimation are the nose and mouth, palate and palatine suture (Figure 3), and mastoid form (Gill, 1998).

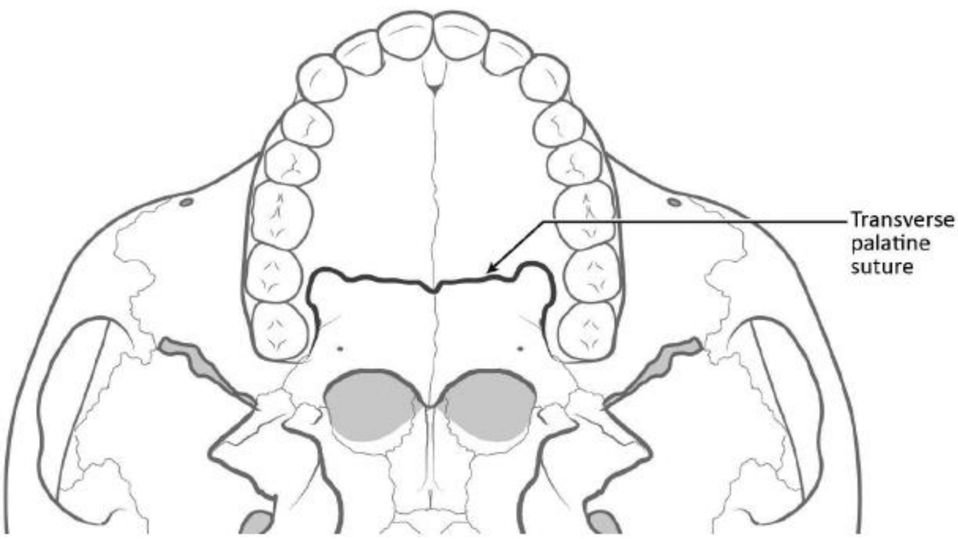

Figure 3. Inferior view of cranium demonstrating approximate location of nonmetric traits [Image adapted from Macromorphoscopics Software Version 1.61 User Manual ("MMS Software – Macromorphoscopic Data", n.d.)]

Table 1 and Figure 4 shows some of the nonmetric traits of the three main ancestral groups whereas Table 2 shows some of the characteristics of the six geographical races.

Table 1. Nonmetric cranial traits of the three main ancestral groups [Adapted from (Hefner, 2003)]

Morphological Trait	Whites	Negroids	Mongoloids
Interorbital Space	Narrowest	Broad	Broad
Upper Nasalia	Arched, high	Broad, flat	Flat, often narrow
Bridge (space)	Narrowest	Broadest	Lowest
Bridge (height)	Highest	Intermediate	Lowest
Nasal Aperture	Narrowest	Broadest	Intermediate
Nasal Sills	Sharpest	Infantile	Least developed
Nasal Spine	Most developed	Usually infantile	Variable

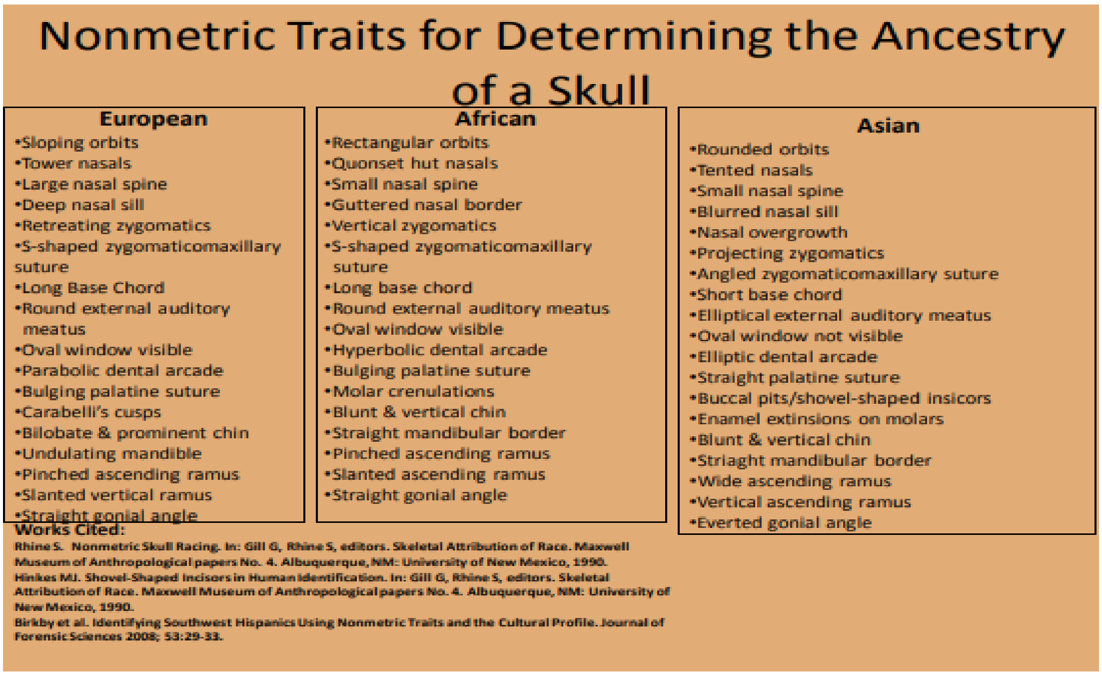

Figure 4. Nonmetric traits of a skull used to determine ancestry [Adapted from (Wheat, 2009)]

Table 2. Nonmetric cranial characteristics of the geographical races [Adapted from (Gill, 1998)]

CRANIOFACIAL TRAIT VARIATIONS COMMON TO EACH GEOGRAPHIC RACE

Characteristics	*East Asian*	*American Indian*	*White*	*Polynesian*	*Black*
Cranial form	broad	medium-broad	medium	highly variable	long
Sagittal outline	high, globular	medium-low sloping frontal	high, rounded	medium	highly variable post-bregmatic depression
Cranial sutures	complex	complex	simple	complex	simple
Nose form	medium	medium	narrow	medium	broad
Nasal bone size	small	medium/large	large	medium	medium/small
Nasal bridge form	flat	medium/tented	high/steeple-like	medium	low/quonset hut
Nasal profile	concave	concavo-convex	straight	concave/concavo-convex	straight/concave
Interorbital projection	very low	low	high, prominent	low	low
Nasal spine	medium	medium, tilted	prominent, straight	highly variable	reduced
Nasal sill	medium	medium	sharp	dull/absent	dull/absent
Incisor form	shovelled	shovelled	blade	blade/shovelled	blade
Facial prognathism	moderate	moderate	reduced	moderate	extreme
Alveolar prognathism	moderate	moderate	reduced	moderate	extreme
Malar form	projecting	projecting	reduced	projecting	reduced
Zygomaticomaxillary suture	angled	angled	curved	curved/angled	curved/angled
Palatal form	parabolic/elliptic	elliptic/parabolic	parabolic	parabolic	hyperbolic/parabolic
Palatine suture	straight/jagged	straight	jagged	highly variable	arched/jagged
Orbital form	round	rhomboid	rhomboid	rhomboid	round
Mastoid form	wide	wide	narrow, pointed	wide	oblique, posterior tubercle
Mandible	robust	robust	medium cupped below incisors	robust rocker form	gracile oblique gonial angle
Chin projection	moderate	moderate	prominent	moderate	reduced
Chin form	median	median	bilateral	median	median

Dental metrics and morphology

Teeth are the hardest tissue in the body and are often well preserved postmortem. In this technique, dental measurements are taken and the mesidistal and buccolingual tooth dimensions are used to differentiate between broad geographically based groups. Generally, Africans have the largest teeth, Asians intermediate-size teeth and Europeans have the smallest teeth (Pilloud et al., 2014).

Additionally, different ancestral groups have been noted to have characteristic dental peculiarities; for instance, Negroids have a midline diastema and an open bite, Caucasoids have the cusp of Carabelli, and Mongoloids have shovel-shaped inscisors (Yaacob, Narnbiar & Naidu, 1996; Rawlani, Rawlani, Bhowate, Chandak & Khubchandani, 2017).

Sex Determination

Sex determination is vital, as determined sex for unidentified remains can be used as a foundation on which other aspects of the biological profile are estimated (Randolph-Quinney et al., 2009; Parsons, 2017; Torimitsu et al., 2017; Bongiovanni & LeGarde, 2017; Dereli et al., 2018), and is a relatively easy task provided that the skeleton is complete (Rogers, 1999; İşcan, 2001; Bongiovanni & LeGarde, 2017). However, this is not often the case as observed in the breaking and dispersal of bones in airplane crashes (İşcan, 2001). The method of sex assessment selected will depend on: (i) skeletal elements available for examination, (ii) condition or relative degree of preservation of the skeletal elements, and (iii) general age of the individual (SWGANTH, 2010).

Sexing methods are divided into two: morphological/nonmetric (shape) aspects that are found in the pelvis and skull, and metric (size) aspects found in the skull and postcranial skeleton (Randolph-Quinney et al., 2009; Dirkmaat, 2012; Tersigni-Tarrant & Shirley, 2013; Parsons, 2017). The two methods complement each other and result in the same levels of accuracy (Rogers, 1999). Of all the methods, the pelvis is the most reliable as there is a common pattern of sexual dimorphism to the whole human race (Schmitt et al., 2010; Dirkmaat, 2012). However, because skeletal dimorphism of the skeleton is controlled and regulated by sexual hormones produced during puberty, sexing from the skeleton is easier in adults and late adolescents as compared to subadults or juveniles whose secondary sexual characteristics are yet to be established (Randolph-Quinney et al., 2009; Schmitt et al., 2010; Tersigni-Tarrant & Shirley, 2013; Parsons, 2017). SWGANTH categorizes the sexing of children under the age of 12 years as an unacceptable practice (SWGANTH, 2010).

Morphological/Nonmetric Method (Based on shape)

Pelvis

The pelvis is the most sexually dimorphic and gives the most reliable and accurate results during sexing. As such, it should be used as the principal indicator of sex when present (Schmitt et al., 2010; Dirkmaat, 2012; Tersigni-Tarrant & Shirley, 2013; Parsons, 2017). This is due to the difference in biological function between the male and female pelvis. While the pelvis provides support for internal organs and the support needed for locomotion in both sexes, the female pelvis has the additional function of childbearing. Following this difference, the male pelvis is thus smaller and narrower while the female pelvis is wider and broader (Figure 5) (Schmitt et al., 2010; Dirkmaat, 2012; Tersigni-Tarrant & Shirley, 2013; Parsons, 2017).

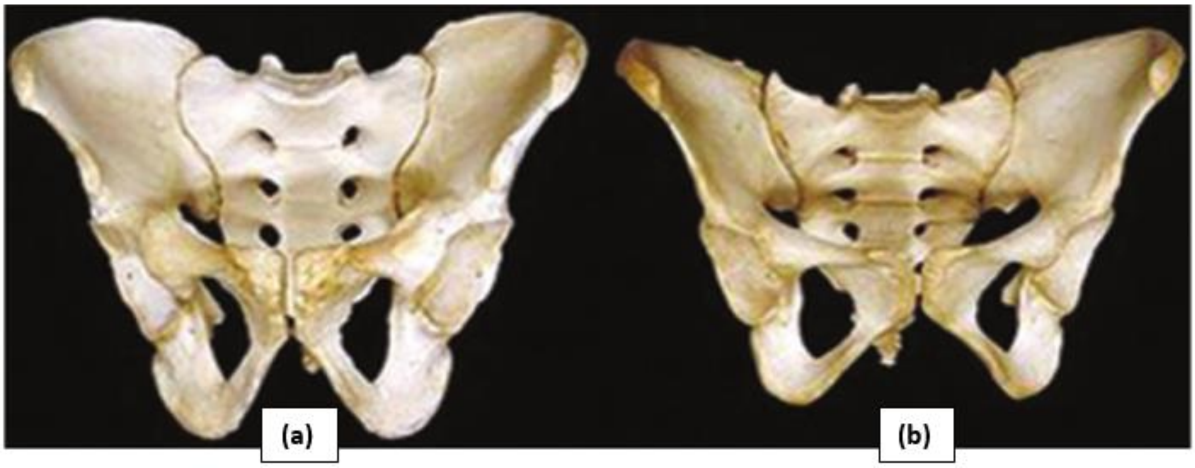

Figure 5. (a) Male pelvis and (b) female pelvis [Adapted from (Tersigni-Tarrant & Shirley, 2013)]

Phenice (1969) developed a sexing method that is considered to be the most accurate with a rate greater than 95%. He examined the ventral arc, subpubic concavity, and medial aspect of the ischiopubic ramus within the subpubic region, which are now known as the "traits of Phenice". If in a pelvis the medial aspect of the ischiopubic ramus is wide and flat and there is an absence of the ventral arc and subpubic concavity, then it belongs to a male; whereas, if it has a sharp medial aspect of the ischiopubic ramus and both the ventral arc and subpubic concavity ae present, then it belongs to a female (Tersigni-Tarrant & Shirley, 2013).

Additional elements of the pelvis that can be used to estimate sex include: (i) sciatic notch, which is present as a wide open notch in females and a narrow U-shaped notch in males (Figure 6) and can be scored on a scale of 1 (female) to 5 (male); (ii) Preauricular suculus, which is more variable and is large and wide with deep pits in females, while it can be absent in males or appear as a small, narrow and shallow groove. It is scored as 0 (absent) or 1-4 depending on its characteristics (Tersigni-Tarrant & Shirley, 2013).

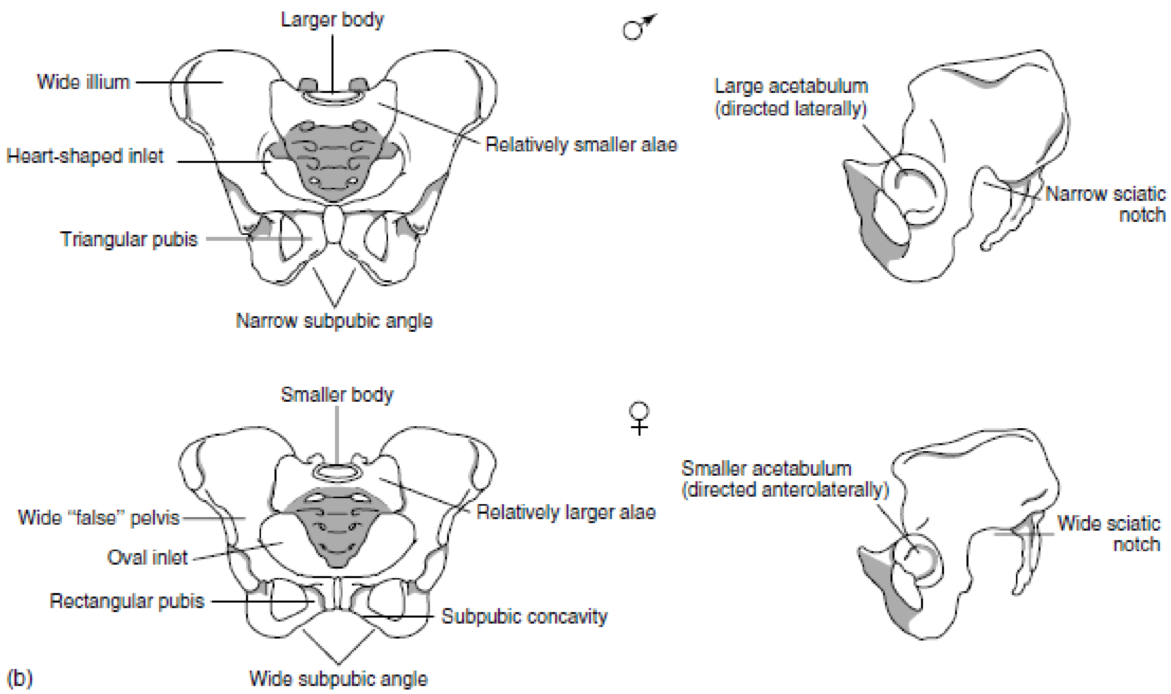

Figure 6. Sex differences in the pelvic girdle of (a) male and (b) female [Adapted from (Randolph-Quinney et al., 2009)]

Table 3 below illustrates some of the classic characteristics and differences between the male and female pelvis.

Table 3. Morphological sex differences in the pelvis [Adapted from (Randolph-Quinney et al., 2009)]

Pubic symphysis	Higher	Lower
Subpubic angle	Narrow V-shaped, acute angle	Wide U-shaped, obtuse angle
Subpubic concavity	Slight to no concavity	Concavity present
Ventral arc	Absent	Present as elevated ridge extending inferolaterally across ventral pubis
Medial ischiopubic ramus	Broad, flat and blunt. Slightly everted	Ridged, sharp edged, everted
Greater sciatic notch	Narrow and deep	Shallow and wide
Obturator foramen	Large and ovoid	Small and triangular
Acetabulum	Large, more laterally oriented	Small, more anteriorly oriented
Auricular surface	Depressed, wide	Raised, narrow
Preauricular sulcus	Not present or illusionary	Often present, well developed
Postauricular space	Narrow	Wide
Sacrum shape	Narrower, more curved, alae narrower than promontory	Wider, less curved, alae wider than promontory
Pelvic inlet shape	Heart shaped, narrow mediolaterally	Circular, elliptical, wide mediolaterally

Skull

Differences in shape of the cranium are primarily due to size. Females tend to have smaller and gracile crania as compared to males (Tersigni-Tarrant & Shirley, 2013). Five particular traits of the skull are focused on during sex estimation: the mastoid process; nuchal crest; mental eminence (chin); supraorbital margin; and supraorbital ridge/glabella (Table 4). These traits are scored from 1-5 with 1 being "very feminine" and 5 being "very masculine" (Dirkmaat, 2012; Tersigni-Tarrant & Shirley, 2013).

Estimating sex from the skull as a nonmetric method is less reliable than using the pelvis, and its dimorphism is dependent upon the population under observation (Schmitt et al., 2010; Parsons, 2017). As a result, it is recommended that sexting should only be attempted after representative samples have been collected from individuals from the population the skull was drawn from as comparatives (Tersigni-Tarrant & Shirley, 2013).

Table 4. Morphological sex differences in the skull [Adapted from (Randolph-Quinney et al., 2009)]

Morphological trait	Male	Female
Overall appearance	Large and rugged	Small and gracile
Supraorbital ridges	Prominent and rounded	Not prominent
Supraorbital margin	Rounded blunt margins	Thinner sharp margins
Orbital shape	Rectangular	Circular
Frontal profile	Sloping anteroposteriorly	Vertical
Frontal eminences	Bosses absent or not pronounced	Pronounced
Mastoid processes	Longer and more pneumatized	Short and small
Suprameatal crest	Extends as a bony crest past the auditory meatus	Root of zygoma does not continue past the auditory meatus
Parietal eminences	Bosses absent or not pronounced	Pronounced
Nuchal region	Muscle markings rugose and pronounced, nuchal crest with external hook may be present	Less rugose and pronounced. Protuberance not marked.
Palate	Larger, broader, tends to U shape	Small, tends to parabolic arc
Teeth	Large	Small
Mandibular symphysis	Pronounced trigonum mentale; projection of mental protuberance in midline with large mandibular tubercles	Small trigonum mentale; reduced projection of mental protuberance with small or absent mandibular tubercles
Mandibular profile	Squared and U-shaped	Narrow and more pointed
Mandibular ramus flexure	Present	Absent
Gonial flaring	Flaring present	Flaring absent
Gonial angle	More acute	More obtuse

Other Postcranial Bones

This method is particularly useful in cases where either the pelvis, skull or both are missing from the remains; or when inconclusive results are drawn from analysis of either the skull or pelvis (Parsons, 2017).

Rogers (1999) developed a morphological method of determining sex from the posterior distal humerus using the following elements: trochlear constriction, trochlear symmetry, olecranon fossa depth and shape, and angle of the medial epicondyle. In females, the olecranon fossa is more oval, the medial epicondyle is angled, and the trochlea is more constricted and symmetrical (Tersigni-Tarrant & Shirley, 2013).

The medial clavicle can also be used to estimate sex by examining for the presence or absence of a rhomboid fossa; male individuals are typically characterized by a deeply pitted rhomboid fossa (Tersigni-Tarrant & Shirley, 2013).

Metric Method (Based on Size)

Generally, males have a larger body size, more massive joints and stronger musculature than females within a given population. As such, measurements of body size such as long bone lengths, articular surface dimensions, humeral and femoral head size, and facial and cranial vault size can be used to help determine the sex of unknown remains (Randolph-Quinney et al., 2009; Dirkmaat, 2012; Schmitt et al., 2010). For instance, in the case of femoral heads, sectioning points have been provided that propose femoral heads less than 42.5mm are female and those greater than 47.5mm are male (Dirkmaat, 2012).

These measurements are then compared to a large reference database and statistical analyses conducted on them in an attempt to obtain an identification (Schmitt et al., 2010; Parsons, 2017). The measurements can also be entered into Fordisc for metric analysis, and the results compared against an existing database (Parsons, 2017). Sex estimation is especially more reliable when the estimation is being made from long bones which include the dimensions that characterize their width or circumference (İşcan, 2001).

Torimitsu et al. (2017) attempted to use hyoid bone measurements from a Japanese population to determine sex as an alternative method in the event that the pelvis and skull are not recovered with skeletal remains. They found that the hyoid bone was indeed highly sexually dimorphic and could be used with a high level of accuracy to determine sex, and in some instances stature. However, the study was conducted on a Japanese population, hence the discriminant equations used may not be applicable to other populations.

Bongiovanni and LeGarde (2017) attempted to establish a univariate standard for estimation of sex using the distal humerus and distal radius from a population of European/American White and American Black individuals. This was in an effort to provide an additional technique that could be applied to remains that were fragmented but were well preserved. The study was successful, and also added the capitulum-trochlea to the common measurements utilized in sex estimation.

Age Estimation

There are two categories of age: Chronological age, which is defined by time, that is, how many literal days or months or years have passed since birth. It is the only way to give an individual's precise age, and without a birth date it cannot be established. The second category of age is the biological age which denotes the physiological state of an individual and is reflected in skeletal remains. It is dependent on genetic and environmental factors, and can only be expressed in ranges or estimates rather than a specific age (Dirkmaat, 2012; Priya, 2017; Boyd & Boyd, 2018). In his book, Dwight (1878) puts forward that an adult skeleton can be divided into four classes based on age: (i) immature stage for ages up to 25 in males or 22 in females; (ii) young stage for ages up to about 30; (iii) mature stage for ages from about 30 to about 60; and (iv) senile stage which begins at a variable period. He however cautions that although analysis of the skeleton will lead to classification into one of the four stages, one must always keep in mind the high degree of individual variation. In a more recent study, Randolph-Quinney et al. (2009) divided the aging process into three phases: growth and development; equilibrium; and senescence, and thus defined new phases of skeletal age, albeit there is a noted overlap with the definition put forward by Dwight: (i) developmental phase which encompasses the intrauterine age to around 18 years, young adult (roughly 18-25 years), middle adult (25-45 years) and mature adults (45 years and above). In their book, Schmitt et al. (2010) also came up with their own developmental subgroups: children up to 12 years (when dental development is crucial); subadults up to 20 years (based on epiphyses); young adults (up to 40 years); mature adults (over 40 years); and senior adults/the elderly (over 65 years).

Forensic anthropologists utilise skeletal indicators that are time-related and associated with bone resorption, deposition and remodelling to estimate the age of an individual (Priya, 2017). SWGANTH states that acceptable age indicators should fulfil four criteria: (i) morphological changes should proceed unidirectionally with age; (ii) features should have a high degree of correlation with chronological age; (iii) changes should occur roughly at the same age in all individuals within a distinguishable subgroup; and (iv) the characteristics should be measured with known intra- and interobserver error rates. It also states that the final age estimate depends on the judgement of the expert after they have evaluated all the information available (SWGANTH, 2013). The basis on which age estimation can be achieved includes developing dentition, growing skeleton or degenerative changes of the skeleton (Priya, 2017). Age estimation and an accurate age range also helps to narrow the list of potential victims or missing individuals (Parsons, 2017).

Juvenile age estimation

Generally depends on a physiological assessment of dental (mineralization and eruption) or skeletal (long bone growth and epiphyseal fusion) maturation (Schmitt et al., 2010; Dirkmaat, 2012; Tersigni-Tarrant & Shirley, 2013; Parsons, 2017). Additional factors that can be considered include the appearance of primary and secondary ossification centers of the cranial and post cranial skeleton and correlation of growth of individual cranial bones with gestational age (Randolph-Quinney et al., 2009). Age estimation in infancy is by examination of the fontanelles/fonticuli (Kewal Krishan, 2013).

Age estimation using dental development is the most preferred method for juvenile age estimation. It makes use of the developmental stages (development, calcification and eruption) of deciduous and permanent teeth, which occur at a regular and predictable rate. (Schmitt et al., 2010; Tersigni-Tarrant & Shirley, 2013). Additionally, human teeth are not only the least affected by environmental influences compared to the rest of the skeleton, but they are also unique enough to differentiate between individuals (Taylor, 2009).

Growth, development and maturation of the skeleton (epiphyseal fusion, diaphyseal lengths) can also be used to reliably estimate juvenile age as these processes occur at predictable rates and known timeframes (Schmitt et al., 2010; Parsons, 2017). Long bone diaphyses will grow at a predictable rate, and further growth is prevented by the fusion of the distal and proximal epiphyses to each of the diaphyses (Figure 7). Consequently, measurement of these diaphyseal lengths can be associated with particular age ranges (Tersigni-Tarrant & Shirley, 2013). If the fusion of the epiphysis with any of the long bones is yet to occur, then the skeleton will be barely over 20 years. Dwight (1878) also recorded a peculiarity of the scapula in an effort to warn others against making errors: the tip of the acromion sometimes remains unfused throughout life. Caution must thus be exercised when examining this component of the skeleton.

Figure 7. An illustration of the growth and maturation of the human femur from infancy (far left) to adulthood (far right) [Adapted from (Tersigni-Tarrant & Shirley, 2013)]

Once fusion of the long bones is complete, late fusing epiphyses are used to age adolescents. Axial skeletal epiphyses develop in a similar manner to those of the long bones, for instance epiphyses of the ribs; hence assessing which epiphyses have already fused and which ones are yet to fuse can help establish an age estimate of the remains (Tersigni-Tarrant & Shirley, 2013).

Additional components used to estimate adolescent age include jugular growth plate of the skull, fusion of thoracic and lumbar vertebral rings, epiphyses of the scapula and pelvis and the medial epiphysis of the clavicle (Randolph-Quinney et al., 2009; Schmitt et al., 2010) (Table 5).

Table 5. Estimation of age from adolescents and young adults from epiphyseal fusion on a select number of bones [Adapted from (Randolph-Quinney et al., 2009)]

Element	Fusion	Age	
		Male	Female
Occipital	Fusion of sphenooccipital synchondrosis	13–18 years	11–16 years
	Closure of jugular growth plate	22–34 years	
Ethmoid	Ethmoid and vomer fuse	20–30 years	
Clavicle	Fusion of medial epiphysis	16–21 years, complete in all individuals by 29+ years	
	Fusion of lateral epiphysis	19–20 years	
Sternum	Sternebra 2 fuses to 3 and 4	11–16 years	
	Sternumebra 1 fuses to mesosternum	15–20 years	
	Sternum essentially complete	21+ years	
	All epiphyseal plaques in costal notches fused	25+ years	
	Xiphoid process commences fusion to mesosternum	40+ years	
Scapula	Coracoid and subcoracoid commence fusion to body	13–16 years	
	Coracoid and subcoracoid fused to body	15–17 years	
	Fusion of glenoid epihysis	17–18 years	
	Fusion of acromial and coracoid epiphysis complete	By 20 years	
	All epiphyses fused and adult form achieved	By 23 years	
Pelvis	Fusion of acetabulum	14–17 years	11–15 years
	Illiac crest commences fusion	17–20 years	
	Anterior iliac spine fused	By 20 years	
	Ischial and iliac crest fully fused	20–23 years	
Sacrum	Fusion between lateral elements and union of lower sacral segments	12–14 years	
	Sacrum complete	25+ years	
Humerus	Distal epiphysis fuses	12–17 years	11–15 years
	Medial epicondyle fuses	14–16 years	13–15 years
	Proximal epiphysis fuses	16–20 years	13–17 years
Radius	Proximal epiphysis fuses	14–17 years	11.5–13 years
	Distal epiphysis fuses	16–20 years	14–17 years
Ulna	Proximal epiphysis fuses	13–16 years	12–14 years
	Distal epiphysis fuses	17–20 years	17 years
Hand	Hook of hamate appears and fuses to body	10–12 years	
	Distal phalangeal epiphyses fuse	16 years	13.5 years
	Base of metacarpal 1 fuses	16.5 years	14–14.5 years
	Proximal and middle phalangeal epiphyses fuse	16.5 years	14–14.5 years
	Heads of metacarpals 2–5 fuse	16.5 years	14.5–15 years
Femur	Head fuses	14–19 years	12–16 years
	Greater trochanter fuses	16–18 years	14–16 years
	Lesser trochanter fuses	16–17 years	
	Distal epiphysis fuses	16–20 years	14–18 years
Tibia	Distal epiphysis fuses	15–18 years	14–16 years
	Proximal epiphysis fuses	15–19 years	13–17 years
Fibula	Distal epiphysis fuses	15–18 years	12–15 years
	Proximal epiphysis fuses	15–20 years	12–17 years
Foot	Calcaneal epiphysis commences fusion	11–14 years	10–12 years
	Distal and middle phalangeal epiphyses fuse	14–16 years	11–13 years
	Heads of metatarsals 2–5 fuse	14–16 years	11–13 years
	Proximal phalangeal epiphyses fuse	16–18 years	13–15 years
	Base of metatarsal 1 fuses	16–18 years	13–15 years
	Calcaneal epiphysis completes fusion	18–20 years	15–16 years

Adult age estimation

Adult age estimation involves analysis of the degenerative changes a skeleton undergoes over time to provide an age range. It relies on the examination of joint surfaces that are not affected by stress associated with body weight, locomotion, or muscle attachments (Randolph-Quinney et al., 2009; Parsons, 2017). It is vital to note however, that these degenerative changes will progress at different rates for different people and/or populations because of genetics, exposure to different environments and lifestyles, congenital anomalies, injuries, pathologies, and different personal habits. Because of this, the age estimation should have a wider range so as to factor in this variation. The surfaces used for adult age estimation include: the pubic symphysis, auricular surface of the ilium, sternal rib end of the fourth rib, cranial and maxillary suture closure (these are the main four methods); medial clavicle epiphyseal fusion; tooth root translucency; dental attrition; acetabulum; costal and thyroid cartilage ossification; and degenerative changes in the vertebral column (Snodgrass, 2004; Randolph-Quinney et al., 2009; Schmitt et al., 2010; Dirkmaat, 2012; Tersigni-Tarrant & Shirley, 2013; Parsons, 2017; Priya, 2017; Boyd & Boyd, 2018).

Pubic Symphysis

The pubic symphysis is suitable for age estimation because it is resistant to stress-related activities, and is considered as the most reliable age estimator of the adult skeleton (Dirkmaat, 2012; Parsons, 2017). The pubic symphysis goes through morphological changes with age, for instance the pubic face exhibits billowing in children and subadults, but with time these billows become worn down leading to a smooth texture of the bone that can become excavated and irregular because of bone porosity in old age. The later stage is also characterized by erosion of the pubic face and erosion, lipping and breakdown of the symphyseal rim (Schmitt et al., 2010; Dirkmaat, 2012; Tersigni-Tarrant & Shirley, 2013).

Todd (1920) described 10 morphological phases that could be used in the assessment of the pubic symphysis to classify them within a given age range. However, his method did not put into consideration that male and female symphyses were adapted for different functions and hence could not be evaluated with the same standards. Additionally, his method was found to over-estimate the age in older individuals. Brooks & Suchey (1990) refined Todd’s method by adding more female pubic symphyses to the original sample and describing a separate set of standards for the evaluation of female symphyses. They also narrowed down the initial 10 morphological phases to 6 (Illustrated in Figure 8; Table 6). This is the method that is preferred by forensic anthropologists today (Dirkmaat, 2012; Tersigni-Tarrant & Shirley, 2013; Parsons, 2017; Priya, 2017). However, it has a shortcoming of using wide age ranges to avoid unintentional exclusion of the unknown individual’s age, hence this affects the method’s accuracy (Parsons, 2017).

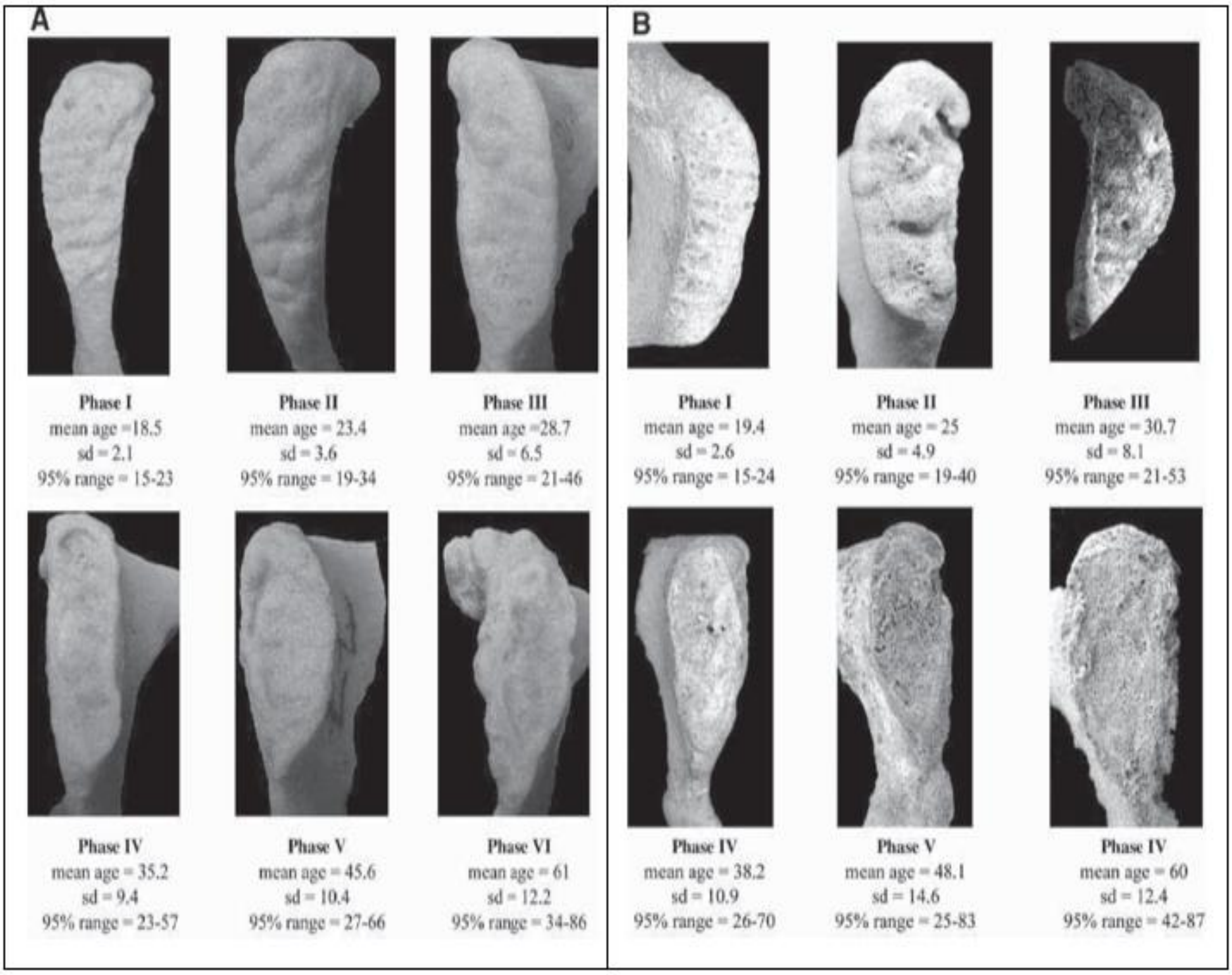

Figure 8. Changes in the pubic symphysis of a male (A) and female (B) with descriptive analysis as described by Suchey-Brooks. sd, standard deviation; 95% range, interval for 95% of the sample. [Adapted from (Schmitt et al., 2010)]

Table 6 shows the phases of morphological changes of the pubic symphysis as described by Brooks & Suchey (1990).

Table 6. Suchey-Brooks phases of pubic symphysis morphological changes [Adapted from (Priya, 2017)]

Phase	Age Range	Description
1.	15-23	Symphyseal face has a billowing surface composed of ridges and furrow which includes the pubic tubercle. The horizontal ridges are well marked. Ventral beveling may be present. Although ossific nodules may occur on the upper extremity, a key feature of this phase is the lack of delimitation for either extremity (upper or lower).
2.	19-34	Symphyseal face may still show ridge development. Lower and upper extremities show early stages of delimitation, with or without ossific nodules. Ventral rampart may begin formation as extension from either or both extremities.
3.	21-46	Symphyseal face shows lower extremity and ventral rampart in process of completion. Fusing ossific nodules may form upper extremity and extend along ventral border. Symphyseal face may either be smooth or retain distinct ridges. Dorsal plateau is complete. No lipping of symphyseal dorsal margin or bony ligamentous outgrowths.
4.	23-57	Symphyseal face is generally fine grained, although remnants of ridge and furrow system may remain. Oval outline usually complete at this stage, though a hiatus may occur in upper aspect of ventral circumference. Pubic tubercle is fully separated from the symphyseal face through definition of upper extremity. Symphyseal face may have a distinct rim. Ventrally, bony ligamentous outgrowths may occur in inferior portion of pubic bone adjacent to symphyseal face. Slight lipping may appear on dorsal border.
5.	27-66	Slight depression of the face relative to a completed rim. Moderate lipping is usually found on the dorsal border with prominent ligamentous outgrowths on the ventral border. Little or no rim erosion, though breakdown possible on superior aspect of ventral border.
6.	34-86	Symphyseal face shows ongoing depression as rim erodes. Ventral ligamentous attachments are marked. Pubic tubercle may appear as a separate bony knob. Face may be pitted or porous, giving an appearance of disfigurement as the ongoing process of erratic ossification proceeds. Crenulations may occur, with the shape of the face often irregular.

Auricular Surface of the Ilium

Changes that occur to the auricular surface with age are systematic and well defied, hence it provides an accurate estimate of age. It also has a higher rate of persistence in archaeological populations, the changes that occur to it are perceptible beyond the age of 50 compared to the pubic symphysis and its morphology is not influenced by either sex or ancestry (Lovejoy, Meindl, Pryzbeck & Mensforth, 1985; Dirkmaat, 2012; Priya, 2017;).

Just like the pubic symphysis, the auricular surface of subadults is characterized by billows that are progressively reduced to transverse striae, and traces of these striae may persist throughout life. With age, the texture of the surface becomes coarse due to granularity increase, the bone becomes more dense and there appears micro- and macroporosity. Ultimately, old age sets in general breakdown, lipping, erosion and irregularities (Dirkmaat, 2012; Tersigni-Tarrant & Shirley, 2013).

Lovejoy et al. (1985) described five general phases of transformation that the auricular surface goes through with age: early post epiphyseal phase (until mid-20s); young adult phase (mid-20s to mid-30s); mid adult phase (mid-30s to mid-40s); early senescent phase (mid-40s to mid-50s); and breakdown (approximate ages of 55-60) (Lovejoy et al., 1985; Priya, 2017). They further recommended 8 phases with corresponding age ranges based on observation for the estimation of age. The first 7 phases had a 5 year range while the eighth one included anyone above 60 years (Lovejoy et al., 1985; Dirkmaat, 2012; Parsons, 2017). This method was however found to underestimate the age of older individuals and overestimate the age of younger individuals (Parsons, 2017).

The apex of the auricular surface on the posterior ilium can also be used to estimate age; it is often a sloping angle with a smooth margin in young individuals but over time the margins become irregular leading to lipping at the apex (Tersigni-Tarrant & Shirley, 2013).

Cranial sutures

Age estimation is by analysis of degree of cranial suture closure. Cranial sutures are unique to an individual and are permanent throughout one's life (Rogers & Allard, 2004). This is however controversial as cranial suture closure is highly variable among individuals (Parsons, 2017; Priya, 2017). Nevertheless, it can be combined with other age estimation techniques to become a significant age indicator because with increasing age there is progressive fusion between the fibrous joints between the skull and bones (Dirkmaat, 2012; Priya, 2017). Meindl & Lovejoy (1985) examined 10 sutures which would be used to estimate age based on degree of closure; and the degree of closure wa scored on a four-point system as follows: 0 = open, no observable closure, 1 = minimal closure, 2 = significant closure, 3 = complete obliteration (Figure 9) (Dirkmaat, 2012; Tersigni-Tarrant & Shirley, 2013; Priya, 2017).

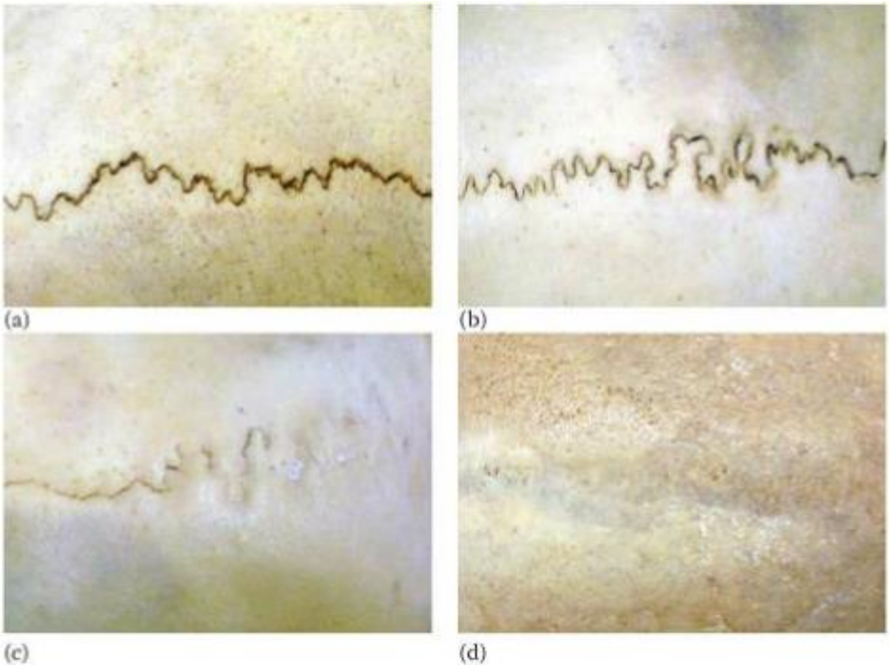

Figure 9. Illustration of the four-point scoring method of degree of suture closure by Meindl & Lovejoy (1985): (a) open (b) minimal closure (c) significant closure (d) complete obliteration. [Adapted from (Tersigni-Tarrant & Shirley, 2013)]

<ins>Sternal Rib Ends</ins>

This is the second most preferred technique by forensic anthropologists (Parsons, 2017). The main components of the sternal rib end that are examined during age estimation are the rim wall, pit shape and pit depth (İşcan, Loth & Wright, 1984). With age, the epiphyseal line disappears, and a deep V-shaped and then wide U-shaped pit forms on the initially flat and billowy surface of the sternal end. Rib rims that are initially rounded eventually become irregular, and there is notable depreciation of bone quality and density of the rib (Dirkmaat, 2012; Tersigni-Tarrant & Shirley, 2013; Priya, 2017).

While this technique is relatively easy to apply and gives narrower age ranges than the Suchey-Brooks method, sternal rib ends are fragile hence may not always be present or well preserved in a forensic context and thus this may impede their use in age estimation (Parsons, 2017). Additionally, various factors such as sex and biomechanical variation between individuals may affect age estimation using this method (İşcan et al., 1984).

Stature Estimation

This is the approximation of the height of the unknown remains, and the method applied for estimation will be determined by what skeletal components are recovered (Parsons, 2017).

Cardoso, Marinho and Albanese (2016) describe three different concepts of stature: (i) living stature, (LS) which is "the actual stature of a person standing in a standardized position as measured using calibrating equipment such as an anthropometer" (Cardoso et al., 2016, p55); (ii) forensic stature (FS), which refers to "the documented stature of an individual as it appears on official government issued documents such as passports" (Cardoso et al., 2016, p56); and (iii) cadaver stature (CS), which describes "the length of the cadaver taken prior to autopsy in a supine position" (Cardoso et al., 2016, p56). They observed that living stature of an individual may vary over 24 hours, with the tallest height being in the morning, because of effects of gravity on the joints and intervertebral discs, and that it changes with age due to cartilage degeneration in the joints. The findings of their study showed that cadaver stature is greater than both living and forensic statures mostly because the gravitational pressure acting on the joints when standing is no longer there, hence this needs to be taken into account during height estimation.

Portions of the skeleton used in estimation include the tibia, femur and sacral and coccygeal vertebrae (Cattaneo, 2007) because the accuracy is usually more reliable when the skeletal components used are found along its length. As such, lower limb dimensions have a higher correlation with body height (because they contribute directly to the stature of a person) as compared to upper limb dimensions (Özaslan, İşcan, Özaslan, Tuğcu & Koç, 2003; Dirkmaat, 2012; Kewal Krishan, 2013). Of importance to note is that different bones will give different resultant estimates (Dirkmaat, 2012). Estimation from fragmentary remains is inaccurate and is not appropriate for statistical analysis hence is inappropriate for forensic use as well (Randolph-Quinney et al., 2009).

There are two methods of stature estimation, anatomical method and mathematical or regression method.

Anatomical method

The anatomical method is only suitable when the skeleton is mostly complete, as it involves measurement of the cranium, all vertebrae except the atlas, sacrum, femur, tibia, talus and calcaneus. This method is not affected by either sex or ancestry and it gives a more accurate estimation of stature. However, it is inapplicable when any of the elements required are missing, which is the most common scenario in forensic contexts (Tersigni-Tarrant & Shirley, 2013).

Mathematical/Regression Approach

The mathematical/regression approach is applicable when skeleton is incomplete. The regression formula chosen varies depending the data available as most methods of estimation used are sex-specific and/or population-specific and/or century-specific (Randolph-Quinney et al., 2009; Cardoso et al., 2016). Although measurements of the lower extremity are preferred, upper limb measurements give acceptable estimates as well, and can be used in their absence (Tersigni-Tarrant & Shirley, 2013).

Personal Identification

Identification refers to “the process of verifying that the individual concerned is the same as the one that is known” (Tersigni-Tarrant & Shirley, 2013, p 398). Personal identifiction is the next step after creation of a biological profile, and is critical for ethical, juridical and civil reasons (Ciaffi, Gibelli & Cattaneo, 2011; Kewal Krishan, 2013). In this field, a forensic anthropologist will have to work with other experts, mostly a forensic pathologist and odontologist, in order to achieve a definitive personal identification. It involves comparing antemortem records of the suspected person and postmortem records of the actual remains to achieve either a positive identification or exclusion. It must always be conducted with a set of data (Cattaneo, 2007; Schmitt et al., 2010; Ciaffi et al., 2011; Vandermeulen et al., 2012; Tersigni-Tarrant & Shirley, 2013).

Personal identification can be categorized into three: tentative (the identity of the remains is suspected), circumstantial or presumptive (stong consistencies between the remains and the suspected person), and positive (Tersigni-Tarrant & Shirley, 2013). The SWGANTH [2010] guidelines for personal identification document titled “Personal Identification” defines positive identification as a case where “the antemortem and postmortem information match in sufficient detail to conclude that they are from the same individual to the exclusion of all other reasonable possibilities” (p2) (Randolph-Quinney et al., 2009; Ubelaker et al., 2018). This can however be challenging because it is difficult to determine just how many morphological elements are adequate for a definite identification as there does not exist a minimum number of points (Kahana & Hiss, 1997; Cattaneo, 2007; Schmitt et al., 2010; Ciaffi et al., 2011; Tersigni-Tarrant & Shirley, 2013), and therefore it is rather subjective. Indeed, some experts assert that expert opinion is sufficient, and that quantifying and standardizing features used in identification is not necessary (Rogers & Allard, 2004). Unfortunately, this approach may face limitations during trial as it falls short of the Daubert criteria (Ciaffi et al., 2011).

Positive identification involves a two-step process: (i) discovery of anatomical features that are common between the examined remains and the antemortem data of the suspected individual; and (ii) determination by the analyst that the features under comparison are sufficiently unique to make a positive identification (Ubelaker et al., 2018). Needless to say, misidentification can lead to disastrous consequences.

The identification method used will be determined by the postmortem condition of the body and the availability, quality and quantity of antemortem information about the victim (Tersigni-Tarrant & Shirley, 2013).

Comparative Radiography

This is a technique that involves the direct visual comparison of antemortem and postmortem radiographs, and is used to attain positive identification. Radiographs are a common diagnostic tool used in the healthcare industry around the world, and facilities exist to store the radiographs over extended periods of time (Kahana & Hiss, 1997; Tersigni-Tarrant & Shirley, 2013; Nikam, Gadgil, Bhoosreddy, Shah & Shirsekar, 2015). This makes their retrieval for comparison with post-mortem radiographs to achieve identification during mass disaster fast considerably quick and easy. Indeed, it is the most common technique used in forensic anthropology to obtain a positive identification from unknown remains (Kahana & Hiss, 1997). Comparison between the antemortem and postmortem images can be done either by side-by-side visual inspection of the images (Figure 10) or by superimposition of the images in an attempt to find any consistencies or inconsistencies of the morphological features captured in the radiograph (Tersigni-Tarrant & Shirley, 2013).

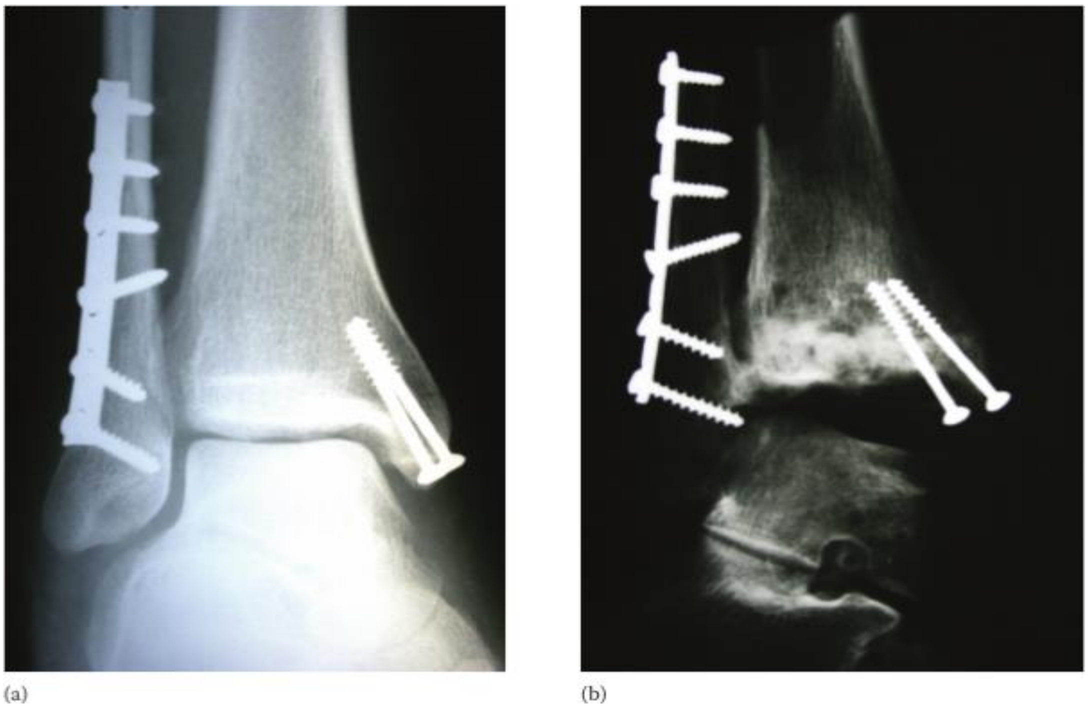

Figure 10. Side by side comparison of an antemortem (a) and a postmortem (b) radiograph of an ankle [Adapted from (Tersigni-Tarrant & Shirley, 2013)]

In order for morphological features captured on radiographs to be of value in identification, they have to be unique to the individual and they have to remain unchanging over time despite ageing (Kahana & Hiss, 1997; Ciaffi et al., 2011). The smallest anatomical, pathological, and therapeutic characteristics must be searched for, as these peculiarities can lead to a positive identification (Schmitt et al., 2010).

Comparative radiography can be done on the various osseous districts of the body in order to achieve identification: head (suture pattern and frontal sinuses), thorax (ribs, vertebrae, clavicle), abdomen and pelvis (vertebrae), arms and legs (Schmitt et al., 2010; Ciaffi et al., 2011; Dirkmaat, 2012). Aside from examining similarity in morphology, such as degree of closure of sutures and frontal sinuses, degenerative changes such as osteophytic lipping and evidence of healed trauma and medical intervention are also used as individualizing markers (Kahana & Hiss, 1997). The post mortem radiographs should be taken with the same orientation, scope and magnification as the antemortem radiographs (see Figure 10) for easier comparison and superimposition (Kahana & Hiss, 1997; Schmitt et al., 2010; Tersigni-Tarrant & Shirley, 2013).

Antemortem records are usually acquired with the aid of law enforcement officers who look for the possible medical facilities that had been visited by the suspected person (Tersigni-Tarrant & Shirley, 2013).

Cranial evidence

The skull is composed of several elements that can be used for comparison to attain a positive identification. Smith, Limbird & Hoffman (2002) put forward that through computed tomography (CT) scans, bony details of the frontal and sphenoid sinuses, ethmoid and mastoid air cells, sagittal cranial suture and the torcula could be used for comparison to attain a positive identification. Rogers & Allard (2004) analysed cranial suture patterns (specifically the location, length, and slope of a suture's component lines) on CT scans and compared this method against the Daubert standard. They concluded that the cranial suture technique met the Daubert standard.

Frontal sinuses

At age 20, frontal sinus growth is complete, and they do not change throughout life after 20. As such, provided the radiograph was taken after the individual was at least 20 years old, the age at which the radiograph was captured does not matter (Nikam et al., 2015). Frontal sinuses are unique and display a wide range of variation, from minimal presence to large formations (Ubelaker et al., 2018). As such, matching antemortem and postmortem radiographs of sinuses provides a mean of positive identification of remains (Nikam et al., 2015).

Christensen (2005) noted that while the use of frontal sinuses for positive identification was generally accepted within the forensic community and had been peer reviewed, it had not undergone any standardization, hence still fell short of meeting the Daubert standard. She assessed the individualization of frontal sinuses using Elliptical Fourier analysis (EFA) and concluded that it was a reliable method with a 96% probability of recognizing a correct identification.

Dental Comparison

Although this is the area of discipline for forensic odontologists, forensic anthropologists also share in the expertise on aspects of dental morphology and can identify evidence useful for positive identification (Ubelaker et al., 2018). Teeth are among the most resilient structures in the human body and can persist through conditions and trauma that destroy or otherwise alter the body (Kahana & Hiss, 1997; Pretty, 2007; Schmitt et al., 2010; Hinchliffe, 2011; (Tersigni-Tarrant & Shirley, 2013)). Additionally, they are unique enough to be able to distinguish between individuals (Taylor, 2009). Anthropologists and odontologists examine the anatomical, pathological and restorative characteristics of teeth such as number of teeth present, antemortem loss of teeth, unusual tooth rotation, and carious lesions, in order to obtain an identification (Kahana & Hiss, 1997; Ubelaker et al., 2018). For instance, if damage to teeth from a trauma was repaired using maxillofacial pins, wires or plates, these implants may be traced if they have a manufacturer's number or code (Hinchliffe, 2011).

In the event that the postmortem radiograph was taken in the same spatial orientation with the antemortem one, then the images can be superimposed and compared to achieve an identification (Schmitt et al., 2010).

Skull-Photo/Craniofacial Superimposition

The foundation of this method is the fact that there exists a strong relationship between the morphology of the skull and the soft tissues of the human face (Sauer, Michael & Fenton, 2012). It involves comparison between the features of a skull recovered from unknown remains with antemortem photographs of the individual suspected to be the victim and is usually applied when all other methods of positive identification have not accomplished an identification. This method can only be used when a complete skull is available for comparison (Ubelaker et al., 2018). The comparison is made by superimposing a photograph of the skull with a semitransparent photograph of the face of the living person, and the craniometrics points of the soft tissues of the face are compared with craniometrics points of the skull. Facial photographs are obtained either from family or through police records. The orientation of the two images must be similar (Schmitt et al., 2010, Sauer et al., 2012). An important factor to note is that this method requires good-quality photographs because the quality of the facial image will affect the accuracy of the results obtained (Schmitt et al., 2010; Ubelaker et al., 2018). The ideal image would be a close-up facial view with the teeth revealed and the individual facing the camera (Tersigni-Tarrant & Shirley, 2013).

Superimposition can also be used in forensic odontology when antemortem dental records of the suspected individual cannot be obtained. An image of the skull of the unidentified remains is superimposed on a photograph of the suspected individual in which the dental elements are clearly visible, and a comparison is made. This method is somewhat more accurate than skull-photo superimposition of the whole face because teeth are considered part of the skeletal system, hence it will be a comparison between skeletal elements, unlike superimposition, which is a comparison between skeletal elements and soft tissues of the face (Schmitt et al., 2010).

This method is often only used for exclusion or to provide corroborative evidence in favour of an identification and not a method of positive identification of remains (Schmitt et al., 2010, Sauer et al., 2012; Tersigni-Tarrant & Shirley, 2013; Ubelaker et al., 2018) as seen from Fenton, Heard & Sauer (2008). They were only able to use skull-photo superimposition to exclude an identity between two skulls, but they were not able to positively identify the skull that was not excluded as belonging to the suspected individual.

Nonimaged Records Comparison

This method involves the comparison of antemortem records such as charts and notes to features of skeletal remains, and is useful when antemortem radiographs and other images are not available. Information in such records may be individualizing and hence useful for identification, such as surgical procedures (like implanted devices), dental patterns, injury treatments (such as a broken bone), and pathologies and anomalies. It is ideal to have antemortem records for all these examples; however, in the absence of such records recollection from family may have to suffice (Tersigni-Tarrant & Shirley, 2013).

Caution should be exercised when using these records however, as at times they may not be current or accurate representations of an individual’s current medical situation for instance if mistakes were made during recording or if the records were fabricated in order to commit insurance fraud (SWGANTH, 2010).

Craniofacial Reconstruction

Craniofacial reconstruction refers to the artistic reproduction of the soft tissue facial features of an individual (Tersigni-Tarrant & Shirley, 2013), and relies on the hypothesized relationship between the soft tissues of the face and the bone structure of the skull underneath (Stavrianos, Stavrianou, Zouloumis & Mastagas, 2007; Vandermeulen et al., 2012). It is a useful forensic technique that endeavours to recreate an individual's face from a skull or skull model for the reason of obtaining identification through recognition (Starbuck & Ward, 2007). It is not a means of personal identification, but a final resort when all other scientific leads have been exhausted or when no other information is available, especially in the case of skeletonized, badly decomposed or mutilated bodies. The goal of this method is to act as a stimulus to capture the attention of the public so as to facilitate identification when there are few to no clues on the identity of remains (Cattaneo, 2007; Stavrianos et al., 2007; Starbuck & Ward, 2007; Vanezis, 2008; Vandermeulen et al., 2012; Tersigni-Tarrant & Shirley, 2013; Gupta, 2015; Santoro et al., 2017; Ubelaker et al., 2018).

Since reconstruction involves reproduction of the facial features, knowledge of human cranial anatomy and artistic ability are vital in order to reproduce useful images. The reconstructions should thus be a collaborative effort between anthropologists, anatomists and artists (SWGANTH, 2011).

Reconstruction techniques can either be two-dimensional (2D) or three-dimensional (3D), and they can be analysed either manually or using specific software (Vandermeulen et al., 2012; Gupta, 2015). 2D reconstructions recreate a face from the skull using soft tissue depth estimates, and can be manual or computer aided (Figure 11). On the other hand, 3D manual reconstructions are accomplished by applying clay, plasticine, wax or plastic directly onto the skull or a replica of the skull (Buzug, 2007; Vanezis, 2008; Gupta, 2015). Markers are placed in holes on the skull at specific landmarks as depth markers to represent the different soft tissue depths of the face (Gupta, 2015).There are three 3D manual methods of reconstruction used on forensic facial reconstruction: Anatomical (Russian), Anthropometrical (American) and Combination Manchester (British) methods (Stephan, 2006; Vandermeulen et al., 2012; Gupta, 2015).

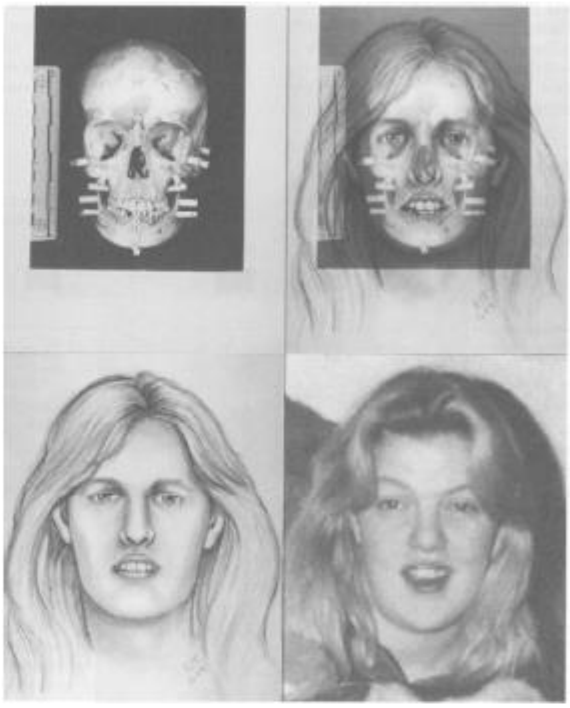

Figure 11. Illustration of a 2D reconstruction. Markers indicating soft tissue depth are placed on the skull and photographed. The artist then draws the face over the photograph according to the markers. [Adapted from (Vanezis, 2008])

3D Manual Facial Reconstruction

The Russian (Anatomical, Morphoscopic) method was developed by Gerasimov in 1971. It involves modelling of the facial tissues according to their anatomical position without consideration for soft tissue depth. Muscles, glands and cartilage are shaped onto the skull layer by layer in order to mimic the skin. It is much slower than the American method, and requires a great degree of anatomical knowledge. It is a technique that is often used in the reconstruction of fossil faces where no statistical data exists. On the other hand, the American (Anthropometrical, Morphometric) method, which was developed by Krogman in 1946, involves building the soft-tissue thickness in bulk using standard sets of statistical tissue thickness measurements at precise positions on the face, without regard to detail or the anatomy of the underlying skull. There have been instances in the past where both soft tissue depths and anatomical facial structures were used in a reconstruction, laying foundation for the combined method (developed by Neave in 1977). As such, the Combination method is the most accepted method of reconstruction currently (Kähler, Haber & Seidel, 2003; Stephan, 2006; Vanezis, 2008; Vandermeulen et al., 2012; Gupta, 2015).

Stephan (2006) in his study concluded that the terms “American” and “Russian” should be avoided as they were imprecise. This is because each method incorporated to a varying degree both approaches, hence both methods were within the spectrum of the Combination method. Additionally, he also recommended that referring to the methods based on locality (“Russian” and “American”) should be avoided as they are a poor indication of what the methods actually entail. He gave an example of the “Manchester/British” method and the “Melbourne” method, which although had different names and hence gave the impression of different methods, both actually incorporated muscle construction and average soft tissue depths.

Manual reconstructive methods remain difficult and highly subjective because of the anatomical and artistic expertise they require. Two different artists can interpret the same skull in two different ways resulting in two substantially different reconstructions (Vandermeulen et al., 2012). The reality of this was seen in the Green River serial killer case where nine different artists were used to create the reconstructions of the unidentified victims. Interpretations of the same victim varied greatly between practitioners, hence there was little success in identification when the reconstructions were shown to the public. Additionally, manual methods are very time consuming and labour intensive (Haglund & Reay, 1991; Davy, Gilbert, Schofield & Evison, 2005; Vandermeulen et al., 2012).

3D Computer-Aided Facial Reconstruction

There has been an advancement in recent years in computer science and an improvement of medical imaging technologies (Greef & Willems, 2005). Computerized methods for 3D facial reconstruction use computer programmes to transform laser-scanned 3D skull images into faces (Stavrianos et al., 2007). This is done by first taking skull measurements using anatomical landmarks for reference and entering them into the computer before capturing an image of the skull in 3D either using a CT scan or laser-scanning (Buzug, 2007). This method was originally used as a solution to the shortcomings of the manual method such as being time-consuming, highly subjective and requiring artistic talent. The main aim was to come up with a process that was flexible, repeatable and accurate (Greef & Willems, 2005). Additional advantages of computer-aided reconstructions over manual reconstructions include: it decreases practitioner training requirements hence is accessible to a wider range of people without need for extensive expertise (Vandermeulen et al., 2012; Gupta, 2015), different variations of the same face (such as slim and obese) can be produced at the push of a button, slight variations in facial expressions can be obtained (Kähler et al., 2003), 3D scans of the skull are acquired contact-free hence reducing the risk or opportunity of damaging the original specimen (Kähler et al., 2003; Davy et al., 2005), ease of visualization (Vandermeulen et al., 2012). The method is not without its limitations, such as the amount of finer detail on the skull that will be captured depends on the maximum resolution of the digital scanner

(Kähler et al., 2003). The greatest limitation is that there are no credible ways to estimate many of the most individualizing aspects of the face that are vital in the recognition of the human face such as eye colour, ears, lips, hair and facial colour and length. These do not have an underlying skeletal feature from which they can be inferred, hence their determination is left to an artistic guess (Tersigni-Tarrant & Shirley, 2013).

Davy et al. (2005) were able to create a fairly accurate computerized reconstruction of the face of a mummy from only the frontal and lateral radiographs of its skull. They used 3ds max™ version 5 (Discreet™, 2002), which is a computer program designed for modelling and animation. They commented that the programme allowed them to view the virtual space in which the skull occupied from multiple angles and in layers, and this helped them in the correct positioning of the vertices of the virtual skull.

THREE-DIMENSIONAL IMAGING

3D imaging has become a common tool especially in the medical field for diagnosis of ailments, and is also applied to medical procedures such as work-up prior to surgery. It is the preferred visualization technique for volume data (Duke & Aguirre, 2010).

Photogrammetry

While 2D documentation is a vital part of forensic documentation and examination, additional 3D surface documentation helps in visualizing findings and contributes to the reconstruction of crime scenes (Kottner et al., 2019). Photogrammetric methods can be utilized in any circumstances where the object to be measured can be recorded using photographs (Luhmann et al., 2013). They use photographs of an object to obtain its precise dimensions

(Santoro et al., 2017). Forensic photogrammetry is a method that enables a 3D image of objects in virtual space by recording and documenting the surface of small objects (Thali et al., 2003b) in digital form (coordinates and derived geometric elements) or graphical form (images, drawings, maps) (Luhmann et al., 2013). This process involves taking a series of overlapping photographs taken from different angles (Koller, Ebert, Martinez & Sieberth, 2019; Kottner et al., 2019) which are entered into a computer system that calculates the position in space of specific points on the surface of the objects and thereafter produces data models of the objects in 3D (Figure 12) (Thali et al., 2003a, Thali et al., 2003b). The resultant image contains a wealth of information and can be re-accessed at any time (Luhmann et al., 2013).

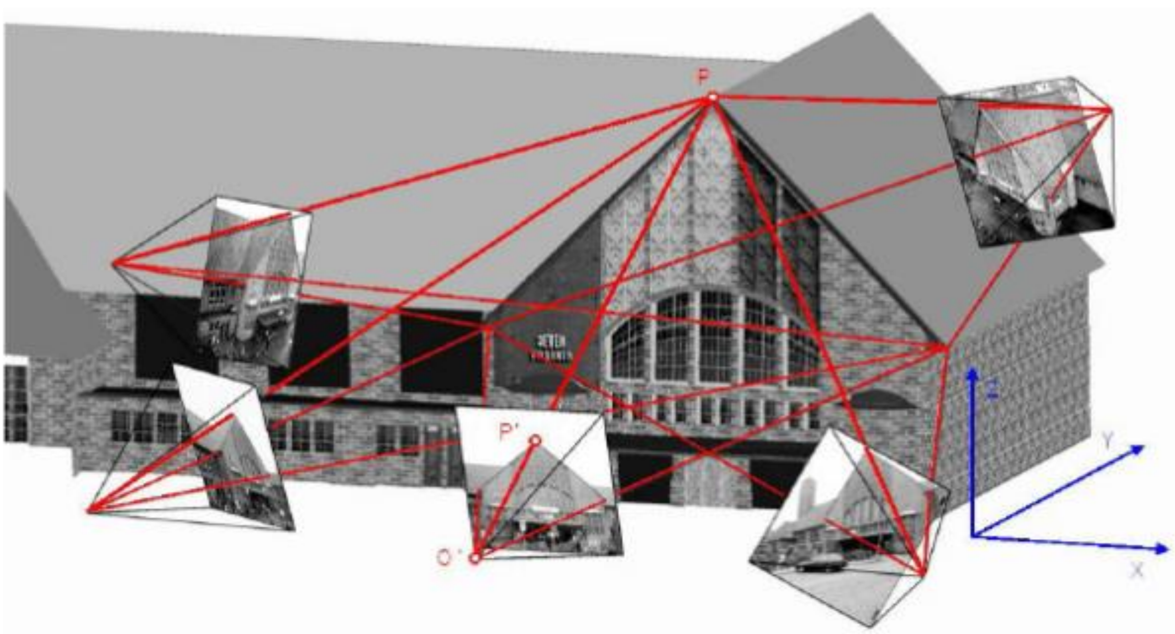

Figure 12. Example of a photogrammetric reconstruction of a building. [Adapted from (Luhmann et al., 2013)]

3D photogrammetry is gaining increasing applicability in quantitative evaluation, for instance in evaluating plastic surgery outcomes. It allows for the analysis of soft tissues with regards to topography and volumes (Linden et al., 2018). In their study whose aim was to determine the accuracy and reliability of 3D stereophotogrammetry, Dindaroğlu et al. (2016) concluded that the measurements using this method were consistent with those of direct anthropometric measurements; and that the method could be used reliably. Additionally, photogrammetry produces high-resolution photorealistic, real sized or easy to calibrate 3D surface models (Urbanová, Hejna & Jurda, 2015), the process is fast and non-invasive, and does not have radiation concerns like CT scans (Linden et al., 2018).

When compared to standard photographs, photogrammetric measurements in 3D are more accurate, and the resultant 3D models can be visualized in different ways which enables a better comprehension and review of forensic-relevant injuries even after they've healed (Koller et al., 2019). Furthermore, it is a non-contact (Osman & Tahar, 2016) and hence non-destructive method (Edelman & Aalders, 2018) because the original objects are never touched or changed, thus there is no loss or damage to evidence (Thali et al., 2003a; Thali et al., 2003b).

All these features, coupled with the fact that photogrammetry is rapid and remote make it suitable as a forensic science analytical tool (Edelman & Aalders, 2018). Furthermore, the method allows for the resultant reconstruction to be re-assessed with great accuracy at any time (Villa, 2016; Luhmann et al., 2013) even after the crime scene was released (Edelman & Aalders, 2018) or the injury or object no longer exist (for instance if the body with the injury was cremated) (Thali et al., 2003a; Thali et al., 2003b; Brüschweiler et al., 2003).

In spite of all its advantages, photogrammetry is not without its shortcomings: it falls short when the surface of the body being scanned is either covered with hair or is reflective due to being moist (Urbanová, Hejna & Jurda, 2015). The procedure of image capture can be time consuming and, depending on the camera being used, may require experienced photographers (Koller et al., 2019; Kottner et al., 2019). Indeed, this technique needs ambient light to illuminate the objects to be photographed, without which this method is not applicable (Buck et al., 2017).

Among the applications of photogrammetry in forensic science include documentation and measurement of forensic-relevant injuries (Thali et al., 2000; Villa, 2016; Koller et al., 2019), determination of injury-causing weapon (Brüschweiler et al., 2003; Thali et al., 2003a), recording crime scenes (Edelman & Aalders, 2018), examining patterned injuries of skin, soft tissues and bones, and comparison of injuries with injury-causing instruments (Brüschweiler et al., 2003), road accident reconstruction (Osman & Tahar, 2016) and facial reconstruction (Santoro et al., 2017).

With the advancement of technology, consumer-grade cameras can now be used in photogrammetric applications. These cameras are everywhere, have a high enough resolution and can give results with medium accuracy required in forensic measurement (Osman & Tahar, 2016).

Close-Range Photogrammetry (CRP)

CRP is an affordable, flexible and accurate technique (Urbanová et al., 2015). It is characterized by much shorter image rages and alternative recording techniques as compared to the longer range photogrammetry (Luhmann et al., 2013). It also offers the option of fast data acquisition and reduced cost of operations (Osman & Tahar, 2016). It has found application in a wide range of fields such as automotive and aerospace industries, architecture, archaeology, engineering and medicine (Luhmann et al., 2013; Villa, 2016). In forensic analysis and police work, it is primarily used during accident recording (Luhmann et al., 2013; Osman & Tahar, 2016; Villa, 2016), crime scene measurements and measurement of individuals (Luhmann et al., 2013).

The images used in CRP require a scale that will define the size of the object or area contained in the photos, this is standard practice in photography. The software used to process the images will recognize the scale in the photos and hence scale the objects accordingly (Colwill, 2016; Edelman & Aalders, 2018).

Forensic three-dimensional/computer aided design (3D/CAD)-supported photogrammetry (FPHG)

3D/CAD- supported photogrammetry is a method that enables 3D image creation of objects in a virtual space by documenting the surface of small objects (Brüschweiler et al., 2003; Thali et al., 2003b). It plays a vital role in forensic documentation from a reconstructive angle, especially when a detailed 3D reconstruction is critical, for instance documenting forensically relevant injuries, and comparing patterned injuries to injury-causing instruments (Figure 13) (Thali et al., 2000; Thali et al., 2003a; Brüschweiler et al., 2003). Thali et al. (2003a) in their paper were able to prove using FPHG that the patterned blunt injury on a victims face was as a result of a blow from the muzzle of a soft air gun. FPHG additionally stands out from other comparative methods because it allows for the analysis of non- protruding injuries as well such as intradermal bleeding (Brüschweiler et al., 2003; Thali et al., 2003b).

Thali et al. (2000) utilized 3D/CAD-supported photogrammetry and radiology (CT) to reconstruct an injury and compare the injury to the object suspected to have caused it. They reconstructed a killing blow from a forensic murder case by striking a representatively constructed 'skin-skull-brain-model' with a characteristically shaped tool, and then photogrammetrically treated both the wound and tool by taking a series of photographs from different angles. The photographs were then scanned and fed into the RolleiMetric multi-image evaluation system, resulting in the creation of a dot matrix data model that formed the basis for a dot-and-line reconstruction for both the injury and injury-causing instrument. The reconstructions were fed into a 3D/CAD program and the resultant models compared in virtual space. Additionally, the patterned injury's internal structure was radiologically scanned using CT, and an additional 3D data model created. The radiologic data and 3D/CAD photogrammetry data were then compared.

The combination of the two methods provides a way of conclusively fitting a tool to an injury in forensic investigations; and additionally opens up a way to a 'scalpel-free' autopsy ('Forensic Digital Autopsy') in the near future due to the non-invasive nature through which the documentation and analysis of injuries to the body is conducted.

Thali et al. (2003b) on the other used FPHG in bite mark analysis. They digitized both the bite mark in question and the suspect's teeth cast and produced 3D models of both the bite mark and cast using3D/CAD software. The two were then compared and the cast was additionally overlayed on the bite mark within the 3D space. At the end of their investigation, Thali et al. (2003b) were able to strongly suggest that the suspect from whom the cast was made was the perpetrator.

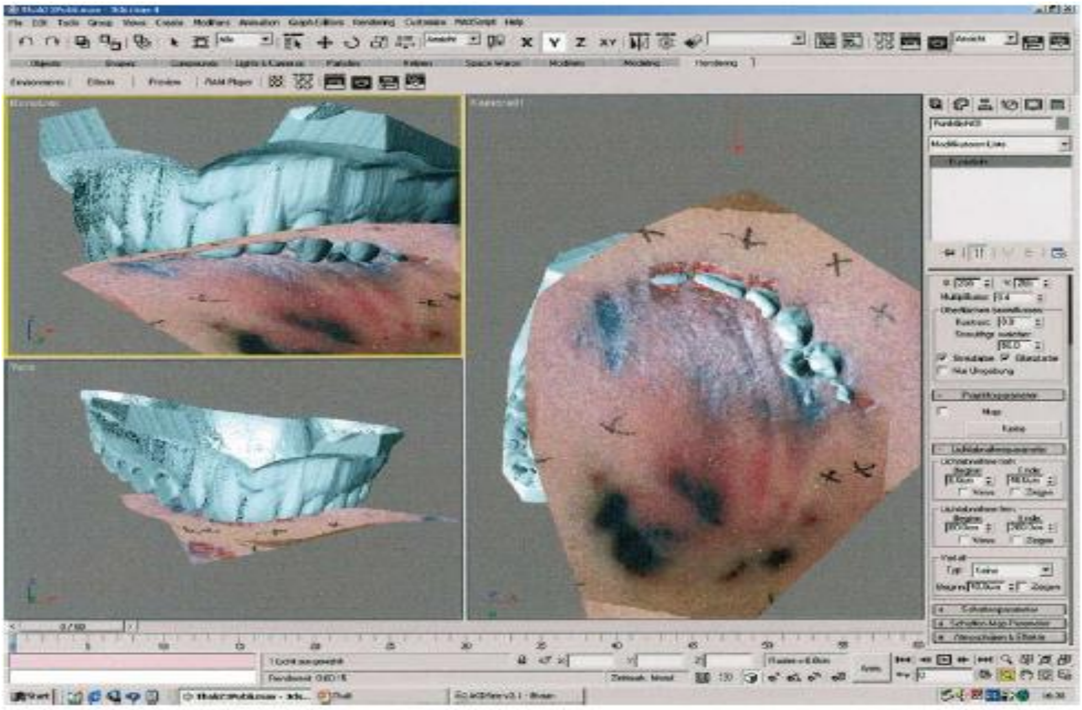

Figure 13. Use of FPHG in comparison between a bite mark injury and a digitized cast of the suspect's teeth. [Adapted from (Thali et al., 2003b)]

It is important to note that successfully evaluating an object of forensic relevance using FPHG relies on the proficient preparation and photographic recording of the object (Brüschweiler et al., 2003) hence appropriate training should be undertaken (Colwill, 2016). Additionally, it is advisable that analysis using 3D/CAD software should be left to experts (Brüschweiler et al., 2003). However, with constant developments in technology and software, one requires only minimal knowledge or training to be able to use the software (Colwill, 2016).

From the information provided here, it is evident that previous research has established FPHG as a valid method of reconstructing forensically relevant injuries especially to the soft tissues such as bite marks or blunt force trauma. The researcher of this paper will thus attempt to validate photogrammetry as a method that can be used in the forensic documentation and analysis of osseous remains.

Agisoft Metashape Professional Software

Formerly known as Agisoft PhotoScan, this is a software that is used to develop a 3D model from 2D photogrammetric photographs by producing a set of 3D coordinates known as a point cloud. A mesh that estimates the shape of the object is then produced by forming polygons between point clouds (Koller et al., 2019). The software automatically adjusts bundle blocks and generates 3D models from photos of both calibrated and non-calibrated cameras. The photos of the area to be documented are taken in an overlapping sequence with a constant focal length and distance to the object (Villa, 2016; Buck, Buße, Campana & Schyma, 2017). The photos can be taken from any position so long as the object to be reconstructed is visible on at least two photos (*Agisoft Metashape User Manual: Professional Edition, Version 1.5*, 2019). The resulting model has high-resolution colour information; although, the quality of the geometry reies on the configuration of the photos around the object and the quality of the photos themselves (Buck et al., 2017).

Agisoft PhotoScan (now Agisoft Metashape) is easy to use, provides good results and has a low purchase price. In terms of accuracy, photogrammetry can exhibit slight deviations in geometry but still give accurate enough results (Buck et al., 2017).

Following previous research, and due to the availability of the software at the researcher's academic institution, this is the software that will be used by the researcher in their work.

Laser Surface Scanning

The mechanism of action of laser surface scanners is using laser beams that move slowly across the scanned surface to rapidly and accurately digitize the surface, and reflect back to a light sensor (Aung, Ngim & Lee, 1995; Urbanová et al., 2015). This method requires that scanned objects avoid motion for long periods of time and it can be slow hence it is not preferred for living persons as it can result in motion artefacts, especially with children or subjects with developmental disabilities (Wong et al., 2008; Fourie, Damstra, Gerrits & Ren, 2011; Urbanová et al., 2015). It is however suitable in a forensic setting for examining crime scenes, corpses and skeletal remains, weapons or personal belongings (Urbanová et al., 2015).

Laser surface scanning is accurate and reliable for identifying craniofacial surface landmarks (Aung et al., 1995; Wong et al., 2008; Fourie et al., 2011). It has proved to be a valuable tool for swift and accurate measurements in particular regions of the face, most especially the longitudinal documentation of morphological changes around the nasal and circumoral regions (Aung et al., 1995).

This method has several advantages: it is noninvasive, allows images to be archived and avoids errors that occur with 2D representations on 3D surfaces (Wong et al., 2008). In addition, it captures an image in a simple and rapid manner with the capability of viewing the reformatted laser scan image immediately at any preferred angle and position, it offers easy retrieval of data, and it can be done repeatedly without any danger of radiation (Aung et al., 1995).

Some of the shortcomings of laser scanning include the fact that it is operator dependent (Aung et al., 1995), the resulting 3D model does not include information about original texture colouring unless the scanner is equipped with an optical camera system (Urbanová et al., 2015), landmarks covered by hair (beards/moustaches/long hairstyles) are obscured, and the equipment and software needed are costly (Farkas & Deutsch, 1996).

Despite the disadvantages, laser scanning has been proven to be accurate and valuable, both in recording surfaces in 3D and in taking accurate measurements.

Radiological Scanning [Computed Tomography (CT) and Magnetic Resonance Imaging (MRI)]

CT has always been preferred for clear high-resolution images, and modern CTs have, on top of improving the quality of image acquisition, advanced so that they operate faster and hence reduce radiation exposure to the patients. MRI on the other hand uses electromagnets instead of radiation to acquire images. However, it is not suitable for patients with metallic implants that can be magnetized (Duke & Aguirre, 2010).

Forensic institutes across the world are adopting CT or MRI scanners or both in their mortuaries and mobile CT for autopsy and mass fatality investigations. CT provides information to a pathologist that may not be available to them, and is a non-destructive permanent record of the body. However, comparison of forensic to antemortem records may become problematic when the CT imaging is performed by clinical radiologists as they have little training in interpreting forensic CTs hence may overlook information that they think is irrelevant, but in essence has forensic value. Additionally, CT may be insensitive in diagnosing some conditions or give a false appearance of some conditions. For instance sub-arachnoid hemorrhage (Rutty, Morgan, O'Donnell, Leth & Thali, 2008), and (particularly Multislice Computed Tomography (MSCT)) in dental identification it cannot distinguish between different types of teeth restorations and artefacts leading to insufficient detail obtained to be compared to antemortem records (Vallis, 2017). Furthermore, CT is a cumbersome tool for screening the entire skeleton (Rybak & Rosenthal, 2001).

Radiological scanning methods allow for the 3D documentation of internal and external aspects of the body including lesions, but their resolution is not adequate for the documentation of skin injuries or facial contours. Additionally, the colour information of the skin is not obtained (Wong et al., 2008; Urbanová et al., 2015; Villa, 2016), and CT scans have the disadvantage of radiation (Linden et al., 2018) and need for general anaesthesia in young subjects (Wong et al., 2008). These radiological methods are used to complement FPHG (Brüschweiler et al., 2003) because they can examine the sub-surface (volumes and depths) whereas photogrammetry only examines the surface (Thali et al., 2000; Brüschweiler et al., 2003).

Photogrammetry (3D external data) can be combined with radiological scanning (3D internal information) to establish individualized 3D human models which describe the precise internal and external wounds and lesions and the individual body proportions (Villa, 2016). An example of this combination is seen in the research of Thali et al. (2000). Of importance to note is that the sensitivity of CT used during post-mortem should be higher than that used during clinical tests (slice thickness of 2.5 mm or less). This may translate to longer scan times and higher radiation doses, but these factors are not important during post-mortems (Rutty et al., 2008).

Anthropometry

Anthropometry is a method for quantifying body size and proportions for instance by measuring the length and width of the body (Wang, Thornton, Kolesnik & Pierson, 2006). Craniofacial anthropometry refers to the quantification of facial characteristics, and is essential for research in various disciplines such as dysmorphology, plastic surgery (Aung et al., 1995; Heike, Cunningham, Hing, Stuhaug & Starr, 2009). Anthropometric measurements enable forensic anthropologists to come up with biological profiles containing precise metric data, and to determine features of an individual that could be used to obtain an identification with time (Cahill, 2017).

There are various methods of anthropology and these involve three elements: location of craniofacial landmarks (Figures 14, Table 7), execution of measurements and evaluation of the findings using normative data. The methods of anthropology include traditional methods such as direct anthropometry and 2D photogrammetry (Fourie et al., 2011), and indirect anthropometry (Farkas & Deutsch, 1996). In the case of direct anthropometry, measurements are taken directly from the subject (Farkas & Deutsch, 1996) and are restricted to linear distances, angles, and area calculations of the body surface (Linden et al., 2018) Measurements are taken using tools such as callipers, and take a considerable amount of time (Aung et al., 1995; Farkas & Deutsch, 1996; Heike et al., 2009). However, the direct measurements are reliable, inexpensive to conduct, and have a vast normative database for reference (Wong et al., 2008; Heike et al., 2009; Fourie et al., 2011). Indirect anthropometry on the other hand is further divided into three: photogrammetry, soft tissue facile-profile cephalometry, and computer-imaged 3D craniofacial surface scans (Farkas & Deutsch, 1996). In this case, images are obtained quickly and can be rotated and enlarged, and archived for later evaluation (Heike et al., 2009). The fact that image acquisition is rapid is especially handy when working with children because quantification of their facial features can be more challenging (Heike et al., 2009; Linden et al., 2018).

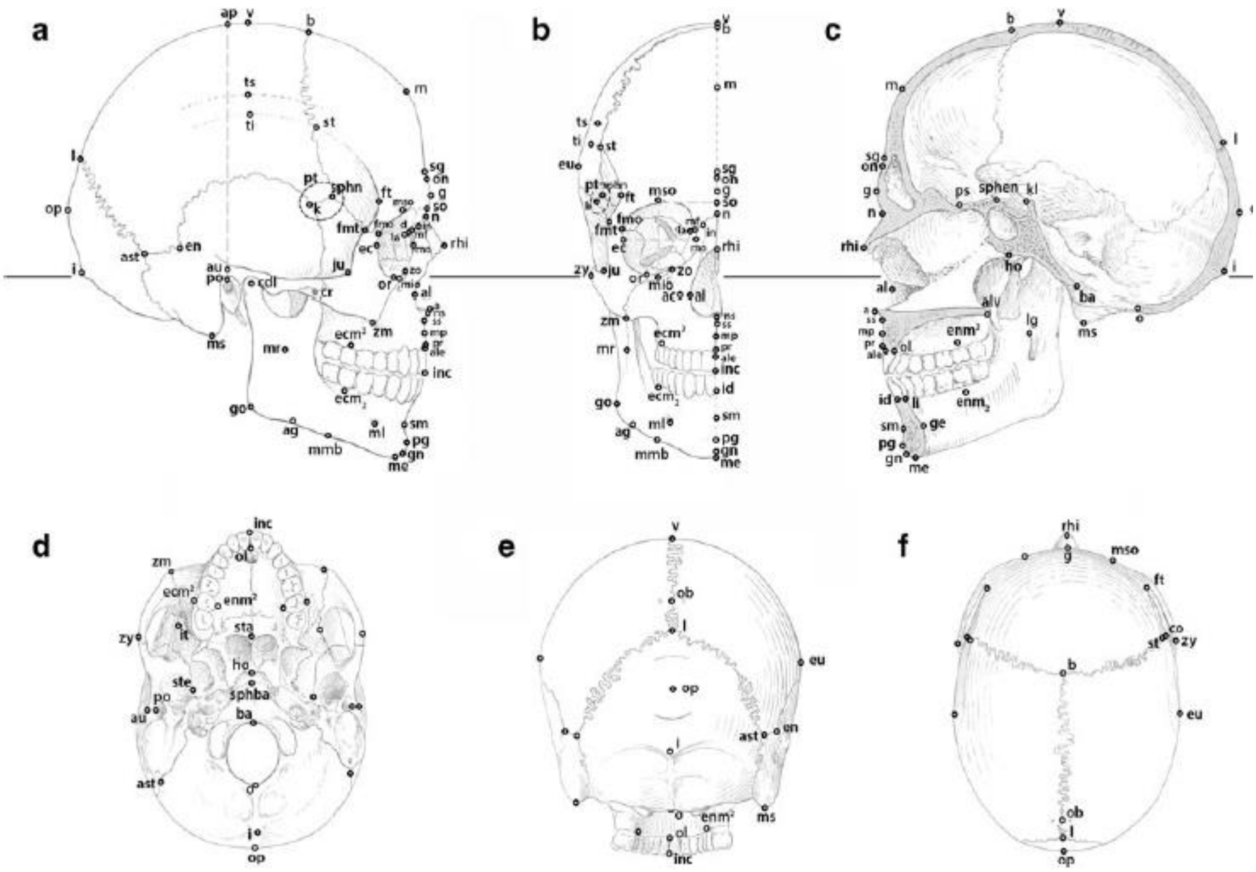

Figure 14. Craniometric landmarks for 3D analysis. a- Norma Lateralis; b- Norma Frontalis; c- Norma Medialis; d- Norma Basalis; e- Norma Occipitalis. Bold line indicates FH[3]. Definitions in Appendix 1 [Adapted from (Caple & Stephan, 2015)]

The most commonly used 3D systems used to obtain anthropometric measurements are photogrammetry and laser surface scanners. Aung et al. (1995) in their study compared the accuracy of a laser scanner against direct anthropometry and utilized 41 anthropometric landmarks, while Fourie et al. (2011) evaluated the anthropometric accuracy, reliability and repeatability of 3D scanning systems (laser surface scanner, cone beam computed tomography (CBCT) and 3D stereophotogrammetry) against direct measurements making use of 15 landmarks. In addition, Wong et al. (2008) compared the validity and reliability of 3D

[3] The Frankfort Horizontal Plane (FH)—an imaginary horizontal line passing through the inferior border of the orbit and the external auditory meatus on both sides of the skull, in an attempt to approximate the natural position of the head in life (Starbuck & Ward, 2007).

photogrammetry against direct measurements of 19 landmarks. For each of the three studies conducted, the conclusion was that the various 3D methods of measurement being tested were indeed precise, accurate and reliable, and hence could be used together with or in the place of direct measurement.

Table 7. A small sample of anthropometric landmarks and linear distances [Adapted from (Wong et al., 2008)]

Abbreviation	*Anthropometric Landmarks*	*Measurement*
en-en	endocanthion	intercanthal distance
ex-ex	exocanthion	biocular (lateral canthal) width
al-al	alare	nasal width
se-sn	sellion, subnasale	nasal height
sn-prn	subnasale, pronasale	nasal tip protrusion
sn-c′	subnasale, highest point of columella	columellar length
sn-ls	subnasale, labiale superius	cutaneous upper labial height
sn-sto	subnasale, stomion	overall upper labial height
cphs-cphs	crista philtri superior	upper prolabial width
cphi-cphi	crista philtri inferior	lower prolabial width
sn-cphi	subnasale, crista philtri inferior	midpoint of columella base to inferior point of philtral column
ac-cphi	alar curvature, crista philtri inferior	facial insertion of alar base to inferior point of philtral column
sbal-cphi	subalare, crista philtri inferior	labial insertion of alar base to inferior point of philtral column
cphi-ch	crista philtri inferior, chelion	inferior point of philtral column to labial fissure
cphi-ch′	crista philtri inferior, chelion′	inferior point of philtral column to the most lateral point of the vermilion cutaneous junction of the upper lip
cphs-cphi	crista philtri superior, crista philtri inferior	philtral length
t′-gn′	tragion′, gnathion′	lower facial depth (gn′ – surface)
t-gn	tragion, gnathion	lower facial depth (gn – bony)

New advances in 3D imaging are having a profound effect in the field of craniofacial anthropometry; however, for the new techniques to be of any applicable use they must be able to precisely and accurately quantify facial features as well as, if not better than, the present alternatives (Fourie et al., 2011). It is important to note, however, that all 3D methods must prove their reliability by being compared against direct measurements (Farkas & Deutsch, 1996).

Above all, the new methods must prove to be accurate, repeatable and have a known error rate in order to meet the minimum threshold of the Daubert criteria of admissibility of scientific evidence in courts of law.

Statistical Analysis

The primary aim of the researcher of this paper is to validate photogrammetry as a forensic science analytical method, and compare it to other methods of 3D image documentation. Among the ways of validating a method is to ensure it is reliable. Intrarclass correlation coefficient calculates reliability of a method (Heike et al., 2009; Fourie et al., 2011). It indicates high reliability when close to 1 and low reliability when close to 0 (Heike et al., 2009) and can be calculated based on a 2-way random analysis of variance (ANOVA) (Fourie et al., 2011). Additionally, intermethod reliability (comparing all the methods used in acquiring anthropometric measurements: direct, photogrammetry, CT) is approximated by calculating the Pearson correlation coefficients; values are between 0 and 1 with higher estimates implying a higher reliability (Heike et al., 2009).

The accuracy of the measurements is expressed using the absolute error (AE) and absolute percentage errors (APE). The absolute measuring error of each method measurement (radiological scanning, 3D photogrammetry) is obtained by the method measurement value (mean of the method measurement values) subtracted by the reference value (mean of the direct measurements). The absolute percentage error is then calculated using the equation: APE = 100 x (AME/reference value) (Fourie et al., 2011).

Validity defines how closely a method matches direct anthropometry measurements, and is defined by accuracy and bias. Accuracy- the agreement between direct measurements and other method measurements- is calculated using the Shapiro-Wilk W test for normality. Bias measures whether other methods have overestimated or underestimated direct values, and is evaluated by assessing the magnitude and direction of the difference between the direct and other methods, and evaluating their statistical significance. Correction factors between the direct measurement and other methods is established using linear regression analysis. Finally, test-retest reliability and precision can be applied in assessing the reproducibility of the methods being tested against the direct measurement method. Reproducibility refers to the consistency of values for repeated sets of measurements using other methods (Wong et al., 2008).

Additional statistics that will be calculated are the standard deviation of each method from the direct measurement, the 95% confidence interval (Heike et al., 2009; Fourie et al., 2011) and the technical error of the measurement, which according to Heike et al. (2009) can be interpreted similar to standard deviation.

EXPERIMENTAL DESIGN

Aims and Objectives

The main aim of this research is to compare the measurements of three human bone clone skull models obtained from 3D photogrammetry using a dedicated software (Agisoft Metashape) to the measurements of the same skulls obtained from CT scanning and using digital calipers, with the ultimate aim of validating photogrammetry as an accurate and reliable forensic anthropology measuring and documentation tool. In order to accomplish this, the following will be the objectives of the study:

i. To obtain accurate 3D reconstructions of all three skulls using Agisoft Metashape.
ii. To introduce interobserver data and error as practised by Garcia De Leon Valenzuela (2014). A total of four observers will be used, with two being "trained" (having background knowledge about the research) and two being "untrained" (having no knowledge whatsoever about the research).
iii. To produce more robust data on the skulls which can then be used to conduct statistical tests that will determine the accuracy and reliability of 3D photogrammetry. This will be achieved by utilizing 16 interlandmark distances (ILDs) around the skull.

Experimental Design

Photography

Overlapping photographs of the entire surface of each of the three skulls will be taken using a Samsung Galaxy S7 camera. The skulls will be elevated on a stand through the foramen magnum to facilitate photography of the entire surface, including the base of the skull.

Physical Measurements

A total of 16 ILDs will be used in the study. The measurements of these distances will be taken using a sliding caliper for the linear distances, and a spreading caliper for distances along curved surfaces such as the cranial length.

A set of distances (non-landmarks) will also be measured in order to set the scale in the photogrammetry software. All the distances (ILDs and calibration) will be measured in triplicate and then averaged to increase precision.

Photogrammetry

Photographs of each of the skulls will be imported into Agisoft Metashape and processed to produce 3D models of the skulls in a virtual space. Each skull will then be scaled/calibrated using the non-landmark distances measured from it; and then the same 16 ILD measurements taken using calipers will be measured from the 3D reconstruction. The measurements will be taken in triplicate and then averaged to increase precison.

CT Scan

All three skulls will be scanned using a CT to obtain their 3D images. The same 16 ILDs will then be measured from the scan images.

Statistics

The statistical tests that will be performed are intrarater, interrater and intermethod reliability. Intrarater reliability tests the accuracy and precision of an individual observer; interrater reliability tests accuracy and precision across the different observers; and intermethod reliability tests the accuracy and precision of one method against the other. These statistics range from 0 to 1, with values closer to 1 indicating a high reliability and values close to 0 indicating a low reliability. An analysis of variance (ANOVA) will also be conducted to test the hypothesis.

CONCLUSION

Forensic anthropologists have a huge role to play when it comes to the identification of osseous remains for which no identity is suspected, or when remains are severely decomposed or burned hence conventional methods such as DNA cannot be used. When establishing personal identification, the forensic anthropologist is required to work together with other experts such as forensic odontologists and pathologists in order to establish a positive identification.

3D imaging methods are used to create 3D models of objects in virtual space from 2D images such as photographs. The 3D models can then be examined further and manipulated in the virtual space in an attempt to reconstruct crime scenes and create a plausible sequence of events leading up to a crime or accident. Photogrammetry is simple, inexpensive, has fairly minor technical requirements and can create accurate 3D models with a single camera without reference points (Urbanová et al., 2015). Additionally it is a non-invasive non-contact method hence the object remains undisturbed, and the resultant 3D model is a permanent record that can be reassessed at any time long after the evidence has been lost. It important to remember, however, that photograph quality will affect the results; thus the higher the resolution of the camera, the better the results obtained. Despite the many advantages of photogrammetry such as being cost-effective, accurate and time-independent; it fails when a body surface is either covered with hair or is reflective due to moisture.

Radiological methods on the other hand give a clear image of the internal structures of the body whereas photogrammetry can only be used on the surface. They are however costly as compared to photogrammetric methods because they require specialized equipment and also require experts to interpret the images. On the other hand, photogrammetry is relatively cheap, and only needs a camera and software.

In anthropometry, there is no standard minimum number of landmarks that can be used to take measurements, it is left to the discretion of whoever is conducting the measurements. It is the opinion of the researcher of this paper however, that the landmarks should be chosen in such a manner that the whole face is well represented, where applicable.

REFERENCES

Agisoft LLC. (2019). *Agisoft Metashape User Manual: Professional Edition, Version 1.5*[PDF]. Retrieved from https://www.agisoft.com/

Anthropology Subcommittee. (2019). Retrieved from https://www.nist.gov/topics/forensic-science/anthropology-subcommittee

Aung, S., Ngim, R., & Lee, S. (1995). Evaluation of the laser scanner as a surface measuring tool and its accuracy compared with direct facial anthropometric measurements. *British Journal Of Plastic Surgery*, *48*(8), 551-558. doi: 10.1016/0007-1226(95)90043-8

Blau, S., & Briggs, C. (2011). The role of forensic anthropology in Disaster Victim Identification (DVI). *Forensic Science International*, *205*(1-3), 29-35. doi: 10.1016/j.forsciint.2010.07.038

Bongiovanni, R., & LeGarde, C. (2017). A Univariate Approach to Sex Estimation for the Fragmentary Upper Limb. *Journal Of Forensic Sciences*, *63*(2), 356-360. doi: 10.1111/1556-4029.13530

Boyd, C., & Boyd, D. (2018). *Forensic Anthropology: Theoretical Framework and Scientific Basis* (pp. 99-107). John Wiley & Sons.

Brooks, S., & Suchey, J. (1990). Skeletal age determination based on the os pubis: A comparison of the Acsádi-Nemeskéri and Suchey-Brooks methods. *Human Evolution*, *5*(3), 227-238. doi: 10.1007/bf02437238

Brüschweiler, W., Braun, M., Dirnhofer, R., & Thali, M. (2003). Analysis of patterned injuries and injury-causing instruments with forensic 3D/CAD supported photogrammetry (FPHG): an instruction manual for the documentation process. *Forensic Science International*, *132*(2), 130-138. doi: 10.1016/s0379-0738(03)00006-9

Buck, U., Buße, K., Campana, L., & Schyma, C. (2017). Validation and evaluation of measuring methods for the 3D documentation of external injuries in the field of forensic medicine. *International Journal Of Legal Medicine*, *132*(2), 551-561. doi: 10.1007/s00414-017-1756-6

Buzug, T. M. (2007). *Facial reconstruction : forensic, medical and archeological methods of the reconstruction of soft facial parts = Gesichtsrekonstruktion : forensische, medizinische und archäologische Methoden der Gesichtsweichteilrekonstruktion.* München: Luchterhand.

Caple, J., & Stephan, C. (2015). A standardized nomenclature for craniofacial and facial anthropometry. *International Journal Of Legal Medicine*, *130*(3), 863-879. doi: 10.1007/s00414-015-1292-1

Cardoso, H., Marinho, L., & Albanese, J. (2016). The relationship between cadaver, living and forensic stature: A review of current knowledge and a test using a sample of adult Portuguese males. *Forensic Science International*, *258*, 55-63. doi: 10.1016/j.forsciint.2015.10.012

Cattaneo, C. (2007). Forensic anthropology: developments of a classical discipline in the new millennium. *Forensic Science International*, *165*(2-3), 185-193. doi: 10.1016/j.forsciint.2006.05.018

Christensen, A. (2005). Testing the Reliability of Frontal Sinuses in Positive Identification. *Journal Of Forensic Sciences*, *50*(1), 1-5. doi: 10.1520/jfs2004145

Ciaffi, R., Gibelli, D., & Cattaneo, C. (2011). Forensic radiology and personal identification of unidentified bodies: a review. *La Radiologia Medica*, *116*(6), 960-968. doi: 10.1007/s11547-011-0677-6

Colwill, S. (2016). *Low-Cost Crime Scene Mapping: Reviewing Emerging Freeware, Low-Cost Methods of 3D Mapping and Applying Them to Crime Scene Investigation and Forensic Evidence* (Masters). Murdoch University.

Daubert v. Merrell Dow Pharmaceuticals, US Supreme Court 509. U.S.579. (1993). 113S.Ct.2786, 125L, Ed.2d 469

Davy, S.L., Gilbert, T., Schofield, D. and Evison, M.P. (2005). Forensic facial reconstruction using computer modelling software. In Clement, J.G. and Marks, M.K. (Eds.), *Computer-Graphic Facial Reconstruction,* New York: Elsevier Academic Press, pp 183-196.

Dereli, A., Zeybek, V., Sagtas, E., Senol, H., Ozgul, H., & Acar, K. (2018). Sex determination with morphological characteristics of the skull by using 3D modeling techniques in computerized tomography. *Forensic Science, Medicine And Pathology*, *14*(4), 450-459. doi: 10.1007/s12024-018-0029-0

Dindaroğlu, F., Kutlu, P., Duran, G., Görgülü, S., & Aslan, E. (2016). Accuracy and reliability of 3D stereophotogrammetry: A comparison to direct anthropometry and 2D photogrammetry. *The Angle Orthodontist*, *86*(3), 487-494. doi: 10.2319/041415-244.1

Dirkmaat, D. (2012). *A companion to forensic anthropology* (pp. 197-330, 432-446). Malden, MA: Wiley-Blackwell.

Dirkmaat, D., Cabo, L., Ousley, S., & Symes, S. (2008). New perspectives in forensic anthropology. *American Journal Of Physical Anthropology*, *137*(S47), 33-52. doi: 10.1002/ajpa.20948

Duke, E., & Aguirre, S. (2010). *3D imaging: Theory, Technology and Applications*. New York: Nova Science Publishers.

Dwight, T. (1878). *The Identification of the Human Skeleton. A medico-legal study: To which was awarded the prize of the Massachusetts Medical Society for 1878*. Boston: D. Clapp.

Edelman, G., & Aalders, M. (2018). Photogrammetry using visible, infrared, hyperspectral and thermal imaging of crime scenes. *Forensic Science International*, *292*, 181-189. doi: 10.1016/j.forsciint.2018.09.025

Elliott, M., & Collard, M. (2009). F ordisc and the determination of ancestry from cranial measurements. *Biology Letters*, *5*(6), 849-852. doi: 10.1098/rsbl.2009.0462

Farkas, L., & Deutsch, C. (1996). Anthropometric determination of craniofacial morphology. *American Journal Of Medical Genetics*, *65*(1), 1-4. doi: 10.1002/ajmg.1320650102

Fenton, T., Heard, A., & Sauer, N. (2008). Skull-Photo Superimposition and Border Deaths: Identification Through Exclusion and the Failure to Exclude. *Journal Of Forensic Sciences*, *53*(1), 34-40. doi: 10.1111/j.1556-4029.2007.00624.x

Fourie, Z., Damstra, J., Gerrits, P., & Ren, Y. (2011). Evaluation of anthropometric accuracy and reliability using different three-dimensional scanning systems. *Forensic Science International*, *207*(1-3), 127-134. doi: 10.1016/j.forsciint.2010.09.018

Gill, G. W. (1998). Craniofacial criteria in the skeletal attribution of race. *Forensic osteology: Advances in the identification of human remains*, 293-317.

Greef, S., & Willems, G. (2005). Three-dimensional Cranio-Facial Reconstruction in Forensic Identification:Latest Progress and New Tendencies in the 21st Century. *Journal Of Forensic Sciences*, *50*(1), 1-5. doi: 10.1520/jfs2004117

Gupta, S. (2015). Forensic Facial Reconstruction: The Final Frontier. *Journal Of Clinical And Diagnostic Research*. doi: 10.7860/jcdr/2015/14621.6568

Haglund, W. D., & Reay, D. T. (1991). Use of facial approximation techniques in identification of Green River serial murder victims. *The American journal of forensic medicine and pathology*, *12*(2), 132-142.

Harris, H., & Lee, H. (2019). Introduction to Forensic Science and Criminalistics, Second Edition. Milton: Chapman & Hall/CRC Press.

Hefner, J. (2003). *Assessing Nonmetric Cranial Traits Currently Used in the Forensic Determination of Ancestry* (Masters). University of Florida.

Hefner, J. (2009). Cranial Nonmetric Variation and Estimating Ancestry. *Journal Of Forensic Sciences*, *54*(5), 985-995. doi: 10.1111/j.1556-4029.2009.01118.x

Heike, C., Cunningham, M., Hing, A., Stuhaug, E., & Starr, J. (2009). Picture Perfect? Reliability of Craniofacial Anthropometry Using Three-Dimensional Digital Stereophotogrammetry. *Plastic And Reconstructive Surgery*, *124*(4), 1261-1272. doi: 10.1097/prs.0b013e3181b454bd

Hinchliffe, J. (2011). Forensic odontology, part 1. Dental identification. *British Dental Journal*, *210*(5), 219-224. doi: 10.1038/sj.bdj.2011.146 https://trace.tennessee.edu/utk_graddiss/4490

İşcan, M. (2001). Global forensic anthropology in the 21st century. *Forensic Science International*, *117*(1-2), 1-6. doi: 10.1016/s0379-0738(00)00433-3

İşcan, M., Loth, S., & Wright, R. (1984). Metamorphosis at the sternal rib end: A new method to estimate age at death in white males. *American Journal Of Physical Anthropology*, *65*(2), 147-156. doi: 10.1002/ajpa.1330650206

Kahana, T., & Hiss, J. (1997). Identification of human remains: forensic radiology. *Journal Of Clinical Forensic Medicine*, *4*(1), 7-15. doi: 10.1016/s1353-1131(97)90002-x

Kähler, K., Haber, J., & Seidel, H. (2003). Reanimating the dead. *ACM SIGGRAPH 2003 Papers On - SIGGRAPH '03*. doi: 10.1145/1201775.882307

Kewal Krishan, T. (2013). Personal Identification in Forensic Examinations. *Anthropology*, *02*(01). doi: 10.4172/2332-0915.1000114

Klales, A., & Kenyhercz, M. (2014). Morphological Assessment of Ancestry using Cranial Macromorphoscopics,. *Journal Of Forensic Sciences*, *60*(1), 13-20. doi: 10.1111/1556-4029.12563

Koller, S., Ebert, L., Martinez, R., & Sieberth, T. (2019). Using virtual reality for forensic examinations of injuries. *Forensic Science International*, *295*, 30-35. doi: 10.1016/j.forsciint.2018.11.006

Kottner, S., Schaerli, S., Fürst, M., Ptacek, W., Thali, M., & Gascho, D. (2019). VirtoScan-on-Rails – an automated 3D imaging system for fast post-mortem whole-body surface documentation at autopsy tables. *Forensic Science, Medicine And Pathology*, *15*(2), 198-212. doi: 10.1007/s12024-019-00095-5

Linden, O., Baratta, V., Gonzalez, J., Byrne, M., Klinge, P., Sullivan, S., & Taylor, H. (2018). Surgical Correction of Metopic Craniosynostosis: A 3-D Photogrammetric Analysis of Cranial Vault Outcomes. *The Cleft Palate-Craniofacial Journal*, *56*(2), 231-235. doi: 10.1177/1055665618775729

Lovejoy, C., Meindl, R., Pryzbeck, T., & Mensforth, R. (1985). Chronological metamorphosis of the auricular surface of the ilium: A new method for the determination of adult skeletal age at death. *American Journal Of Physical Anthropology*, *68*(1), 15-28. doi: 10.1002/ajpa.1330680103

Luhmann, T., Robson, S., Kyle, S., & Boehm, J. (2013). *Close-Range Photogrammetry and 3D Imaging* (2nd ed., pp. 1-27, 619-621). De Gruyter, Inc.

Meindl, R., & Lovejoy, C. (1985). Ectocranial suture closure: A revised method for the determination of skeletal age at death based on the lateral-anterior sutures. *American Journal Of Physical Anthropology*, *68*(1), 57-66. doi: 10.1002/ajpa.1330680106

MMS Software – Macromorphoscopic Data. Retrieved from http://macromorphoscopic.com/mms-software/

Nikam, S. S., Gadgil, R. M., Bhoosreddy, A. R., Shah, K. R., & Shirsekar, V. U. (2015). Personal Identification in Forensic Science Using Uniqueness of Radiographic Image of Frontal Sinus. *The Journal of forensic odonto-stomatology*, *33*(1), 1–7.

Osman, M., & Tahar, K. (2016). 3D accident reconstruction using low-cost imaging technique. *Advances In Engineering Software*, *100*, 231-237. doi: 10.1016/j.advengsoft.2016.07.007

Özaslan, A., İşcan, M., Özaslan, İ., Tuğcu, H., & Koç, S. (2003). Estimation of stature from body parts. *Forensic Science International*, *132*(1), 40-45. doi: 10.1016/s0379-0738(02)00425-5

Parsons, H. (2017). *The accuracy of the biological profile in casework: an analysis of forensic anthropology reports in three medical examiners' offices* (PhD). The University of Tennessee.

Pexa, T., Krajsa, J., Šaňková, M., Velemínský, P., Havrda, J., Kotrlý, T., & Drábek, J. (2018). Identification of the skeletal remains of the Czech communist regime crime victim, priest Josef Toufar. *Forensic Science International*, *291*, e13-e17. doi: 10.1016/j.forsciint.2018.07.002

Phenice, T. (1969). A newly developed visual method of sexing the os pubis. *American Journal Of Physical Anthropology*, *30*(2), 297-301. doi: 10.1002/ajpa.1330300214

Pilloud, M., Hefner, J., Hanihara, T., & Hayashi, A. (2014). The Use of Tooth Crown Measurements in the Assessment of Ancestry. *Journal Of Forensic Sciences*, *59*(6), 1493-1501. doi: 10.1111/1556-4029.12540

Pretty, I. (2007). Forensic Dentistry: 1. Identification of Human Remains. *Dental Update*, *34*(10), 621-634. doi: 10.12968/denu.2007.34.10.621

Priya, E. (2017). Methods of Skeletal Age Estimation used by Forensic Anthropologists in Adults: A Review. *Foresic Research & Criminology International Journal*, *4*(2). doi: 10.15406/frcij.2017.04.00104

Randolph-Quinney, P.S., Mallett, X. and Black, S.M. (2009). Forensic Anthropology. In A. Jamieson and A. Moenssens (eds.) *Wiley Encylopedia of Forensic Science*. London: John Wiley and Son Ltd. pp 1-27.

Rawlani, S., Rawlani, S., Bhowate, R., Chandak, R., & Khubchandani, M. (2017). Racial characteristics of human teeth. *International Journal Of Forensic Odontology*, *2*(1), 38. doi: 10.4103/ijfo.ijfo_21_16

Rogers, T. (1999). A Visual Method of Determining the Sex of Skeletal Remains Using the Distal Humerus. *Journal Of Forensic Sciences*, *44*(1), 14411J. doi: 10.1520/jfs14411j

Rogers, T., & Allard, T. (2004). Expert Testimony and Positive Identification of Human Remains Through Cranial Suture Patterns. *Journal Of Forensic Sciences*, *49*(2), 1-5. doi: 10.1520/jfs2003095

Rutty, G., Morgan, B., O'Donnell, C., Leth, P., & Thali, M. (2008). Letters to the Editor. *The Journal Of Trauma: Injury, Infection, And Critical Care*, *65*(2), 493-494. doi: 10.1097/ta.0b013e31817de420

Rybak, L. D., & Rosenthal, D. I. (2001). Radiological imaging for the diagnosis of bone metastases. *QJ Nucl Med*, *45*(1), 53-64.

Santoro, V., Lubelli, S., De Donno, A., Inchingolo, A., Lavecchia, F., & Introna, F. (2017). Photogrammetric 3D skull/photo superimposition: A pilot study. *Forensic Science International*, *273*, 168-174. doi: 10.1016/j.forsciint.2017.02.006

Sauer, N., Michael, A., & Fenton, T. (2012). Human Identification Using Skull-Photo Superimposition and Forensic Image Comparison. *A Companion To Forensic Anthropology*, 432-446. doi: 10.1002/9781118255377.ch21

Schmitt, A., Cunha, E. and Pinheiro, J. (2010). *Forensic anthropology and medicine*. Totowa, NJ: Humana Press, pp.39-69, 225-332, 359-379.

Sholts, S., Walker, P., Kuzminsky, S., Miller, K., & Wärmländer, S. (2011). Identification of Group Affinity from Cross-sectional Contours of the Human Midfacial Skeleton Using Digital Morphometrics and 3D Laser Scanning Technology*,‡. *Journal Of Forensic Sciences*, *56*(2), 333-338. doi: 10.1111/j.1556-4029.2011.01701.x

Sierp, I., & Henneberg, M. (2015). Can ancestry be consistently determined from the skeleton?. *Anthropological Review*, *78*(1), 21-31. doi: 10.1515/anre-2015-0002

Smith, D., Limbird, K., & Hoffman, J. (2002). Identification of Human Skeletal Remains by Comparison of Bony Details of the Cranium Using Computerized Tomographic (CT) Scans. *Journal Of Forensic Sciences*, *47*(5), 15499J. doi: 10.1520/jfs15499j

Snodgrass, J. (2004). Sex Differences and Aging of the Vertebral Column. *Journal Of Forensic Sciences*, *49*(3), 1-6. doi: 10.1520/jfs2003198

Snow, C. (1982). Forensic Anthropology. Annual Review Of Anthropology, 11(1), 97-131. doi:10.1146/annurev.an.11.100182.000525

Starbuck, J., & Ward, R. (2007). The affect of tissue depth variation on craniofacial reconstructions. *Forensic Science International*, *172*(2-3), 130-136. doi: 10.1016/j.forsciint.2007.01.006

Stavrianos, C., Stavrianou, I., Zouloumis, L., & Mastagas, D. (2007). An introduction to facial reconstruction. *Balkan Journal of Stomatology*, *11*(2), 76-83.

Stephan, C. (2006). Beyond the Sphere of the English Facial Approximation Literature: Ramifications of German Papers on Western Method Concepts*. *Journal Of Forensic Sciences*, *51*(4), 736-739. doi: 10.1111/j.1556-4029.2006.00175.x

Stewart, T. (1979). *Essentials of forensic anthropology, especially as developed in the United States*. Springfield, Ill.: Thomas.

Taylor, J. (2009). *Development of the Disaster Victim Identification Forensic Odontology Guide for the Australian Society of Forensic Odontology* (Ph.D). The University of Newcastle, Australia.

Tersigni-Tarrant, M., & Shirley, N. (2013). *Forensic anthropology: An Introduction*. Boca Raton, FL: CRC Press LLC.

Thali, M., Braun, M., Brueschweiler, W., & Dirnhofer, R. (2003a). 'Morphological imprint': determination of the injury-causing weapon from the wound morphology using forensic 3D/CAD-supported photogrammetry. *Forensic Science International*, *132*(3), 177-181. doi: 10.1016/s0379-0738(03)00021-5

Thali, M., Braun, M., Kneubuehl, B., Brueschweiler, W., Vock, P., & Dirnhofer, R. (2000). Improved Vision in Forensic Documentation: Forensic 3D/CAD-supported Photogrammetry of bodily injury external surfaces combined with Volumetric Radiologic Scanning of bodily injury internal structures provides more investigative leads and stronger forensic evidence. *28Th AIPR Workshop: 3D Visualization For Data Exploration And Decision Making*. doi: 10.1117/12.384876

Thali, M., Braun, M., Markwalder, T., Brueschweiler, W., Zollinger, U., & Malik, N. et al. (2003b). Bite mark documentation and analysis: the forensic 3D/CAD supported photogrammetry approach. *Forensic Science International*, *135*(2), 115-121. doi: 10.1016/s0379-0738(03)00205-6

Todd, T. (1920). Age changes in the pubic bone. I. The male white pubis. *American Journal Of Physical Anthropology*, *3*(3), 285-334. doi: 10.1002/ajpa.1330030301

Torimitsu, S., Makino, Y., Saitoh, H., Ishii, N., Yajima, D., & Inokuchi, G. et al. (2017). Determination of sex on the basis of hyoid bone measurements in a Japanese population using multidetector computed tomography. *International Journal Of Legal Medicine*, *132*(3), 907-914. doi: 10.1007/s00414-017-1728-x

Ubelaker, D., Shamlou, A., & Kunkle, A. (2018). Contributions of forensic anthropology to positive scientific identification: a critical Review. *Forensic Sciences Research*, *4*(1), 45-50. doi: 10.1080/20961790.2018.1523704

Urbanová, P., Hejna, P., & Jurda, M. (2015). Testing photogrammetry-based techniques for three-dimensional surface documentation in forensic pathology. *Forensic Science International*, *250*, 77-86. doi: 10.1016/j.forsciint.2015.03.005

Vallis, J. (2017). The Role of Radiography in Disaster Victim Identification. In T. Thompson & D. Errickson, *Human Remains - Another Dimension: The Application of 3D Imaging in the Funerary Context*. Elsevier Science & Technology.

Vandermeulen, D., Claes, P., De Greef, S., Willems, G., Clement, J., & Suetens, P. (2012). Automated facial reconstruction. *Craniofacial Identification*, 203-221. doi: 10.1017/cbo9781139049566.017

Vanezis, M. (2008). *Forensic facial reconstruction using 3-D computer graphics: evaluation and improvement of its reliability in identification* (Ph.D). University of Glasgow.

Villa, C. (2016). Forensic 3D documentation of skin injuries. *International Journal Of Legal Medicine*, *131*(3), 751-759. doi: 10.1007/s00414-016-1499-9

Wheat, A. (2009). *Assessing ancestry through nonmetric traits of the skull: a test of education and experience* (Masters). Texas State University.

Wong, J., Oh, A., Ohta, E., Hunt, A., Rogers, G., Mulliken, J., & Deutsch, C. (2008). Validity and Reliability of Craniofacial Anthropometric Measurement of 3D Digital Photogrammetric Images. *The Cleft Palate-Craniofacial Journal*, *45*(3), 232-239. doi: 10.1597/06-175

Yaacob, H., Narnbiar, P., & Naidu, M. D. (1996). Racial characteristics of human teeth with special emphasis on the Mongoloid dentition. *Malaysian Journal of Pathology*, *18*(1), 1-7.

APPENDICES

Appendix 1

Craniometric landmarks including their abbreviations, definitions, and various classifications [Adapted from (Caple & Stephan, 2015)]

Landmark	3D Notation	Definition	Bookstein type
Median points			
Alveolare[a]	ale	Median point at the inferior tip of the bony septum between the upper central incisors. Equivalent to Infradentale superius	II
Alveolon	alv	Median point, at the rear of the hard palate, of a line joining the posterior most alveolar margins	II
Acanthion[b]	a	Most anterior tip of the anterior nasal spine	II
Apex[a]	ap	Instrumentally determined median point on the superior surface of the cranial vault at the coronal plane connecting left and right *po*	III
Basion	ba	Basion encompasses a small region, on the median plane at the anterior most extent of the foramen magnum. Its position as a landmark varies slightly depending on the measurement being taken. It can be the most posterior aspect of the foramen magnum's anterior rim or the most inferior median point on the foramen magnum's anterior rim (such as used for taking cranial height measurements)	II
Bregma	b	Where the sagittal and coronal sutures meet. Impossible to determine in juvenile skulls with anterior fontanelle, or with complete suture obliteration	I
Genion	ge	Most projecting tip of the internal mental spine on the lingual surface of the mandible	II
Glabella	g	Most projecting anterior median point on lower edge of the frontal bone, on the brow ridge, in between the superciliary arches and above the nasal root. In adults, glabella usually represents the most anterior point of the frontal bone	II
Gnathion[c]	gn	Median point halfway between *pg* and *me*	III
Hormion	ho	Median point where the vomer and sphenoid bones meet	I
Incision[a]	inc	Point at the occlusal surface where the upper central incisors meet	II
Infradentale[d]	id	Median point at the superior tip of the septum between the mandibular central incisors	II
Inion	i	Median point between the apices of the superior nuchal lines and at the base of the external occipital protuberance (not the tip of the protuberance)	II
Klition	kl	Median endocranial point at the center of the highest extent of the posterior margin of the sella turcica	II
Lamda	l	Point at which the two legs of the lambdoid suture and sagittal suture meet (project from the main direction of the sutures in cases of obliteration or presence of wormian bones)	I
Linguale	li	Median most superior point of the mandibular symphysis, on the lingual surface	II
Menton[c]	me	Most inferior median point of the mental symphysis (may not be the inferior point on the mandible as the chin is often clefted on the inferior margin)	III
Metopion[a]	m	Median point, instrumentally determined on the frontal bone as the greatest elevation from a cord between *n* and *b*. In juveniles, the *m*, rather than the *g*, may be the most anterior point of the frontal bone.	III
Mid-philtrum[e]	mp	Median point midway between *ss* and *pr*	II
Nasion	n	Intersection of the nasofrontal sutures in the median plane	I
Nasospinale	ns	The point where a line drawn between the inferior most points of the nasal aperture crosses the median plane. Note that this point is not necessarily at the tip of the nasal spine	II
Obelion	ob	Median point where the sagittal suture intersects with a transverse line connecting parietal foramina	II
Ophryon	on	Median point that intersects the smallest frontal bone chord width	II
Opisthion	o	Median point on the anterior side of the foramen magnum's posterior rim	II
Opisthocranion	op	Most posterior median point of the occipital bone, instrumentally determined as the greatest chord length from *g*. Usually above the external occipital protuberance	III
Orale	ol	Median most inferior point of the maxillary symphysis, on the lingual surface	II
Pogonion	pg	Most anterior median point on the mental eminence of the mandible	III

Landmark	3D Notation	Definition	Bookstein type
Prosphenion	ps	Median endocranial point, at the center of the sphenoethmoidal suture	I
Prosthion	pr	Median point between the central incisors on the anterior most margin of the maxillary alveolar rim	II
Rhinion	rhi	Most rostral (end) point on the internasal suture. Cannot be determined accurately if nasal bones are broken distally	I
Sphenobasion	sphba	Median point at the spheno-occipital synchondrosis	I
Sphenoidale	sphen	Median endocranial point on the anterior clinoid process, marking the anterior margin of the sella turcica	I
Staphylion	sta	Median point of a line drawn between the anterior most apices of the posterior notches (free edges) of the horizontal plates of the palatine bones	I
Subspinale[b]	ss	The deepest point seen in the profile view below the anterior nasal spine (orthodontic point A)	II
Supraglabellare	sg	Deepest part of the supraglabella fossa in the median plane (cannot be determined in skulls without a supraglabella fossa)	II
Supramentale[f]	sm	Deepest median point in the groove superior to the mental eminence (orthodontic point B)	II
Supraorbitale	so	Median point at the height of the line joining the most superior points of the left and right superior orbital rims	II
Vertex	v	Most superior point of the skull	III
Bilateral Points			
Alare[d]	al	Instrumentally determined as the most lateral point on the nasal aperture in a transverse plane	III
Alar curvature point[g]	ac	Hard tissue approximation of soft tissue *ac*, approximately 5 mm lateral to *al*	II
Antegonion[h]	ag	Apex of the antegonial notch	II
Asterion	ast	Where the lambdoidal, parietomastoid, and occipitomastoid suture meet	I
Auriculare	au	On the zygomatic root, vertically above the center of the external auditory meatus	II
Condylion laterale	cdl	Most lateral point on the mandibular condyle	III
Condylion mediale	cdm	Most medial point on the mandibular condyle	III
Coronale	co	Most lateral point on the coronal suture	III
Coronion	cr	The tip of the coronoid process of the mandible	II
Dacryon[d]	d	The point on the medial border of the orbit where the lacrimomaxillary suture meets the frontal bone. There is often a small foramen at this point	I
Ectoconchion	ec	Lateral point on the orbit at a line that bisects the orbit transversely	II
Ectomolare[g]	ecm	Most lateral point on the buccal alveolar margin, at the center of the second molar position. Superscript number designates the maxillary landmark; subscript number designates the mandibular landmark	III
Endomolare[g]	enm	Most lateral point on the lingual alveolar margin, at the center of the second molar position. Superscript number designates the maxillary landmark; subscript number designates the mandibular landmark	III
Entomion	en	Where the squamous and parietomastoid sutures meet	I
Euryon	eu	Instrumentally determined as the most lateral point of the cranial vault, on the parietal bone	III
Frontomalare orbitale	fmo	Point on the orbital rim marked by the zygomaticofrontal suture	II
Frontomalare temporale	fmt	Most lateral part of the zygomaticofrontal suture	III
Frontotemporale	ft	Most anterior and medial point of the inferior temporal line, on the zygomatic process of the frontal bone	II
Gonion	go	Point on the rounded margin of the angle of the mandible, bisecting two lines one following vertical margin of ramus and one following horizontal margin of corpus of mandible	II

Landmark	3D Notation	Definition	Bookstein type
Infranasion	in	Intersection of the maxillonasal and nasofrontal sutures	I
Infratemporale	it	Most medial point on the infratemporal crest of sphenoid	II
Jugale	ju	Vertex of the posterior zygomatic angle, between the vertical edge and horizontal part of the zygomatic arch	II
Krotaphion	k	Posterior end of sphenoparietalis suture, where it meets the squamosal part of the temporal bone	I
Lacrimale[a]	la	Intersection of the posterior lacrimal crest with the frontolacrimal suture	I
Lingulare	lg	Superior most point of the lingula of the mandible	II
Mastoidale	ms	The inferior most projecting point of the tip of the mastoid process	II
Maxillofrontale	mf	Intersection of the anterior lacrimal crest with the frontomaxillary suture	I
Medial orbit[g]	mo	Point on the anterior lacrimal crest at the same level as ectoconchion	II
Mentale	ml	Most inferior point on the margin of the mandibular mental foramen	II
Mid-infraorbital[e]	mio	Point on the anterior aspect of the inferior orbital rim, at a line that vertically bisects the orbit	II
Mid-mandibular border[e]	mmb	Point on the inferior border of the corpus of the mandible midway between *pg* and *go*	II
Mid-ramus[e]	mr	Midpoint along the shortest antero-posterior depth of the ramus, in the masseteric fossa, and usually close to the level of the occlusal plane	III
Mid-supraorbital[e]	mso	Point on the anterior aspect of the superior orbital rim, at a line that vertically bisects the orbit	II
Orbitale	or	Most inferior point on the inferior orbital rim. Usually falls along the lateral half of the orbital margin	II
Porion	po	Most superior point on the upper margin of the external auditory meatus	II
Pterion	pt	A circular region, marked by the sphenoparietalis suture at its center. This region marks the thinnest part of the cranial vault	I
Sphenion	sphn	Anterior end of the sphenoparietalis suture, where it meets the frontal bone	I
Stenion	ste	Most medial point on the spheno-squamosal suture (near foramen ovale)	II
Stephanion	st	The point at which the inferior temporal line crosses the coronal suture	I
Temporale inferius[g]	ti	Most superior point on the arc of the inferior temporal line	III
Temporale superius[g]	ts	Most superior point on the arc of the superior temporal line	III
Zygion	zy	Instrumentally determined as the most lateral point on the zygomatic arch	III
Zygomaxillare	zm	Most inferior point on the zygomaticomaxillary suture	III
Zygoorbitale[b]	zo	Intersection of the orbital margin and the zygomaticomaxillary suture	II

Landmarks are positioned assuming the FH position. Definitions are sourced from Martin [25, 27] unless otherwise noted

[a] after White [78]

[b] after Howells [15, 31]

[c] after Krogman & Sassouni [30]

[d] after Buikstra and Ubelaker [32]

[e] after Stephan and Simpson [72]

[f] after Phulari [56] and George [62]

[g] defined by the authors

[h] after Legrell et al. [85] and Stephan [86]

Part Two

MANUSCRIPT

VIRTUAL ANTHROPOLOGY? RELIABILITY OF THREE-DIMENSIONAL PHOTOGRAMMETRY AS A FORENSIC ANTHROPOLOGY MEASUREMENT AND DOCUMENTATION TECHNIQUE

Virtual Anthropology? Reliability of Three-Dimensional Photogrammetry as a Forensic Anthropology Measurement and Documentation Technique

Rita Omari[1], Cahill Hunt, John Coumbaros[1,2], Brendan Chapman[1]

[1] Murdoch University, Murdoch University Forensic Science, Perth, WA.
[2] Forensic Science Laboratory, ChemCentre, Perth, WA.

ABSTRACT

The skull is perhaps the most utilized part of the skeleton by forensic anthropologists to draw up information about a set of remains. By taking different measurements from it and visually analysing it, an anthropologist can come up with a vast amount of information such as the sex and age of the individual to whom the remains belong [1,2]. Traditionally, measurements were taken using tools such as calipers. However, with advancement of technology, there has been a slow but gradual shift from traditional direct methods of measurement to indirect measurement methods such three-dimensional (3D) imaging, which includes computed tomography (CT) scanning and 3D photogrammetry. Although CT scanning is more widely used and preferred, photogrammetry has also found application in a wide gamut of fields such as architecture, geographical mapping and road accident reconstruction. However, the application of modern-day photogrammetry for forensic anthropology purposes has not been discussed extensively. As such, this paper aims to compare (and hence validate) 3D photogrammetry against CT scanning and physical measurements using a caliper.

Intrarater, interrater and intermethod reliability tests were conducted on the data obtained from the three methods; and these tests have a range of 0-1 with values closer to 1 indicating a high reliability. An analysis of variance (ANOVA) was also conducted. The results of the intrarater, interrater and intermethod reliability tests were correlation coefficient values of greater than or equal to 0.98616228 across the three tests for all three measurement methods. This implies that each observer was precise and accurate in their measurements when compared against the other observers; and that photogrammetry is indeed reliable and accurate to 98% when compared against CT scanning and physical measurements. P-values of greater than 0.05 were from the ANOVA conducted between all the data sets except one, hence favouring the rejection of the acceptance of the stated hypothesis and the rejection of the null hypothesis.

Key Words:

Photogrammetry, skull, interlandmark distances, CT scan, 3D reconstruction, measurement

LIST OF FIGURES

LIST OF TABLES

LIST OF ABBREVIATIONS

ILD	Interlandmark distance
2D	Two-dimensional
3D	Three-dimensional
MPR	Multiplanar reconstruction
CT	Computed tomography
CM	Caucasian male
AAF	African American female
AM	Asian male
ANOVA	Analysis of variance

INTRODUCTION

Establishing the identity of unknown remains is a vital role of forensic science, and when conventional methods such as DNA analysis fail due to extensive decomposition or presence of only skeletonized remains [3,4], a forensic anthropologist will be called upon to aid in the identification. The skull is perhaps the part of the skeleton that most utilized in the endeavour to establish the identity of osseous remains: it can be used in building the biological profile such as classification of ancestry [5,6]; sex determination [1,2]; age estimation [1,2,7,8]; and calculation of stature [2]. It can also be used during the efforts by the anthropologist to establish a positive identification of the remains through comparative radiography [7,9], and skull-photo/craniofacial superimposition [4].

Craniofacial anthropometry refers to the quantification of facial characteristics [10], and this quantification can be done by directly taking measurements from the subject using tools such as calipers [10,11,12]. The measurements are restricted to liner distances, angles, and area calculations of the body surface; and they take a considerable amount of time. However, direct measurements are reliable, inexpensive to conduct, and have a vast normative database for reference [10,13,14,15].

Digital technologies have been developed that can supplement and often replace direct craniofacial anthropometric measurements [10]. These indirect anthropometry methods can be divided into three: photogrammetry, soft tissue facile-profile cephalometry, and computer-imaged 3D craniofacial surface scans [12]. With indirect anthropometry, images are obtained quickly and can be rotated and enlarged, and archived for later evaluation [10]. Additionally, the method is non-invasive; and this is especially valuable when the remains are fragile because they can be studied without damaging the original sample [16].

For the purposes of this study, only 3-dimensional (3D) photogrammetry and computed tomography (CT) scanning were used.

CT scanning has always been preferred for clear high-resolution images, and modern CTs have, on top of improving the quality of image acquisition, advanced so that they operate faster [17]. On the other hand, although photogrammetry has found application in some forensic fields such as documentation and measurement of forensic-relevant injuries [18,19,20], recording crime scenes [21], examining patterned injuries of skin, soft tissues and bones, and comparison of injuries with injury-causing instruments [22], and road accident reconstruction [23]; the application of modern-day photogrammetry for forensic purposes has not been discussed extensively [24] especially in the context of forensic anthropology.

New advances in 3D imaging are having a profound effect in the field of craniofacial anthropometry; though for the new techniques to be of applicable use they must be able to precisely and accurately quantify facial features as well as, if better than, the present alternatives [15]. Additionally, that all 3D methods must prove their reliability by being compared against direct measurements [12].

The main aim of this research, therefore, is to compare the measurements of three human bone clone skull models obtained from 3D photogrammetry using a dedicated software (Agisoft Metashape) to the measurements of the same skulls obtained from CT scanning and using digital calipers, with the ultimate aim of validating photogrammetry as an accurate and reliable forensic anthropology measuring and documentation tool. The reliability and accuracy of the data obtained was assessed by conducting intrarater, interrater and method reliability tests, as well conducting an analysis of variance (ANOVA).

Agisoft Metashape

This is a software that is used to develop a 3D model from 2D photogrammetric photographs by producing a set of 3D coordinates known as a point cloud [20]. The creation of the 3D model proceeds in two phases:

(a) Structure from motion(SfM) where the camera's shooting position for each image is obtained and

(b) Multi-view Stereo (MVS) in which a 3D point cloud of the photographed subject is produced [25]. A mesh that estimates the shape of the object is then produced by forming polygons between point clouds [20].

The software automatically adjusts bundle blocks and generates 3D models from photos of both calibrated and non-calibrated cameras. The photos of the area to be documented are taken in an overlapping sequence with a constant focal length and distance to the object [19]. The photos can be taken from any position so long as the object to be reconstructed is visible on at least two photos [26]. The resulting model has high-resolution colour information; although, the quality of the geometry relies on the configuration of the photos around the object and the quality of the photos themselves [27].

Agisoft Metashape is easy to use, provides good results and has a low purchase price. In terms of accuracy, photogrammetry can exhibit slight deviations in geometry but still give accurate enough results [27]. A brief overview of how the software works, and the minimal and recommended system configurations for the software are in Appendix 1.

Research Hypothesis

The hypothesis for this paper states that Agisoft Metashape software will give results accurate to 98% compared to physical measurements by digital calipers and CT scan measurements by Canon Aquilion Lighting 80 scanner on 3 bone clone human skull models (Caucasian male, African American female and Asian male) across 16 facial landmarks.

MATERIALS AND METHODS

Materials

Three bone clone human skulls were used in this study (Figure 1). Overlapping photographs of the entire surface of each skull were taken using a Samsung Galaxy S8 model SM-G950F running on Android version 9 with a camera resolution of 12 megapixels. The camera was used on auto-focus mode, and the constant aperture was F1.7 and the focal length was 4.20mm.

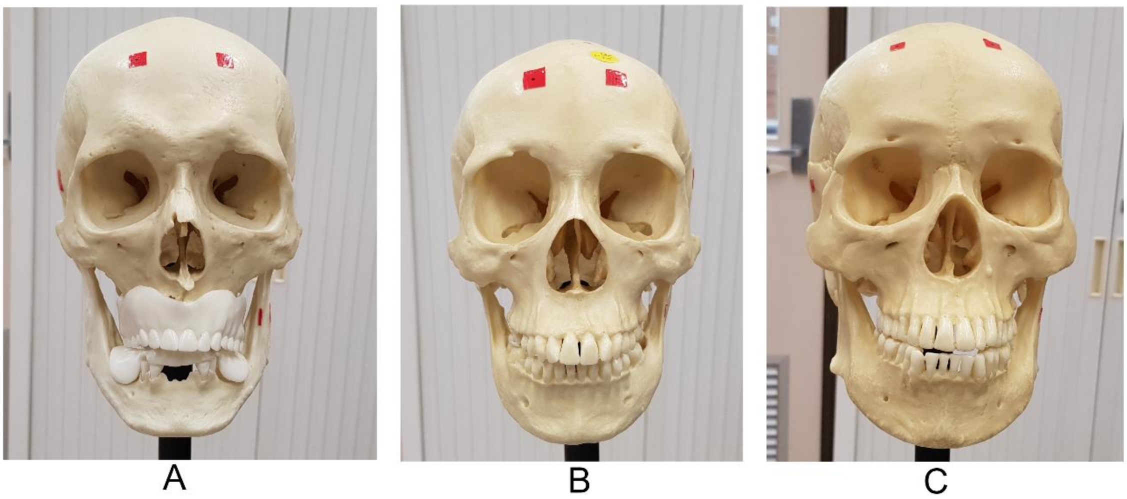

Figure 15. The three bone clone skulls that was used in this study: A- Caucasian male; B- African American female; and C- Asian male.

The photographs were then imported into Agisoft Metashape 1.5.5 Professional Edition software [Copyright © 2019 Agisoft LLC] (formerly Agisoft PhotoScan 1.4.5) (https://www.agisoft.com/) for processing to produce a 3D model for each skull.

The standard instruments used in taking physical measurements in anthropology are made of metal (calipers) and fabric (metric tape graduated with a millimetre scale) [28]. For this study, two different calipers (one spreading and one sliding) were used to conduct the measurements of the skulls. The specifications of the instruments are as follows:

i. Craftright® 0-150mm digital Vernier Caliper (sliding)

ii. Moore & Wright 0-150mm/6" Digital Outside Caliper (spreading)

The sliding caliper measures linear distances between two landmarks on either the same or neighbouring planes whereas the spreading caliper is used when the linear distances to be measured are on different planes, and are far apart [28].

Methods

Physical Measurements

Physical measurements of each of the skulls were taken. A spreading caliper was used for the measurements that were along the curved surface of the skull such as the cranial length and breadth whereas a sliding caliper was used was used for more linear measurements such as the orbital and nasal heights and breadths.

Apart from the interlandmark distances (ILDs), an additional five representative measurements from the norma frontalis, occipitalis and lateralis were taken. The measurements were taken from the forehead in a clockwise direction, with the forehead measurement being labelled "A" and the final measurement which was on the left side of the mandible being labelled as "E" (Figure 2). These measurements were used to set the reference scale in the software, from which the approximation of the ILDs would be made. All the physical and photogrammetric measurements were taken in triplicate and then averaged in order to increase precision [28]. The averaged measurements of A to E for each skull from each of the observers were then added together and five resultant grand averages obtained. These were the figures that was used as the reference measurements in the software. These measurements can be found in Appendix 2.

The calipers gave the distances in millimetres. These distances were converted into meters in order to align with the measurement unit from the software.

Procedure of taking reference measurements

Square pieces of duct rape approximately 7mm by 7mm were placed between the selected distances on each aspect of the skull. A black dot was then drawn at the approximate center of the square, this would be the point from which measurements would be taken using the sliding caliper.

The same approximate distances were chosen for all three skulls for uniformity.

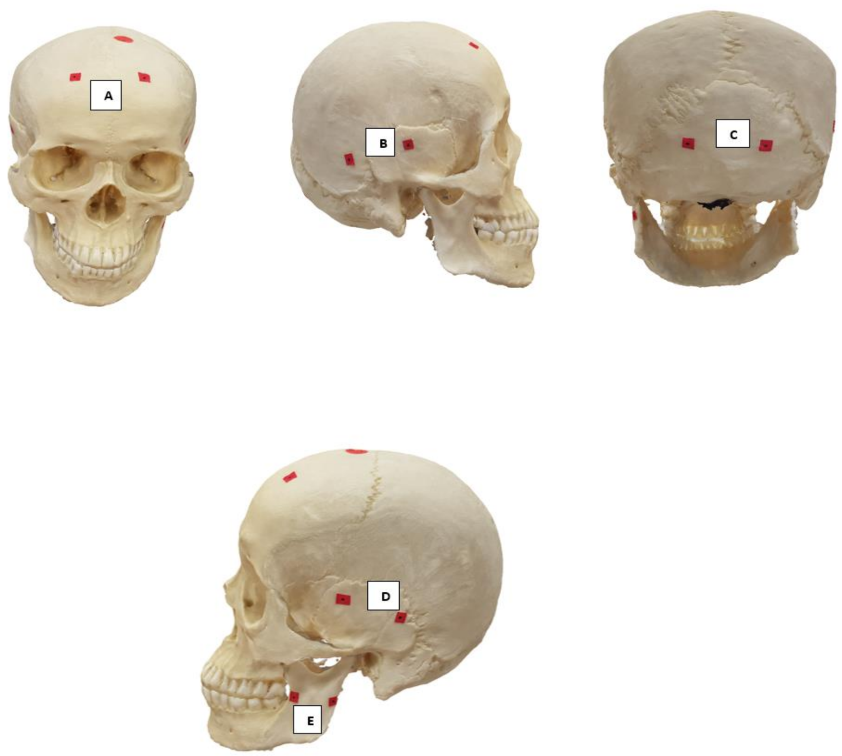

Figure 16. Measurements A to E which were used in setting the reference scale in the software.

In order to introduce interobserver error (and hence increase confidence in the method) as suggested by García de León Valenzuela [16], measurements of each skull were made by four different readers. Two of the readers were “trained” (had prior knowledge of the area of research) while the other two were “untrained” (had no knowledge whatsoever about the research). The measurements were made independently to avoid bias, and each set of measurements between methods was recorded separately by each observer to make sure that they were blinded to preceding results [10] and hence no opportunity for comparison. However, the “untrained” observers were given direction on where the various landmarks that were used in the study were located, and were further provided a diagrammatic representation depicting the landmark positions. At the end of data collection, all data was entered into Microsoft Excel 2016 spreadsheet software for subsequent statistical analysis.

Table 1 below shows a summary of all the ILDs that were measured. For the raw data of each of the skulls refer to Appendix 2, and for the definitions of the landmarks in Table 1 refer to Appendix 3.

Table 8. ILDs used in this study

HEAD/VAULT		
Measurement	**Landmarks**	**Caliper type**
Max. cranial length	g-op	Spreading
Max. cranial breadth	eu-eu	Spreading
Min. frontal breadth	ft-ft	Sliding
FACE		
Facial (max. bizygomatic) breadth	zy-zy	Spreading
Morphological facial height	n-gn	Sliding
Upper facial height	n-pr	Sliding
EYES		
Orbital height	Upper & lower margins of orbital cavity (L&R)	Sliding
Orbital breadth	ec-mf	Sliding
Inter-orbital breadth	d-d	Sliding
Bi-orbital breadth	ec-ec	Sliding

NOSE		
Nasal height	n-ns	Sliding
Nasal breadth	al-al	Sliding
MANDIBLE		
Bicondylar breadth	cdl-cdl	Sliding
Bigonal breadth	go-go	Sliding

The landmarks selected are among those used in standard cranial measurements and they indicate the general size and shape of the cranial vault, the face, the masticatory process, the nasal and the orbital areas [29]. Additionally, these landmarks are used in characterizing facial features [10]. Figures 3 and 4 show the anterior and lateral views of the skull, with the craniofacial landmarks used in the study indicated. Table 2 shows the full names of the landmarks.

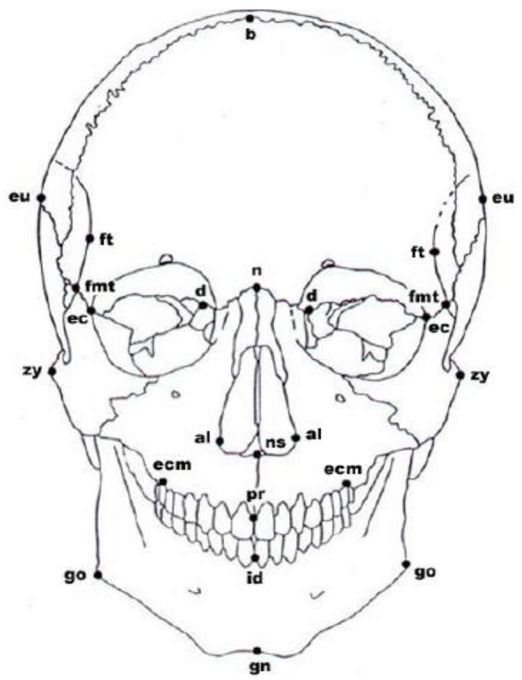

Figure 17. Anterior view of skull showing the craniometric landmarks of the anterior aspect [Adapted from Gordon [30]]

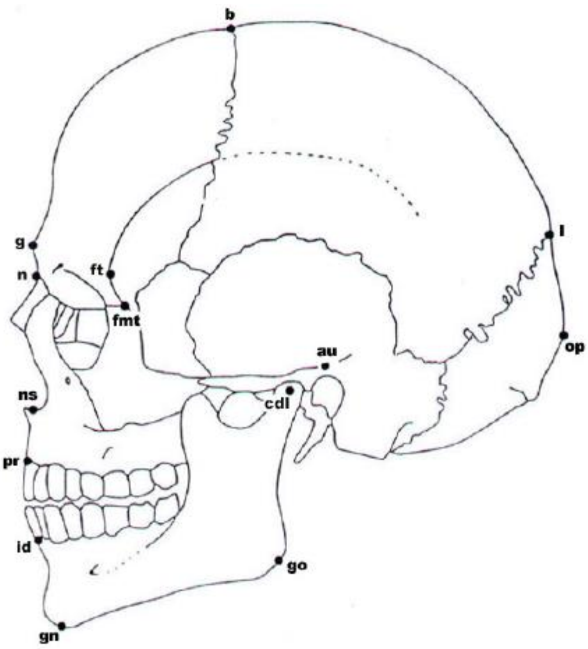

Figure 18. Lateral view of skull showing the craniometric landmarks of the lateral aspect [Adapted from Gordon [30]]

Table 9. Abbreviations of the landmarks in Figures 2 & 3 in full [Adapted from Gordon [30]]

Landmark abbreviation	Landmark name
al	Alare
b	Bregma
d	Dacryon
ec	Ectochonchion
fmt	Frontomalare temporale
ft	Frontotemperale
eu	Eurion
gn	Gnathion
go	Gonion
id	Infradentale
n	Nasion
ns	Nasospinale
pr	Prosthion
zy	Zygion
au	Auriculare
l	Lambda
g	Glabella
op	Opisthocranion
cdl	Condylion laterale

Photogrammetry

Photography

In order to enable photography of the entire external surface of the skulls, the skulls were elevated on a cylindrical stand that was 1220x15mm through the foramen magnum. Overlapping photographs of each of the skulls were taken from four different angles: the first angle was overhead, and was aimed at capturing the top of the skull (frontal and parietal bones); the second angle was the camera directly pointed at the anterior of the skull from which the frontal, lateral and occipital aspects of the skull were captured; the third angle of photography was at the mandible level, and the final angle was at the base of the skull, aimed at capturing the basalis aspect.

All photography began from the frontal aspect of the face and proceeded in a clockwise direction until the researcher circled back to the frontal aspect. A total of 73 phots were taken of the Caucasian male skull, 109 photos for the African American female skull, and 75 photos for the Asian male skull.

3D Reconstruction

Each skull was reconstructed separately. The whole reconstruction process was automated, hence the default settings in the software for each of the steps that led to the final 3D reconstruction (alignment – dense cloud – mesh – texture) were used as they were and not adjusted in any way (Figure 5). The 'Workflow menu' on the menu bar is the only one that was used for the whole reconstruction process. It lists the reconstruction steps in order in which they should be carried out, and the next process could not commence if the previous one had not been carried out or completed. Images of the result of each reconstruction step can be found in Appendix 1.

The photographs were first loaded into the software and then aligned with the accuracy setting of the alignment on “High”. When all the photos aligned (as with the Asian male skull), a sparse point cloud displayed at the end of the alignment. However, when some photos did not align (as with the Caucasian male and African American Female skulls), the incorrectly aligned photos had to be removed and the alignment done again. The number of photos that did not align were seen from the “Workspace” tab to the left of the reconstruction workspace in the software, with the actual photos being seen in the “Photos” tab below the reconstruction workspace. All the aligned photos were checked whereas the unaligned photos were not. 72 of the 73 photos of the Caucasian male skull aligned whereas 105 of the 109 photos of the African American female skulls aligned. All 75 photos of the Asian male skull aligned. Unaligned photographs could be realigned manually. However, because the photos that did not align were very few, and they had no impact on the final 3D reconstruction, the researcher opted to delete them.

Building a dense cloud followed the alignment process, and this was based on the estimated camera positions. The only reconstruction parameter used was the quality, and it was set on medium. A mesh was then built from the data derived from the dense cloud. The “Arbitrary” surface type can be used for modelling any object, but especially closed objects such as statues as it does not make assumptions on the object type being modelled. The face count describes the maximum number of polygons in the final mesh; with the values “low, medium, high” describing the optimal number of polygons required for a mesh of corresponding level of detail to either of the values to be reconstructed [26].

The final step in the reconstruction process was building the texture, which determines how the object texture will be packed in the texture atlas and hence, ultimately, the visual quality of the resultant model. The “Generic” mapping mode is the default for arbitrary geometry and attempts to create as uniform a texture as possible. On the other hand, the blending mode refers to how the pixel values from the different constituent photos will be merged in the final texture. The texture size/count defines the size (in terms of width and height) of the texture atlas in pixels [26].

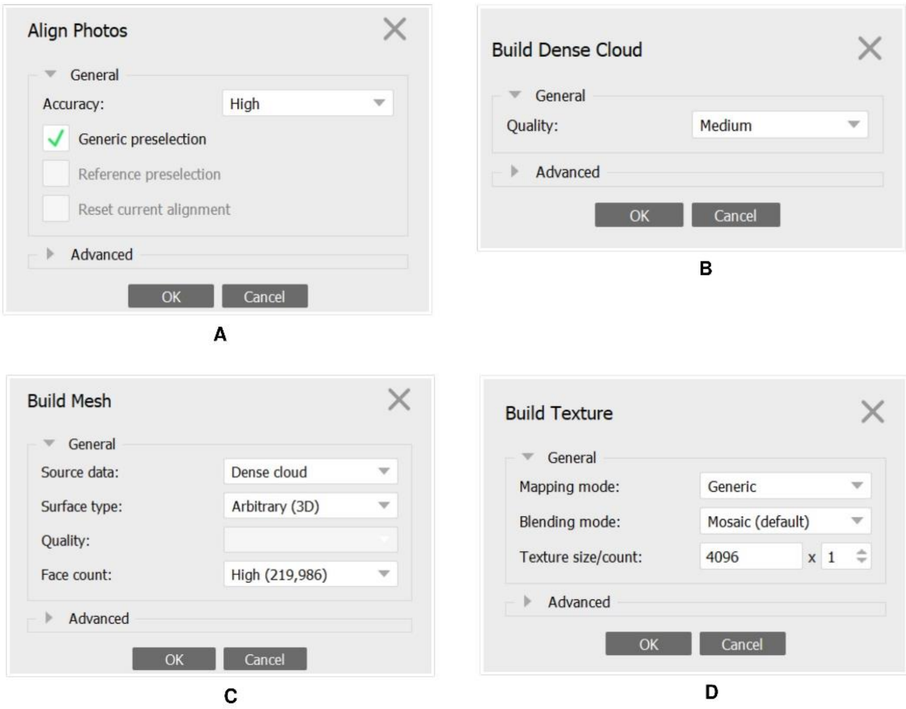

Figure 19. Reconstruction settings at each stage of reconstruction: A- Alignment; B- Dense Cloud; C- Mesh and D- Texture

Software Measurements

The 3D reconstruction of each skull was first scaled using the five reference measurements in Table 3 below that were obtained from the physical measurements. Each of the ILDs used in the study (Table 1) was then measured and recorded. The measurements were done in triplicate, and were done independently to avoid bias. However, a diagrammatic representation of the ILDs and guidance on how to use the software was provided to the "untrained" observers.

The default calibration unit in the software was meters.

Table 10. The five reference measurements (means of A-E) for each skull used to set the scale in Agisoft software. This was the scale from which the ILDs were approximated

Caucasian Male Skull					
Measurement	Obs 1	Obs 2	Obs 3	Obs 4	Mean
A	0.04223	0.04235	0.04218	0.04261	0.042343
B	0.04178	0.04173	0.04162	0.04127	0.0416
C	0.05346	0.05399	0.0535	0.05325	0.05355
D	0.03959	0.03996	0.0402	0.04035	0.040025
E	0.02389	0.02381	0.02378	0.02328	0.02369
African American Female Skull					
Measurement	Obs 1	Obs 2	Obs 3	Obs 4	Mean
A	0.03642	0.03666	0.0369	0.03652	0.036625
B	0.03285	0.03288	0.03249	0.03252	0.032685
C	0.04256	0.043	0.04271	0.04275	0.042755
D	0.03724	0.03657	0.03699	0.03658	0.036845
E	0.02444	0.02415	0.02408	0.02455	0.024305
Asian Male Skull					
Measurement	Obs 1	Obs 2	Obs 3	Obs 4	Mean
A	0.04641	0.04597	0.0463	0.04531	0.045998
B	0.04333	0.04336	0.04357	0.04288	0.043285
C	0.04113	0.04122	0.04139	0.04117	0.041228
D	0.03439	0.03424	0.03419	0.03445	0.034318
E	0.02397	0.02431	0.02426	0.02415	0.024173

CT Scanning

The skulls were scanned using a Conon Aquilion Lighting 80 scanner. The scan parameters used were as follows: (a) power of 100 kilovolts (kV); (b) current of 100 milliamperes (mA); (c) slice thickness of 0.5 mm; (d) rotation time of 0.75 seconds, which was the shortest time;

(e) pitch factor of 0.63; and (f) the reconstruction kernel or the display algorithm used was the bone window which was represented as FC 30.

The CT scan images were saved in a Digital Imaging and Communications in Medicine (DICOM) format.

Measurements

A software called 'RadiAnt DICOM Viewer' (Version 5.0.2) (https://www.radiantviewer.com/) was used to open the CT scan images. The software has two main reconstructions: 3D reconstruction and Multiplanar Reconstruction (MPR). MPR breaks down the 3D image into 2D slices, and has three views namely axial (anterior to posterior), sagittal (lateral left to right), and coronal (superior to inferior). All the measurements except two (upper facial height and nasal height) were obtained from the axial and sagittal MPR views, and hence were taken from the 2D version of the CT image. As such, unlike with the physical and photogrammetric measurements (3D) which were taken in triplicate and averaged due to the high level of subjectivity, only one measurement was made for each ILD for the CT scan.

The upper facial height and nasal height measurements were made from the 3D reconstruction.

Statistical Analyses

The diagram below (Figure 6) summarizes the three main statistical analyses conducted in this study: intrarater reliability, interrater reliability, and intermethod reliability.

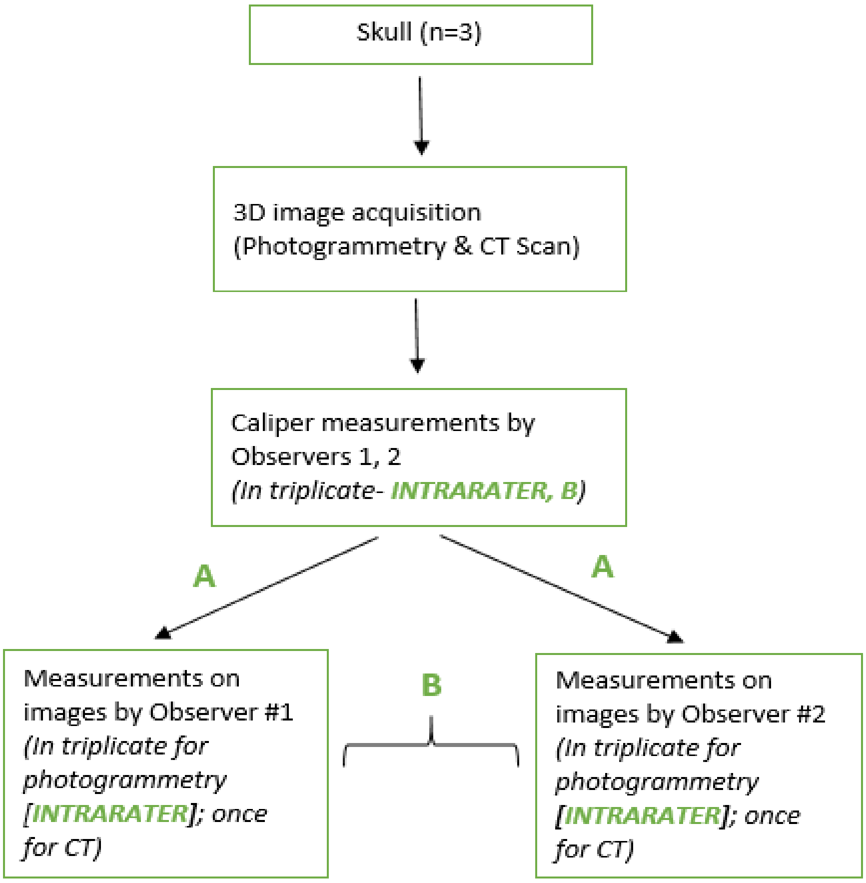

Figure 20. Summary of statistical tests conducted in this study. A- Intermethod reliability between physical and 3D measurements; B- Interrater reliability. Note that interrater reliability was conducted for both caliper (physical) measurements and 3D image measurements.

Intrarater and interrater correlation coefficient values range between 0 and 1 with values close to 1 indicating a higher reliability and those closer to zero indicating lower reliability. Intermethod reliability (comparison between physical, photogrammetric and CT scan measurements) was evaluated by calculating the Pearson correlation coefficient which also ranges between 0 and 1, with values closer to 1 indicating a higher reliability.

In addition to the three main statistics, an ANOVA test of the physical and photogrammetric measurements of each skull was conducted to determine whether there was a statistical difference between the measurements taken by the different observers.

RESULTS

I. 3D Reconstruction

Photogrammetry

The reconstruction process using Agisoft Metashape software yielded an accurate representation of the skull being reconstructed. Figure 7 shows the reconstruction of the Asian skull from all six norma angles using a total of 75 photos and 26,298 points. The reconstruction of the Caucasian male and African American female can be found in Appendix 4 (I). Because only visible parts of the surface can be documented [24], a hole remained when most of the pole on which the skull was resting was trimmed after reconstruction (see Figure 7 picture D, norma basalis).

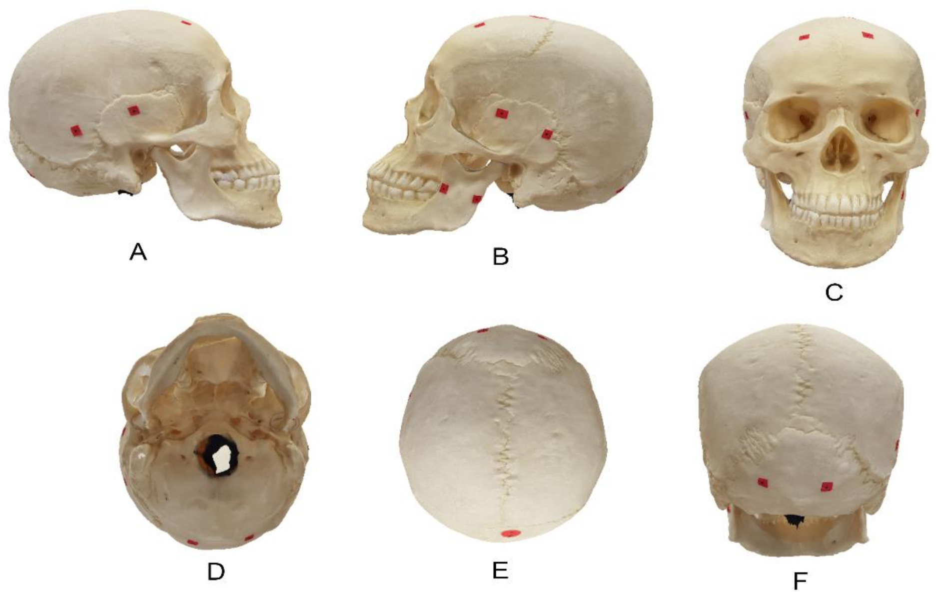

Figure 21. 3D reconstructed Asian male skull model using Agisoft Metashape software from 6 angles: A&B- Norma lateralis; C- Norma frontalis; D- Norma basalis; E- Norma verticalis; and F- Norma occipitalis

When the photogrammetric measurements made by the different observers for each of the skulls were compared side by side against the physical measurements they had already made for each skull (intrarater), and a comparison also made across the measurements of the different observers for the different skulls (interrater), they appeared to be visually similar.

CT Scan

Figure 8 shows the MPR (axial, sagittal) and 3D reconstruction views from the software, and the various ILDs measured from each view. Photographs of all the ILDs used in the study as measured from the CT scan slices can be found in Appendix 4 (II).

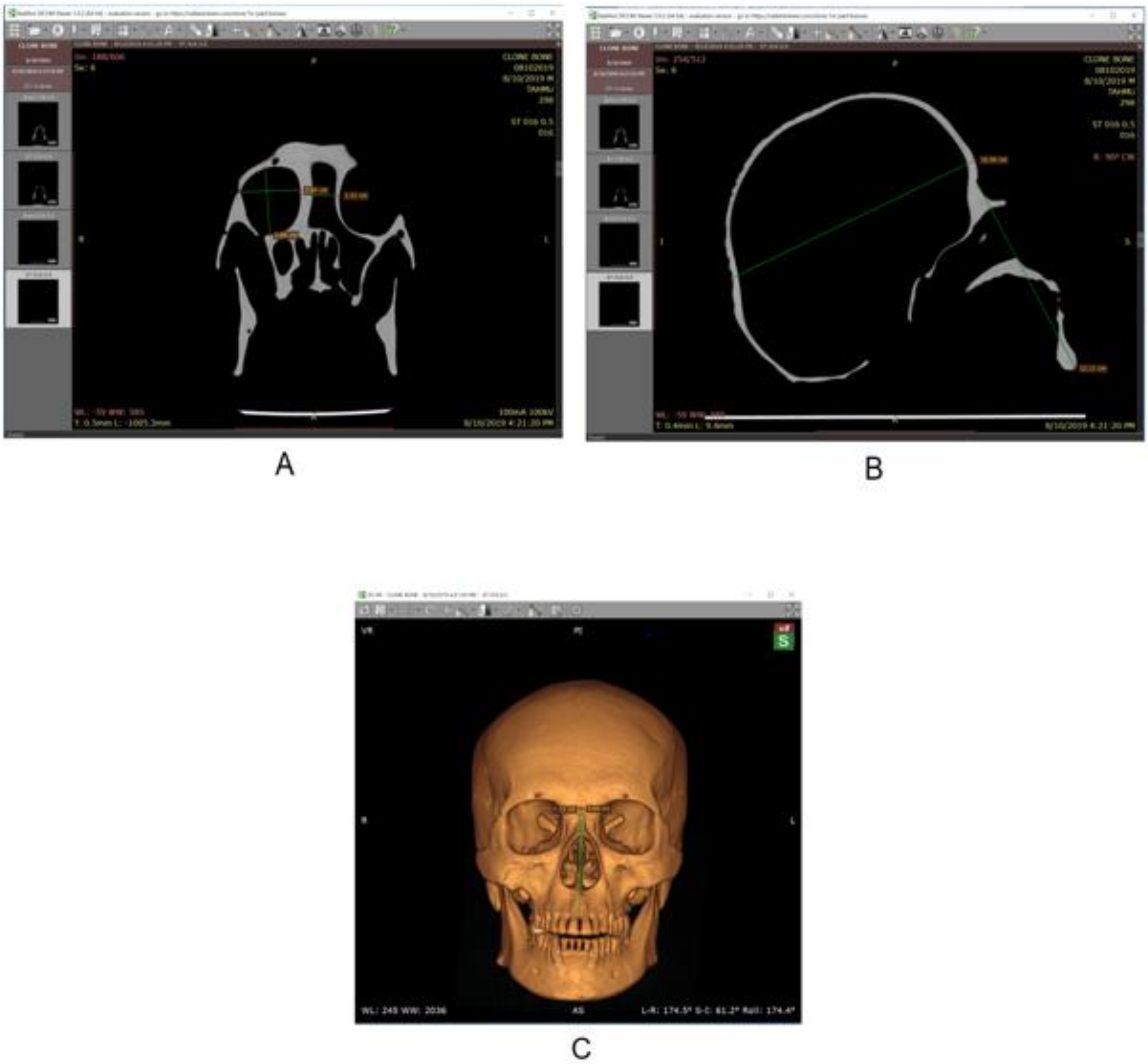

Figure 22. 3D reconstructed Asian male skull using RadiAnt DICOM Viewer software. In the figure is A- axial view and B- sagittal view of the MPR (from slices); and C- 3D reconstruction

When measurements from the CT slices made by the different observers for each of the skulls were compared side by side against the physical measurements they had already made (intrarater), and a comparison also made across the measurements of the different observers for the different skulls (interrater), they appeared to be visually similar.

When all the measurements (physical, photogrammetric, CT) made by the different observers for each of the skulls were compared side for each individual observer (intrarater) and also across the different observers for the different skulls (interrater), there was a high degree of similarity in measurements across the different methods.

II. Statistics

Intrarater Reliablity

The intraclass correlation coefficient for the physical measurements of all the observers across all the three skulls was greater than or equal to 0.9993216. On the other hand, the intraclass correlation coefficient for the photogrammetric measurements was greater or equal to 0.9980488 (Table 4).

Table 11. Intraclass correlation coefficient values for the physical and photogrammetric measurements for all three skulls

Summary of the Intraclass Correlation Coefficients (mean n=3)				
Physical measurements				
	Observer 1	Observer 2	Observer 3	Observer 4
CM Skull	0.99996972	0.99982965	0.9993216	0.99988858
AAF Skull	0.99995302	0.99965715	0.99960746	0.99993394
AM Skull	0.99997641	0.99978576	0.99963604	0.99990282
Photogrammetry measurements				
	Observer 1	Observer 2	Observer 3	Observer 4
CM Skull	0.99988143	0.9995544	0.99916143	0.9980488
AAF Skull	0.99987481	0.99956339	0.99932934	0.99936166
AM Skull	0.99986093	0.99988119	0.99847225	0.99950339

An intraclass correlation was also done for each observer across all three methods of measurements to determine their precision from method to method. The resultant correlation coefficient was greater or equal to 0.98616228 (Table 5).

Table 12. Intraclass Correlation Coefficient Across The 3 Methods of Measurement

Intraclass Correlation Coefficient Across All 3 Methods (Physical:CT:Photogrammetry)				
	Observer 1	Observer 2	Observer 3	Observer 4
CM Skull	0.99763865	0.99669118	0.99413945	0.99801804
AAF Skull	0.99939337	0.99932311	0.99816028	0.99937067
AM Skull	0.99930202	0.99789141	0.98616228	0.99889741

Interrater Reliability

The averaged approximate interclass correlation coefficient for the physical measurements across all the three skulls was greater than or equal to 0.98713394, while those of CT scan measurements and photogrammetric measurements were greater than or equal to 0.99584569 and greater than or equal to 0.98713394 respectively (Table 6).

Table 13. Summary of the interclass correlation coefficients for the three methods of measurement

Summary of the Interclass Correlation Coefficient	
Physical measurements (Observer1:Observer2:Observer3:Observer4)	
	AVERAGE
CM Skull	0.99927573
AAF Skull	0.992037827
AM Skull	0.98713394
CT measurements (Observer1:Observer2:Observer3:Observer4)	
	AVERAGE
CM Skull	0.995845689
AAF Skull	0.99864503
AM Skull	0.998442011
PG measurements (Observer1:Observer2:Observer3:Observer4)	
	AVERAGE

CM Skull	0.995600108
AAF Skull	0.992037827
AM Skull	0.98713394

One Way ANOVA

A one way analysis of variance (ANOVA) was done for the physical and photogrammetric measurements of all three skulls. Table 7 below gives a summary of the results.

Table 14. Summary of the ANOVA carried out for the physical and photogrammetric measurements

	F statistic	p-value
Physical Measurements		
CM Skull	8.8957	0.00629
AAF Skull	8.3469	0.00759
AM Skull	8.7103	0.00669
Photogrammetric Measurements		
CM Skull	20.0042	0.00045
AAF Skull	3.4957	0.06968
AM Skull	5.0732	0.02949

DISCUSSION

There is a growing interest in the use of computer-based techniques to overcome the limitations of direct anthropometry; and over the last three decades, several non-invasive, 3D imaging techniques such as different forms of stereophotogrammetry, computer assisted tomography, have been developed. Aside from being non-invasive, these techniques have the additional advantages of being fast in acquiring craniofacial surface images, allowing images to be archived and avoiding errors in measurement that occur when 3D surfaces are represented in 2D. The investigations are also repeatable and verifiable [14,15,31].

CT has always been preferred for clear high-resolution images, and modern CTs have, on top of improving the quality of image acquisition, advanced so that they operate faster and hence reduce radiation exposure to the patients [17]. Forensic institutes across the world are adopting CT or magnetic resonance imaging (MRI) scanners or both in their mortuaries and mobile CT for autopsy and mass fatality investigations. CT provides information to a pathologist that may not be available to them, and is a non-destructive permanent record of the body [32]. Additionally, CT scanning has been introduced into forensic anthropology [33]. Despite these advantages, training is needed to understand CT images, and the CT images can only be read by certified radiologists [16,33]. Additionally, CT scans lack colour information, have poor resolution of facial contours, have high associated costs and risks of exposure to ionizing radiation, and CT is a cumbersome tool for screening the entire skeleton [14,24,34]

3D photogrammetry is a technique that is well used in multiple fields such as topography, architecture, police investigations such as reconstruction of road accidents and forensic anthropology. It allows the reconstruction of surfaces in three dimensions by making reliable measurements using images taken from different viewpoints. A computer system then produces a 3D data model of the object by calculating the position of particular points on the surface of the object in space [19,24,31,35,36]. Once the original photographs have been captured, their evaluation can happen at a later date long after the object of interest is no longer physically present for instance if the remains have already been buried or the crime scene has been released [19,22,33]. The application of modern-day photogrammetry for forensic purposes has not been discussed extensively [24]. Among the reasons could be because until recently, the required metric cameras were very costly; and they could only be operated by skilled professionals [21].

Perhaps the most important criterion for assessing any measurement technology is the ability to obtain reliable and accurate measurement data [15]. As such, the primary goal of scientists should be the accuracy of measurements in order to avoid statistical errors [37]. All these factors, in addition to ensuring the measurement methods are repeatable and have a known error rate, qualify the measurement methods and technology to meet the minimum threshold of the Daubert criteria of admissibility of scientific evidence in courts of law.

From the statistical analysis conducted in the study, an intraclass correlation coeffieient of greater than or equal to 0.9993216 and 0.9980488 was obtained for the physical and photogrammetric measurements respectively. These values are very high, and imply that all the observers were precise in both their physical and photogrammetric measurements. The intraclass correlation coefficient of greater or equal to 0.98616228 obtained when a correlation was done for each observer across the three measurement methods implies that regardless which of the observers made the measurements at any particular time, their values would still be precise.

The interclass correlation coefficients obtained for the physical, CT scan and photogrammetric measurements were greater than or equal to 0.98713394, 0.99584569 and 0.98713394 respectively. These results imply that each measurement method was accurate and precise, that is, regardless of the method of measurement one chose, they would get nearly the same measurement across the methods.

An ANOVA was additionally conducted in an attempt to determine whether there were any differences between the group averages that were large enough to be statistically significant. The p-values for all the measurements except the photogrammetric of the AAF skull were above 0.05; hence the conclusion that for these groups of data, there were no statistically significant differences between their group averages, that is, the averages of all the groups were considered to be equal. The data set that had a p-value of less than 0.05 could be explained by the fact that one of the observers was under personal and external pressure, hence at a point during the measurement process, they lost concentration and worked hard to finish without much regard to accuracy or precision.

Taking into consideration all the results of the statistical analyses conducted, the researcher reached the conclusion that the statistics favoured the acceptance of the stated hypothesis and the rejection of the null hypothesis. Therefore, photogrammetry gave accurate results compared to physical and CT scan measurements.

The past decade has seen advances in digital camera technology which has led to the rise of numerous new applications that can be used by untrained personnel using any kind of digital camera, for instance metric or non-metric, smartphones, normal consumer cameras, in any possible wavelength [21]. Photogrammetry is a safe, affordable, flexible and precise technique that can provide reliable, reproducible and accurate data. Importantly, it outputs a high resolution colour representation [14,15,24,36]. The major disadvantages of photogrammetry and indeed, the software (Agisoft) are their reliance on photograph quality, hence poor resolution photographs will lead to poor reconstruction, and their difficulties in reconstructing non-textured, shiny, highly reflective, transparent or shadowed surfaces [14,26].

Sources of Error

The most common sources of error in anthropometry are: (i) improper identification of landmarks such as glabella, eurion; (ii) improper measuring technique; and (iii) inadequate use of measuring equipment. Errors in measurement can be greatly decreased by marking the position of the landmarks [28]. However, in order to prevent bias, and because two of the statistical tests were (a) the measure of variability between the measurements taken by an individual observer (intrarater error) and (b) the variability between measurements by the different observers (interrater error), the positions of the landmarks used in this study were not marked.

Depending on the region being measured and the examiner's experience, errors may arise during measurements. For instance, with the spreading calipers, errors in measurement may be up to 3 mm. It is also worth noting that due to its blunt edges, the spreading calipers is less accurate compared to the sliding calipers which has pointed branches [28].

CONCLUSION

This study demonstrated that indeed, photogrammetry could give results that were as accurate as those obtained from physical and CT scan measurements, and that it was a reliable and repeatable method. It further demonstrated that photogrammetry does not have to be carried out using a DSLR camera, but any camera (including phone cameras) can be used as long as they have a high resolution. Additionally, the photogrammetric software is easy to use and does not require much training as evidenced by the observer variability tests. This eliminates the need for skilled professionals who are sometimes in short supply, especially in a mass disaster scenes.

In future, the results of this research could help anthropologists make analyses and determinations on remains which they cannot access physically due to geographical constraints from behind a desk using only the photographs of the remains. Additionally, it could foster collaborations between anthropologists who are in different geographic locations and make it easier to compare opinions about anthropological remains and their context. In instances where police officers or even construction personnel come across remains in the field and they have a good resolution camera, they can be directed on how to capture the photographs needed for reconstruction, hence save on the cost and time it would take to get an anthropologist to the field. This is especially useful when the remains are very fragile and can easily be affected or altered by weather elements.

ACKNOWLEDGEMENTS

The author would like to thank the Anatomy Department of Murdoch University for supplying me with two out of the three bone clone skull models which I used in my research. Additionally, I would like to acknowledge The Murdoch University Animal Hospital for facilitating the CT scans of her bone clone skull models. Finally, I would like to thank my co-authors for their valuable input into this project.

REFERENCES

[1] Dirkmaat D. A companion to forensic anthropology. Malden, MA: Wiley-Blackwell; 2012.

[2] Tersigni-Tarrant M, Langley N. Forensic anthropology. Boca Raton, FL: CRC Press LLC; 2013.

[3] Gupta S. Forensic Facial Reconstruction: The Final Frontier. Journal Of Clinical And Diagnostic Research. 2015.

[4] Ubelaker D, Shamlou A, Kunkle A. Contributions of forensic anthropology to positive scientific identification: a critical Review. Forensic Sciences Research. 2018;4(1):45-50.

[5] Wheat A. Assessing ancestry through nonmetric traits of the skull: A test of education and experience [Masters]. Texas State University; 2009.

[6] Parsons H. The accuracy of the biological profile in casework: an analysis of forensic anthropology reports in three medical examiners' offices [PhD]. The University of Tennessee; 2017.

[7] Rogers T, Allard T. Expert Testimony and Positive Identification of Human Remains Through Cranial Suture Patterns. Journal of Forensic Sciences. 2004;49(2):1-5.

[8] Priya E. Methods of Skeletal Age Estimation used by Forensic Anthropologists in Adults: A Review. Foresic Research & Criminology International Journal. 2017;4(2).

[9] Smith D, Limbird K, Hoffman J. Identification of Human Skeletal Remains by Comparison of Bony Details of the Cranium Using Computerized Tomographic (CT) Scans. Journal of Forensic Sciences. 2002;47(5):15499J.

[10] Heike C, Cunningham M, Hing A, Stuhaug E, Starr J. Picture Perfect? Reliability of Craniofacial Anthropometry Using Three-Dimensional Digital Stereophotogrammetry. Plastic and Reconstructive Surgery. 2009;124(4):1261-1272.

[11] Aung S, Ngim R, Lee S. Evaluation of the laser scanner as a surface measuring tool and its accuracy compared with direct facial anthropometric measurements. British Journal of Plastic Surgery. 1995;48(8):551-558.

[12] Farkas L, Deutsch C. Anthropometric determination of craniofacial morphology. American Journal of Medical Genetics. 1996;65(1):1-4.

[13] Linden O, Baratta V, Gonzalez J, Byrne M, Klinge P, Sullivan S et al. Surgical Correction of Metopic Craniosynostosis: A 3-D Photogrammetric Analysis of Cranial Vault Outcomes. The Cleft Palate-Craniofacial Journal. 2018;56(2):231-235.

[14] Wong J, Oh A, Ohta E, Hunt A, Rogers G, Mulliken J et al. Validity and Reliability of Craniofacial Anthropometric Measurement of 3D Digital Photogrammetric Images. The Cleft Palate-Craniofacial Journal. 2008;45(3):232-239.

[15] Fourie Z, Damstra J, Gerrits P, Ren Y. Accuracy and Repeatability of Anthropometric Facial Measurements Using Cone Beam Computed Tomography. The Cleft Palate-Craniofacial Journal. 2011;48(5):623-630.

[16] García de León Valenzuela M. Three-dimensional image technology in forensic anthropology: assessing the validity of biological profiles derived from CT-3D

images of the skeleton (Master). Boston University. [Master]. Boston University; 2014.

[17] Duke E, Aguirre S. 3D Imaging: Theory, Technology and Applications. New York: Nova Science Publishers, Inc.; 2010.

[18] Thali M, Braun M, Kneubuehl B, Brueschweiler W, Vock P, Dirnhofer R. Improved vision in forensic documentation: forensic 3D/CAD-supported photogrammetry of bodily injury external surfaces combined with volumetric radiologic scanning of bodily injury internal structures provides more investigative leads and stronger forensic evidence. 28th AIPR Workshop: 3D Visualization for Data Exploration and Decision Making. 2000.

[19] Villa C. Forensic 3D documentation of skin injuries. International Journal of Legal Medicine. 2016;131(3):751-759.

[20] Koller S, Ebert L, Martinez R, Sieberth T. Using virtual reality for forensic examinations of injuries. Forensic Science International. 2019;295:30-35.

[21] Edelman G, Aalders M. Photogrammetry using visible, infrared, hyperspectral and thermal imaging of crime scenes. Forensic Science International. 2018;292:181-189.

[22] Brüschweiler W, Braun M, Dirnhofer R, Thali M. Analysis of patterned injuries and injury-causing instruments with forensic 3D/CAD supported photogrammetry (FPHG): an instruction manual for the documentation process. Forensic Science International. 2003;132(2):130-138.

[23] Osman M, Tahar K. 3D accident reconstruction using low-cost imaging technique. Advances in Engineering Software. 2016;100:231-237.

[24] Urbanová P, Hejna P, Jurda M. Testing photogrammetry-based techniques for three-dimensional surface documentation in forensic pathology. Forensic Science International. 2015;250:77-86.

[25] Del Cesta F. Computer Vision techniques for the reconstruction of road accidents [Internet]. 2015 [cited 19 December 2019]. Available from: http://www.softwarericostruzioneincidentistradali.it/tecnica/11-tecniche-di-computer-vision-per-la-ricostruzione-degli-incidenti-stradali.html

[26] Agisoft Metashape User Manual: Professional Edition, Version 1.5 [Internet]. Agisoft LLC; 2019. Available from: https://www.agisoft.com/

[27] Buck U, Buße K, Campana L, Schyma C. Validation and evaluation of measuring methods for the 3D documentation of external injuries in the field of forensic medicine. International Journal of Legal Medicine. 2017;132(2):551-561.

[28] Farkas L. Anthropometry of the head and face. 2nd ed. New York: Raven Press; 1994.

[29] Krecioch J. Human craniofacial variation and dental anomalies: An anthropological investigation into the relationship between human craniometric variation and the expression of orthodontic anomalies. Hamburg: Anchor Academic Publishing; 2014.

[30] Gordon G. An investigation into the accuracy and reliability of skull-photo superimposition in a South African sample [PhD]. University of Pretoria; 2011.

[31] Uldin T. Virtual anthropology – a brief review of the literature and history of computed tomography. Forensic Sciences Research. 2017;2(4):165-173.

[32] Rutty G, Morgan B, O'Donnell C, Leth P, Thali M. Letters to the Editor. The Journal of Trauma: Injury, Infection, and Critical Care. 2008;65(2):493-494.

[33] Bolliger S, Thali M, Ross S, Buck U, Naether S, Vock P. Virtual autopsy using imaging: bridging radiologic and forensic sciences. A review of the Virtopsy and similar projects. European Radiology. 2007;18(2):273-282.

[34] Rybak L, Rosenthal D. Radiological imaging for the diagnosis of bone metastases. Quarterly Journal Of Nuclear Medicine. 2001;45(1):53-56.

[35] Thali M, Braun M, Markwalder T, Brueschweiler W, Zollinger U, Malik N et al. Bite mark documentation and analysis: the forensic 3D/CAD supported photogrammetry approach. Forensic Science International. 2003;135(2):115-121.

[36] Ege A, Seker D, Tuncay I, Duran Z. Photogrammetric Analysis of the Articular Surface of the Distal Radius. Journal of International Medical Research. 2004;32(4):406-410.

[37] Ozsoy U, Demirel B, Yildirim F, Tosun O, Sarikcioglu L. Method selection in craniofacial measurements: Advantages and disadvantages of 3D digitization method. Journal of Cranio-Maxillofacial Surgery. 2009;37(5):285-290.

[38] Caple J, Stephan C. A standardized nomenclature for craniofacial and facial anthropometry. International Journal of Legal Medicine. 2015;130(3):863-879.

APPENDICES

Appendix 1

Agisoft Metashape Professional Edition, Version 1.5

Publication date 2019

Overview

Agisoft Metashape is an advanced image-based 3D modeling solution aimed at creating professional quality 3D content from still images. Based on the latest multi-view 3D reconstruction technology, it operates with arbitrary images and is efficient in both controlled and uncontrolled conditions. Photos can be taken from any position, providing that the object to be reconstructed is visible on at least two photos. Both image alignment and 3D model reconstruction are fully automated.

How it works

Generally the final goal of photographs processing with Metashape is to build 3D surface, orthomosaic and DEM. The processing procedure includes four main stages.

1. The first stage is camera alignment. At this stage Metashape searches for common points on photographs and matches them, as well as it finds the position of the camera for each picture and refines camera calibration parameters. As a result a sparse point cloud and a set of camera positions are formed.

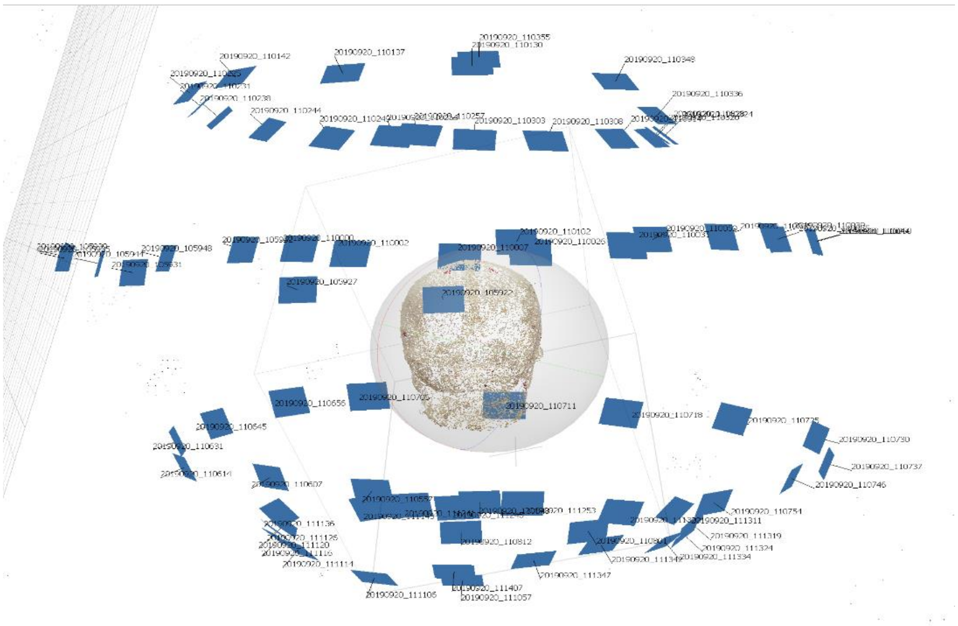

The sparse point cloud represents the results of photo alignment and will not be directly used in further processing (except for the sparse point cloud based reconstruction method, that is not recommended). However it can be exported for further usage in external programs. For instance, the sparse point cloud model can be used in a 3D editor as a reference.

On the contrary, the set of camera positions is required for further 3D surface reconstruction by Metashape.

2. The next stage is generating dense point cloud, that is built by Metashape based on the estimated camera positions and pictures themselves. Dense point cloud may be edited and classified prior to export or proceeding to the next stage.

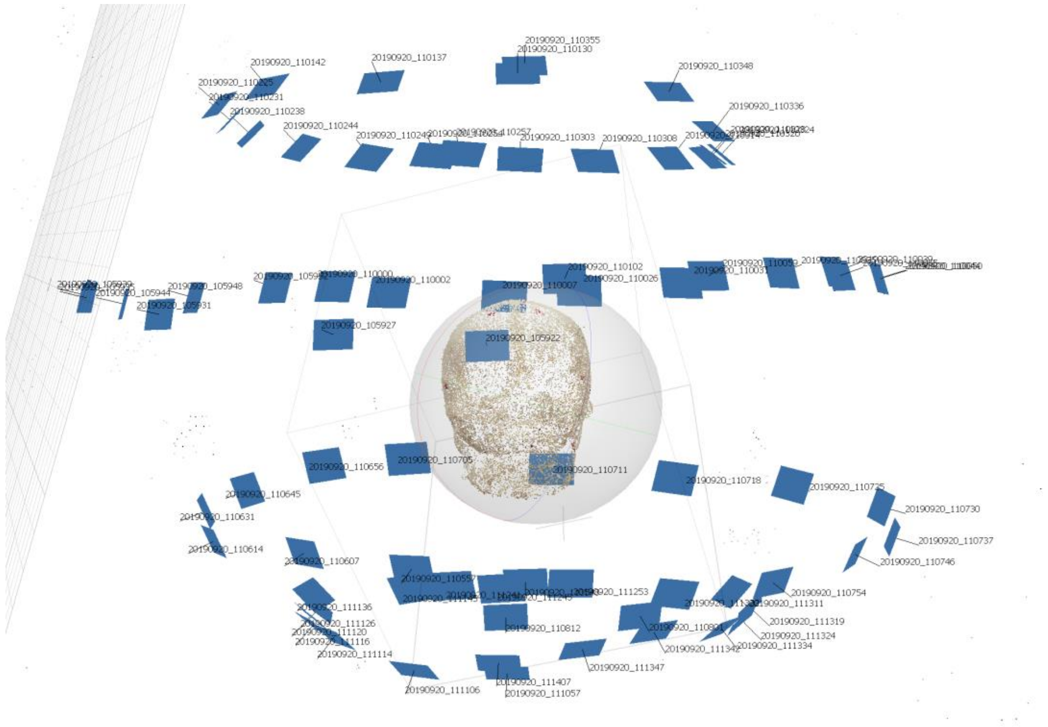

3. The third stage is generation of a surface: Mesh and/or DEM. 3D polygonal mesh model represents the object surface based on the dense or sparse point cloud, this type of surface representation is not always required, so the user may choose to skip mesh model generation step. Digital Elevation Model (DEM) can be built in Geografic, Planar or Cylindrical projections according to the user's choice. If the dense point cloud had been classified on the previous stage - it is possible to use particular point classes for DEM generation.

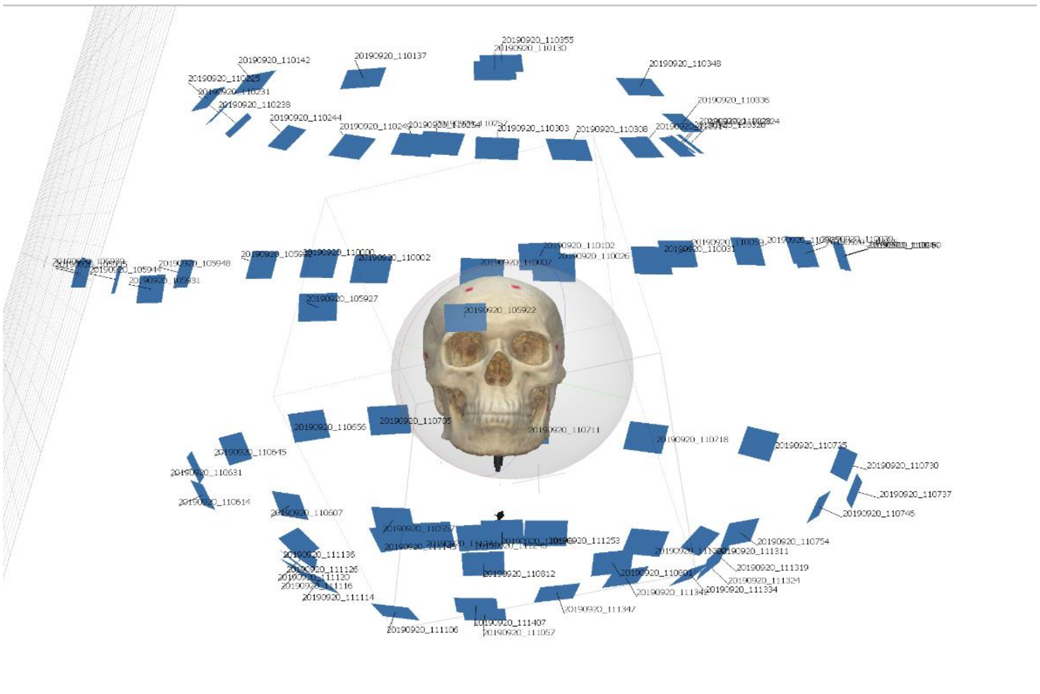

4. After the surface is reconstructed, it can be textured (relevant for mesh model only) or an Orthomosaic can be generated. Orthomosaic is projected on a surface of user's choice: DEM or Mesh model (if it had been generated for the project).

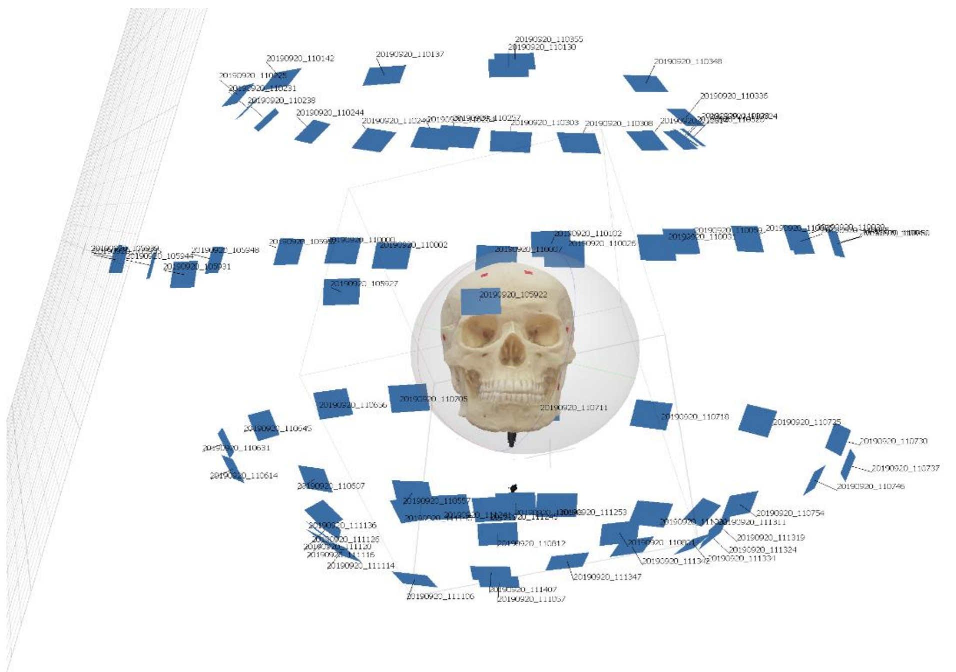

System requirements

Minimal configuration

- Windows XP or later (32 or 64 bit), Mac OS X Mountain Lion or later, Debian/Ubuntu with GLIBC 2.13+ (64 bit)

- Intel Core 2 Duo processor or equivalent

- 4 GB of RAM

Recommended configuration

- Windows 7 SP 1 or later (64 bit), Mac OS X Mountain Lion or later, Debian/Ubuntu with GLIBC 2.13+ (64 bit)

- Intel Core i7 or AMD Ryzen 7 processor

- Discrete NVIDIA or AMD GPU

- 32 GB of RAM

The number of photos that can be processed by Metashape depends on the available RAM and reconstruction parameters used. Assuming that a single photo resolution is of the order of 10 MPix, 4 GB RAM is sufficient to make a model based on 30 to 50 photos. 16 GB RAM will allow to process up to 300-400 photographs.

(Adapted from *Agisoft Metashape User Manual: Professional Edition, Version 1.5*[PDF]. All images obtained from the software after every stage of reconstruction. A detailed discussion on the workflow can be found in Chapter 3: General Workflow).

Appendix 2

RAW PHYSICAL MEASUREMENTS (IN METERS) USED IN SETTING SCALE IN AGISOFT

Caucasian Skull

	Observer 1					Observer 2					Observer 3					Observer 4				
Measurement	r1	r2	r3	Mean	SD	r1	r2	r3	Mean	SD	r1	r2	r3	Mean	SD	r1	r2	r3	Mean	SD
A	0.04212	0.04235	0.04222	0.04223	0.000115	0.04223	0.04248	0.04233	0.042347	0.000126	0.04225	0.04238	0.04191	0.04218	0.000243	0.04229	0.04287	0.04268	0.042613	0.000296
B	0.04194	0.04193	0.04146	0.041777	0.000274	0.04186	0.04164	0.0417	0.041733	0.000114	0.04174	0.0423	0.04081	0.041617	0.000753	0.04148	0.0413	0.04103	0.04127	0.000226
C	0.0524	0.05353	0.05362	0.053183	0.00068	0.05412	0.05406	0.0538	0.053993	0.00017	0.05357	0.05336	0.05356	0.053497	0.000118	0.0535	0.0532	0.05305	0.05325	0.000229
D	0.03958	0.03949	0.03971	0.039593	0.000111	0.03978	0.04003	0.04007	0.03996	0.000157	0.04054	0.03998	0.04008	0.0402	0.000299	0.04011	0.04026	0.04069	0.040353	0.000301
E	0.02391	0.02381	0.02395	0.02389	7.21E-05	0.0243	0.02384	0.02329	0.02381	0.000506	0.02356	0.02374	0.02404	0.02378	0.000242	0.02349	0.02306	0.0233	0.023283	0.000215

African American Skull

	Observer 1					Observer 2					Observer 3					Observer 4				
Measurement	r1	r2	r3	Mean	SD	r1	r2	r3	Mean	SD	r1	r2	r3	Mean	SD	r1	r2	r3	Mean	SD
A	0.03593	0.03667	0.03665	0.036417	0.000422	0.03644	0.03688	0.03665	0.036657	0.00022	0.03644	0.03723	0.03704	0.036903	0.000412	0.03616	0.03683	0.03657	0.03652	0.000338
B	0.03255	0.03283	0.03318	0.032853	0.000316	0.03304	0.03293	0.03267	0.03288	0.00019	0.03184	0.03254	0.03309	0.03249	0.000626	0.03177	0.03282	0.03297	0.03252	0.000654
C	0.04228	0.04284	0.04255	0.042557	0.00028	0.04307	0.04299	0.04293	0.042997	7.02E-05	0.04267	0.04276	0.04271	0.042713	4.51E-05	0.0429	0.04281	0.04253	0.042747	0.000193
D	0.03746	0.03688	0.03737	0.037237	0.000312	0.03651	0.03673	0.03648	0.036573	0.000137	0.03711	0.038.29	0.03558	0.036345	0.001082	0.03641	0.03675	0.03658	0.03658	0.00017
E	0.02424	0.02418	0.0249	0.02444	0.000399	0.02422	0.02409	0.02413	0.024147	6.66E-05	0.02427	0.02397	0.024	0.02408	0.000165	0.02451	0.02465	0.0245	0.024553	8.39E-05

Asian Skull

	Observer 1					Observer 2					Observer 3					Observer 4				
Measurement	r1	r2	r3	Mean	SD	r1	r2	r3	Mean	SD	r1	r2	r3	Mean	SD	r1	r2	r3	Mean	SD
A	0.04631	0.04647	0.04645	0.04641	8.72E-05	0.04577	0.04607	0.04607	0.04597	0.000173	0.04653	0.04626	0.04612	0.046303	0.000208	0.04506	0.04511	0.04575	0.045307	0.000385
B	0.04305	0.04343	0.04352	0.043333	0.000249	0.04318	0.04337	0.04353	0.04336	0.000175	0.04353	0.04353	0.04366	0.043573	7.51E-05	0.04266	0.04271	0.04326	0.042877	0.000333
C	0.04126	0.04117	0.04096	0.04113	0.000154	0.0411	0.04109	0.04147	0.04122	0.000217	0.04114	0.0413	0.04172	0.041387	0.0003	0.04145	0.04106	0.04101	0.041173	0.000241
D	0.03448	0.03446	0.03424	0.034393	0.000133	0.03406	0.03416	0.03449	0.034237	0.000225	0.03444	0.0338	0.03433	0.03419	0.000342	0.03437	0.03467	0.0343	0.034447	0.000197
E	0.02392	0.024	0.02399	0.02397	4.36E-05	0.0244	0.02426	0.02427	0.02431	7.81E-05	0.02463	0.024	0.02416	0.024263	0.000327	0.02441	0.02406	0.02395	0.02414	0.00024

RAW PHYSICAL MEASUREMENTS (IN METERS) FOR THE THREE SKULLS

	Caucasian Skull																			
	Physical																			
	Observer 1					Obserever 2					Observer 3					Observer 4				
Measurement	r1	r2	r3	Mean	SD	r1	r2	r3	Mean	SD	r1	r2	r3	Mean	SD	r1	r2	r3	Mean	SD
g-op	0.181	0.1808	0.1797	0.1805	0.0007	0.1785	0.1783	0.179	0.1786	0.0003606	0.1778	0.179	0.1826	0.1798	0.002498	0.182	0.1817	0.182	0.1819	0.0001732
eu-eu	0.1434	0.1439	0.1434	0.1435667	0.0002887	0.1424	0.1411	0.1444	0.1426333	0.0016623	0.1423	0.1428	0.1428	0.1426333	0.0002887	0.1445	0.1443	0.1441	0.1443	0.0002
ft-ft	0.09326	0.09353	0.09355	0.0934467	0.000162	0.0937	0.0943	0.0946	0.0942	0.0004583	0.09372	0.09389	0.09462	0.0940767	0.0004782	0.0956	0.0954	0.0957	0.0955667	0.0001528
zy-zy	0.1362	0.1362	0.1359	0.1361	0.0001732	0.1354	0.136	0.1364	0.1359333	0.0005033	0.1377	0.1338	0.1343	0.1352667	0.0021221	0.1354	0.1361	0.1366	0.1360333	0.0006028
n-gn	0.12559	0.12515	0.12533	0.1253567	0.0002212	0.12616	0.12619	0.12627	0.1262067	5.686E-05	0.12311	0.1222	0.12248	0.1225967	0.0004661	0.12616	0.12677	0.12663	0.12652	0.0003195
n-pr	0.07898	0.07828	0.0786	0.07862	0.0003504	0.07864	0.07827	0.07985	0.07892	0.0008264	0.07835	0.07717	0.07725	0.07759	0.0006594	0.07916	0.07885	0.07923	0.07908	0.0002022
left orbital height	0.03739	0.03766	0.03765	0.0375667	0.0001531	0.03663	0.03748	0.03667	0.0369267	0.0004796	0.03598	0.03812	0.03632	0.0368067	0.00115	0.03706	0.03714	0.03629	0.03683	0.0004694
right orbital height	0.03808	0.03804	0.0383	0.03814	0.00014	0.03641	0.03765	0.03696	0.0370067	0.0006213	0.03603	0.03578	0.03606	0.0359567	0.0001537	0.3924	0.4039	0.3897	0.3953333	0.0075408
left ec-mf	0.04375	0.0439	0.04365	0.0437667	0.0001258	0.04271	0.04131	0.04261	0.04221	0.000781	0.04523	0.0456	0.04459	0.04514	0.000511	0.04143	0.04164	0.04183	0.0416333	0.0002001
right ec-mf	0.04478	0.04435	0.04472	0.0446167	0.0002329	0.04392	0.04353	0.04311	0.04352	0.0004051	0.0418	0.04066	0.04185	0.0414367	0.0006731	0.04357	0.04312	0.04304	0.0432433	0.0002857
d-d	0.01828	0.0188	0.01809	0.01839	0.0003676	0.02178	0.02233	0.0206	0.02157	0.0008839	0.02465	0.0224	0.02233	0.0231267	0.0013197	0.02414	0.02415	0.02508	0.0244567	0.0005398
ec-ec	0.10213	0.1025	0.10298	0.1025367	0.0004262	0.10224	0.10219	0.10105	0.1018267	0.0006731	0.10425	0.10335	0.10337	0.1036567	0.0005139	0.10184	0.10124	0.10184	0.10164	0.0003464
n-ns	0.05813	0.05827	0.05825	0.0582167	7.572E-05	0.05745	0.05799	0.05906	0.0581667	0.0008194	0.05733	0.05811	0.05842	0.0579533	0.0005616	0.05755	0.05687	0.05673	0.05705	0.0004386
al-al	0.02258	0.02256	0.02264	0.0225933	4.163E-05	0.02276	0.02288	0.02273	0.02279	7.937E-05	0.02421	0.02613	0.02683	0.0257233	0.0013565	0.02332	0.02276	0.02276	0.0229467	0.0003233
cdl-cdl	0.1193	0.1193	0.1192	0.1192667	5.774E-05	0.12093	0.12105	0.12074	0.1209067	0.0001563	0.11978	0.1153	0.1176	0.11756	0.0022403	0.1181	0.1184	0.1176	0.1180333	0.0004041
go-go	0.1021	0.102	0.1022	0.1021	0.0001	0.1056	0.10547	0.10562	0.1055633	8.145E-05	0.1017	0.1048	0.1031	0.1032	0.0015524	0.102	0.1042	0.1044	0.1035333	0.0013317

	African American Skull																			
	Physical																			
	Observer 1					Obserever 2					Observer 3					Observer 4				
Measurement	r1	r2	r3	Mean	SD	r1	r2	r3	Mean	SD	r1	r2	r3	Mean	SD	r1	r2	r3	Mean	SD
g-op	0.1651	0.1652	0.165	0.1651	0.0001	0.1662	0.168	0.1659	0.1667	0.0011358	0.1649	0.1626	0.1647	0.1640667	0.0012741	0.1653	0.165	0.1652	0.1651667	0.0001528
eu-eu	0.1301	0.1299	0.1301	0.1300333	0.0001155	0.1305	0.1307	0.1317	0.1309667	0.0006429	0.1289	0.1302	0.1302	0.1297667	0.0007506	0.1304	0.1307	0.1306	0.1305667	0.0001528
ft-ft	0.0883	0.0881	0.0887	0.0883667	0.0003055	0.08876	0.08881	0.0911	0.0895567	0.0013368	0.08911	0.08927	0.08923	0.0892033	8.327E-05	0.0889	0.0884	0.0883	0.0885333	0.0003215
zy-zy	0.1235	0.124	0.1238	0.1237667	0.0002517	0.1239	0.1234	0.1242	0.1238333	0.0004041	0.1237	0.1236	0.1245	0.1239333	0.0004933	0.1235	0.1236	0.124	0.1237	0.0002646
n-gn	0.1122	0.11247	0.11238	0.11235	0.0001375	0.11197	0.11248	0.11242	0.11229	0.0002787	0.11151	0.11176	0.11135	0.11154	0.0002066	0.11111	0.10983	0.10908	0.1100067	0.0010265
n-pr	0.07132	0.07158	0.07165	0.0715167	0.0001739	0.06998	0.07098	0.07093	0.07063	0.0005635	0.07159	0.0721	0.07186	0.07185	0.0002551	0.07181	0.07268	0.0717	0.0720633	0.0005369
left orbital height	0.03819	0.03908	0.03889	0.03872	0.0004687	0.03837	0.03881	0.03937	0.03885	0.0005012	0.03788	0.03745	0.0383	0.0378767	0.000425	0.03763	0.03811	0.03792	0.0378867	0.0002417
right orbital height	0.03974	0.03933	0.03937	0.03948	0.0002261	0.03908	0.0394	0.03985	0.0394433	0.0003868	0.03885	0.03775	0.03795	0.0381833	0.0005859	0.04146	0.04159	0.04147	0.0415067	7.234E-05
left ec-mf	0.04004	0.04077	0.04005	0.0402867	0.0004186	0.03887	0.0392	0.0392	0.03944	0.0002341	0.04285	0.0384	0.03887	0.04004	0.0024449	0.0374	0.03749	0.03744	0.0374433	4.509E-05
right ec-mf	0.04141	0.04111	0.04087	0.04113	0.0002706	0.03676	0.03723	0.03733	0.0371067	0.0003044	0.03665	0.0358	0.03645	0.0363	0.0004444	0.03667	0.03615	0.03652	0.0364467	0.0002676
d-d	0.01815	0.01782	0.0177	0.01789	0.000233	0.01849	0.01709	0.01897	0.0181833	0.0009768	0.02097	0.02122	0.02095	0.0210467	0.0001504	0.02073	0.02082	0.0208	0.0207833	4.726E-05
ec-ec	0.09514	0.095	0.09506	0.0950667	7.024E-05	0.09318	0.09446	0.09407	0.0939033	0.0006561	0.09713	0.09774	0.09667	0.09718	0.0005367	0.09503	0.09455	0.09445	0.0946767	0.0003101
n-ns	0.0519	0.05081	0.05197	0.05156	0.0006505	0.0561	0.0529	0.05187	0.0536233	0.0022058	0.0529	0.05294	0.05284	0.0528933	5.033E-05	0.04678	0.04743	0.04646	0.04689	0.0004943
al-al	0.02804	0.02779	0.02769	0.02784	0.0001803	0.02687	0.02709	0.02768	0.0272133	0.0004188	0.02548	0.02667	0.02717	0.02644	0.0008682	0.02662	0.02659	0.02613	0.0264467	0.0002747
cdl-cdl-	0.1111	0.1116	0.1112	0.1113	0.0002646	0.11161	0.11159	0.1116	0.1116	1E-05	0.111	0.1104	0.1109	0.1107667	0.0003215	0.1105	0.1107	0.1107	0.1106333	0.0001155
go-go	0.08752	0.08737	0.08771	0.0875333	0.0001704	0.08702	0.08748	0.08715	0.0872167	0.0002371	0.087	0.0866	0.089	0.0875333	0.0012858	0.0873	0.0871	0.087	0.0871333	0.0001528

	Asian Skull																			
	Physical																			
	Observer 1					Obserever 2					Observer 3					Observer 4				
Measurement	r1	r2	r3	Mean	SD	r1	r2	r3	Mean	SD	r1	r2	r3	Mean	SD	r1	r2	r3	Mean	SD
g-op	0.1767	0.1762	0.1767	0.1765333	0.0002887	0.1771	0.1778	0.1803	0.1784	0.0016823	0.1728	0.1718	0.1727	0.1724333	0.0005508	0.1762	0.1758	0.1755	0.1758333	0.0003512
eu-eu	0.143	0.1425	0.1421	0.1425333	0.0004509	0.1409	0.1403	0.1418	0.141	0.000755	0.1418	0.1422	0.1421	0.1420333	0.0002082	0.1411	0.1409	0.1422	0.1414	0.0007
ft-ft	0.0958	0.0957	0.0961	0.0958667	0.0002082	0.096	0.0964	0.0961	0.0961667	0.0002082	0.0981	0.0971	0.0962	0.0971333	0.0009504	0.0984	0.0987	0.0989	0.0986667	0.0002517
zy-zy	0.1372	0.1367	0.137	0.1369667	0.0002517	0.1367	0.1366	0.1375	0.1369333	0.0004933	0.137	0.1361	0.1368	0.1366333	0.0004726	0.1367	0.1364	0.1369	0.1366667	0.0002517
n-gn	0.12586	0.12602	0.126	0.12596	8.718E-05	0.1245	0.1232	0.12554	0.1244133	0.0011724	0.12338	0.12521	0.12555	0.1247133	0.0011671	0.12511	0.12572	0.12559	0.1254733	0.0003213
n-pr	0.07157	0.072	0.07159	0.07172	0.0002427	0.07112	0.07159	0.07218	0.07163	0.0005311	0.07161	0.07237	0.07072	0.0715667	0.0008259	0.07645	0.07694	0.07702	0.0768033	0.0003086
left orbital height	0.03594	0.03588	0.03595	0.0359233	3.786E-05	0.03567	0.03528	0.03544	0.0354633	0.000196	0.0351	0.03765	0.03691	0.0365533	0.0013119	0.03377	0.03501	0.03498	0.0345867	0.0007074
right orbital height	0.03642	0.03653	0.0364	0.03645	7E-05	0.0364	0.03562	0.03556	0.03586	0.0004686	0.03514	0.03547	0.0379	0.03617	0.0015073	0.0358	0.03581	0.03567	0.03576	7.81E-05
left ec-mf	0.04213	0.04133	0.04128	0.04158	0.000477	0.04103	0.04146	0.04021	0.0409	0.0006351	0.0418	0.04275	0.04169	0.04208	0.0005828	0.03856	0.03852	0.03853	0.0385367	2.082E-05
right ec-mf	0.04183	0.04142	0.0413	0.0415167	0.0002779	0.04384	0.04387	0.04299	0.0435667	0.0004996	0.04059	0.04041	0.04022	0.0404067	0.000185	0.0388	0.0386	0.0389	0.0387667	0.0001528
d-d	0.022	0.02185	0.02198	0.0219433	8.145E-05	0.02666	0.02291	0.02261	0.02406	0.0022567	0.02094	0.02085	0.02095	0.0209133	5.508E-05	0.02659	0.02669	0.02616	0.02648	0.0002816
ec-ec	0.10248	0.10279	0.1029	0.1027233	0.0002178	0.10181	0.1017	0.10096	0.10149	0.0004623	0.10356	0.10463	0.10459	0.10426	0.0006065	0.1017	0.10257	0.10123	0.1018333	0.0006799
n-ns	0.05478	0.05472	0.05469	0.05473	4.583E-05	0.05272	0.05302	0.05195	0.0525633	0.0005519	0.05487	0.0545	0.05473	0.0547	0.0001868	0.0532	0.05422	0.05472	0.0540467	0.0007747
al-al	0.02827	0.02825	0.02831	0.0282767	3.055E-05	0.02777	0.02786	0.02791	0.0278467	7.095E-05	0.02783	0.02866	0.0276	0.02803	0.0005576	0.02777	0.02717	0.02706	0.0273333	0.0003821
cdl-cdl-	0.1151	0.1153	0.1152	0.1152	0.0001	0.11566	0.11536	0.11511	0.1153767	0.0002754	0.01154	0.01153	0.0115	0.0115233	2.082E-05	0.1149	0.114	0.116	0.1149667	0.0010017
go-go	0.10623	0.10658	0.10654	0.10645	0.0001916	0.10715	0.10714	0.10633	0.1068733	0.0004706	0.10567	0.10672	0.10656	0.1063167	0.0005657	0.1065	0.1065	0.1064	0.1064667	5.774E-05

RAW CT SCAN MEASUREMENTS (IN METERS) FOR THE THREE SKULLS

	Caucasian Skulll			
	CT			
Measurement	Observer 1	Observer 2	Observer 3	Observer 4
g-op	0.1809	0.1798	0.1794	0.1822
eu-eu	0.1394	0.1427	0.1353	0.1419
ft-ft	0.0918	0.0904	0.0901	0.0967
zy-zy	0.1334	0.1144	0.1309	0.1354
n-gn	0.126	0.1301	0.131	0.1265
n-pr	0.0728	0.0792	0.0795	0.0786
left orbital height	0.0426	0.0448	0.0418	0.0414
right orbital height	0.0416	0.0422	0.0407	0.0419
left ec-mf	0.0391	0.0397	0.0384	0.038
right ec-mf	0.0382	0.0374	0.0365	0.0368
d-d	0.0244	0.0215	0.0263	0.0269
ec-ec	0.102	0.105	0.1015	0.1001
n-ns	0.0501	0.055	0.0561	0.0546
al-al	0.0221	0.0222	0.0218	0.0207
cdl-cdl	0.1187	0.1184	0.1211	0.1202
go-go	0.1046	0.1038	0.1042	0.1046

	African American Skull			
	CT			
Measurement	Observer 1	Observer 2	Observer 3	Observer 4
g-op	0.1607	0.165	0.1636	0.1619
eu-eu	0.1264	0.1274	0.1224	0.1232
ft-ft	0.0882	0.082	0.0888	0.0888
zy-zy	0.1215	0.1203	0.1209	0.1205
n-gn	0.1075	0.1075	0.1117	0.1121
n-pr	0.0697	0.069	0.0709	0.0689
left orbital height	0.0414	0.0419	0.0406	0.0414
right orbital height	0.0417	0.0422	0.0401	0.0414
left ec-mf	0.0373	0.0382	0.0375	0.0371
right ec-mf	0.0377	0.0363	0.0368	0.0368
d-d	0.0211	0.0201	0.0208	0.0208
ec-ec	0.096	0.0936	0.0947	0.097
n-ns	0.0511	0.0523	0.0526	0.051
al-al	0.0267	0.0276	0.0268	0.0274
cdl-cdl-	0.1102	0.11	0.107	0.1099
go-go	0.084	0.085	0.0843	0.0828

	Asian Skull			
	CT			
Measurement	Observer 1	Observer 2	Observer 3	Observer 4
g-op	0.1696	0.1722	0.1691	0.1689
eu-eu	0.1371	0.1419	0.1313	0.1351
ft-ft	0.0935	0.0986	0.0915	0.0919
zy-zy	0.1348	0.1357	0.1313	0.132
n-gn	0.1211	0.1238	0.1281	0.1258
n-pr	0.0732	0.0704	0.0742	0.0743
left orbital height	0.0405	0.04	0.0386	0.0405
right orbital height	0.0384	0.0386	0.0384	0.0383
left ec-mf	0.0368	0.0357	0.0378	0.0372
right ec-mf	0.0384	0.0368	0.0394	0.0383
d-d	0.0252	0.0266	0.0263	0.0267
ec-ec	0.1003	0.0975	0.1013	0.1015
n-ns	0.0566	0.0554	0.0582	0.0573
al-al	0.0263	0.0271	0.0247	0.026
cdl-cdl-	0.113	0.1136	0.1129	0.1126
go-go	0.1034	0.1051	0.1046	0.1044

RAW PHOTOGRAMMETRIC MEASUREMENTS (IN METERS) FOR THE THREE SKULLS

	Caucasian Skull																			
	Photogrammetry																			
	Observer 1					Observer 2					Observer 3					Observer 4				
Measurement	r1	r2	r3	Mean	SD	r1	r2	r3	Mean	SD	r1	r2	r3	Mean	SD	r1	r2	r3	Mean	SD
g-op	0.182452	0.182254	0.182176	0.182294	0.0001423	0.182575	0.182127	0.181521	0.1820743	0.000529	0.179894	0.181106	0.180594	0.1805313	0.0006084	0.179411	0.178048	0.179905	0.1791213	0.0009618
eu-eu	0.140607	0.140624	0.140572	0.140601	2.651E-05	0.138074	0.140793	0.140868	0.1399117	0.0015919	0.131447	0.134001	0.129665	0.1317043	0.0021794	0.139978	0.140437	0.138521	0.1396453	0.0010004
ft-ft	0.091993	0.091566	0.091565	0.091708	0.0002468	0.092446	0.092103	0.094364	0.092971	0.0012185	0.094271	0.094753	0.094128	0.094384	0.0003275	0.095841	0.096733	0.096572	0.096382	0.0004754
zy-zy	0.133667	0.133804	0.133693	0.1337213	7.276E-05	0.132658	0.134886	0.134691	0.1340783	0.0012339	0.133688	0.131033	0.132455	0.132392	0.0013286	0.13426	0.133177	0.133221	0.1335527	0.000613
n-gn	0.125921	0.125049	0.1249	0.12529	0.0005515	0.128366	0.126609	0.127961	0.1276453	0.0009201	0.134457	0.134463	0.133016	0.1339787	0.0008337	0.125772	0.126402	0.126562	0.1262453	0.0004177
n-pr	0.079002	0.078556	0.07806	0.0785393	0.0004712	0.077836	0.077848	0.078921	0.0782017	0.000623	0.0917	0.091717	0.090649	0.0913553	0.0006118	0.080811	0.072617	0.079365	0.0775977	0.0043736
left orbital height	0.039548	0.040034	0.039838	0.0398067	0.0002445	0.038872	0.03856	0.038795	0.0387423	0.0001625	0.039079	0.037544	0.037371	0.037998	0.0009402	0.036413	0.039286	0.039046	0.0382483	0.001594
right orbital height	0.039657	0.040195	0.04024	0.0400307	0.0003244	0.040594	0.040032	0.038217	0.0396143	0.0012423	0.041408	0.039122	0.036196	0.0389087	0.0026125	0.039042	0.042626	0.039186	0.0402847	0.0020289
left ec-mf	0.047418	0.045132	0.045457	0.0460023	0.0012367	0.044249	0.040884	0.040975	0.042036	0.0019171	0.046437	0.043412	0.046649	0.0454993	0.0018108	0.03809	0.038278	0.035279	0.0372157	0.0016798
right ec-mf	0.046707	0.046235	0.047389	0.046777	0.0005802	0.044063	0.047217	0.044558	0.0452793	0.0016962	0.045802	0.045008	0.042672	0.044494	0.0016271	0.038955	0.036878	0.034982	0.0369383	0.0019872
d-d	0.02109	0.018541	0.020619	0.0200833	0.0013563	0.023099	0.023227	0.021732	0.022686	0.0008287	0.034471	0.028897	0.026782	0.03005	0.0039721	0.023432	0.031447	0.023894	0.0262577	0.0045
ec-ec	0.104184	0.104258	0.104133	0.1041917	6.285E-05	0.102446	0.101571	0.101997	0.1020047	0.0004376	0.110926	0.112757	0.110606	0.1114297	0.0011606	0.096805	0.098473	0.098573	0.0979503	0.0009931
n-ns	0.056428	0.057396	0.056838	0.0568873	0.0004859	0.057839	0.05862	0.057395	0.0579513	0.0006202	0.05972	0.060576	0.059828	0.0600413	0.0004662	0.058697	0.059527	0.0512	0.0564747	0.0045868
al-al	0.023432	0.02263	0.022642	0.0229013	0.0004596	0.021744	0.023305	0.02192	0.022323	0.000855	0.022454	0.020894	0.022388	0.021912	0.0008822	0.022429	0.021864	0.022204	0.0221657	0.0002844
cdl-cdl	0.118982	0.119135	0.119256	0.1191243	0.0001373	0.121425	0.120476	0.120969	0.1209567	0.0004746	0.116477	0.11847	0.119103	0.1180167	0.0013704	0.119397	0.119894	0.117233	0.1188413	0.0014149
go-go	0.102494	0.102313	0.102636	0.102481	0.0001619	0.103912	0.104275	0.104061	0.1040827	0.0001825	0.103309	0.102816	0.103668	0.1032643	0.0004278	0.1043	0.103469	0.10112	0.102963	0.0016493

	African American Skull																			
	Photogrammetry																			
	Observer 1					Observer 2					Observer 3					Observer 4				
	r1	r2	r3	Mean	SD	r1	r2	r3	Mean	SD	r1	r2	r3	Mean	SD	r1	r2	r3	Mean	SD
g-op	0.162764	0.162713	0.162871	0.1627827	8.064E-05	0.163324	0.163298	0.163431	0.163351	7.049E-05	0.160779	0.16141	0.161992	0.1613937	0.0006067	0.161816	0.162239	0.16114	0.1617317	0.0005543
eu-eu	0.124645	0.125017	0.124888	0.12485	0.0001889	0.127435	0.125235	0.124003	0.1255577	0.0017386	0.117574	0.113522	0.115291	0.1154623	0.0020314	0.126474	0.127535	0.125915	0.1266413	0.0008229
ft-ft	0.086559	0.086948	0.087244	0.086917	0.0003436	0.087794	0.091381	0.089251	0.0894753	0.001804	0.086605	0.086904	0.086613	0.0867073	0.0001704	0.087647	0.091342	0.092126	0.0903717	0.002392
zy-zy	0.12019	0.120828	0.120686	0.120568	0.000335	0.120892	0.120628	0.121685	0.1210683	0.0005501	0.119673	0.117663	0.120941	0.1194257	0.0016529	0.121146	0.121101	0.120078	0.120775	0.000604
n-gn	0.110359	0.110058	0.110516	0.110311	0.0002327	0.112289	0.111764	0.111774	0.1119423	0.0003003	0.120037	0.116872	0.118001	0.1183033	0.001604	0.11166	0.109365	0.110126	0.1103837	0.001169
n-pr	0.069256	0.06915	0.068944	0.0691167	0.0001586	0.070022	0.070092	0.071367	0.0704937	0.0007571	0.0803	0.077841	0.078046	0.078729	0.0013644	0.072776	0.074305	0.074285	0.0737887	0.0008771
left orbital height	0.03925	0.040312	0.039229	0.039597	0.0006193	0.038893	0.038576	0.038694	0.038721	0.0001602	0.03845	0.0384	0.038256	0.0383687	0.0001007	0.037149	0.03475	0.036448	0.0361157	0.0012335
right orbital height	0.042998	0.041423	0.042243	0.0422213	0.0007877	0.038664	0.038809	0.039173	0.038882	0.0002622	0.037416	0.038086	0.037621	0.0377077	0.0003433	0.03919	0.03951	0.039965	0.039555	0.0003895
left ec-mf	0.042182	0.042499	0.042033	0.042238	0.000238	0.038603	0.038849	0.039439	0.0389637	0.0004296	0.034651	0.036397	0.033852	0.0349667	0.0013015	0.035735	0.035718	0.033645	0.0350327	0.0012018
right ec-mf	0.043092	0.044289	0.043985	0.0437887	0.0006222	0.03675	0.036035	0.036892	0.036559	0.0004593	0.033021	0.036921	0.035015	0.0349857	0.0019502	0.035775	0.035678	0.036995	0.0361493	0.000734
d-d	0.017738	0.017206	0.017576	0.0175067	0.0002727	0.015545	0.0198275	0.016859	0.0174105	0.0021939	0.020545	0.020442	0.021448	0.0208117	0.0005535	0.020222	0.02008	0.022317	0.020873	0.0012526
ec-ec	0.093977	0.095282	0.095657	0.094972	0.0008819	0.094147	0.093556	0.0934393	0.0937141	0.0003794	0.113554	0.114832	0.114952	0.114446	0.0007748	0.090898	0.091179	0.09065	0.090909	0.0002647
n-ns	0.050995	0.052107	0.051177	0.0514263	0.0005965	0.051716	0.052132	0.052845	0.052231	0.000571	0.057232	0.056122	0.056468	0.0566073	0.000568	0.047766	0.050734	0.052159	0.0502197	0.0022412
al-al	0.026513	0.026621	0.026788	0.0266407	0.0001386	0.026551	0.02667	0.026776	0.0266657	0.0001126	0.026918	0.024601	0.026843	0.0261207	0.0013166	0.025477	0.02633	0.025984	0.0259303	0.000429
cdl-cdl-	0.108402	0.107974	0.108355	0.1082437	0.0002347	0.109144	0.110159	0.109978	0.1097603	0.0005414	0.107424	0.107986	0.108264	0.1078913	0.0004279	0.107816	0.107847	0.107719	0.107794	6.678E-05
go-go	0.086085	0.085784	0.084907	0.085592	0.000612	0.086133	0.085533	0.085839	0.085835	0.0003	0.08543	0.084448	0.084429	0.084769	0.0005725	0.083617	0.085224	0.084186	0.0843423	0.0008148

	Asian Skull																			
	Photogrammetry																			
	Observer 1					Observer 2					Observer 3					Observer 4				
Measurement	r1	r2	r3	Mean	SD	r1	r2	r3	Mean	SD	r1	r2	r3	Mean	SD	r1	r2	r3	Mean	SD
g-op	0.170376	0.169961	0.17036	0.1702323	0.0002351	0.177952	0.17786	0.177754	0.1778553	9.908E-05	0.172865	0.173226	0.173136	0.1730757	0.0001879	0.175757	0.176803	0.176203	0.1762543	0.0005249
eu-eu	0.140551	0.140005	0.140671	0.140409	0.000355	0.141792	0.141792	0.140968	0.1415173	0.0004757	0.129203	0.122387	0.121535	0.124375	0.0042028	0.137484	0.141348	0.14162	0.1401507	0.0023134
ft-ft	0.092579	0.092293	0.09322	0.0926973	0.0004747	0.095049	0.095437	0.094323	0.0949363	0.0005655	0.094081	0.093124	0.092499	0.0932347	0.0007968	0.098311	0.098472	0.098583	0.0984553	0.0001368
zy-zy	0.135356	0.135397	0.135046	0.1352663	0.0001919	0.1325	0.132103	0.130922	0.1318417	0.0008208	0.134576	0.133106	0.131219	0.132967	0.0016828	0.134401	0.134818	0.134821	0.13468	0.0002416
n-gn	0.124463	0.124056	0.122727	0.1237487	0.0009079	0.124702	0.125452	0.125678	0.1252773	0.0005109	0.130572	0.134632	0.132852	0.1326853	0.0020351	0.124646	0.125943	0.125959	0.125516	0.0007535
n-pr	0.072807	0.071957	0.072542	0.0724353	0.0004349	0.073021	0.073809	0.074011	0.0736137	0.0005231	0.079421	0.073644	0.073846	0.075637	0.0032786	0.078049	0.077371	0.077798	0.0777393	0.0003428
left orbital height	0.03826	0.038134	0.037821	0.0380717	0.000226	0.037336	0.036882	0.037333	0.0371837	0.0002613	0.037655	0.038192	0.038585	0.038144	0.0004669	0.035445	0.034347	0.03416	0.0346507	0.0006942
right orbital height	0.039764	0.039524	0.040332	0.0398733	0.0004149	0.038722	0.038343	0.03827	0.038445	0.0002426	0.038687	0.035807	0.03461	0.036368	0.0020956	0.038333	0.038227	0.038332	0.0382973	6.091E-05
left ec-mf	0.042591	0.042563	0.042347	0.0425003	0.0001335	0.0426	0.043309	0.042404	0.042771	0.0004761	0.038958	0.038048	0.038317	0.038441	0.0004675	0.035891	0.034763	0.033701	0.034785	0.0010952
right ec-mf	0.043482	0.042283	0.042534	0.0427663	0.0006324	0.042411	0.042541	0.042879	0.0426103	0.0002416	0.038582	0.035816	0.037715	0.037371	0.0014147	0.037653	0.037584	0.03756	0.037599	4.828E-05
d-d	0.023446	0.020137	0.020825	0.0214693	0.0017461	0.022609	0.020006	0.020365	0.0209933	0.0014107	0.019292	0.018785	0.019734	0.0192703	0.0004749	0.025291	0.022121	0.022341	0.023251	0.0017701
ec-ec	0.102897	0.10295	0.102822	0.1028897	6.431E-05	0.102214	0.102123	0.101905	0.1020807	0.0001588	0.133512	0.127812	0.128834	0.1300527	0.0030391	0.095863	0.099285	0.099652	0.0982667	0.0020897
n-ns	0.055968	0.055619	0.055504	0.055697	0.0002416	0.054333	0.054175	0.054842	0.05445	0.0003486	0.074064	0.077514	0.073587	0.075055	0.0021429	0.054359	0.053162	0.054201	0.0539073	0.0006503
al-al	0.028346	0.028399	0.026788	0.0278443	0.0009152	0.02878	0.02799	0.028388	0.028386	0.000395	0.027421	0.02716	0.028165	0.027582	0.0005215	0.026629	0.025557	0.025604	0.02593	0.0006058
cdl-cdl-	0.113526	0.113483	0.113043	0.1133507	0.0002673	0.115404	0.115747	0.115587	0.1155793	0.0001716	0.115123	0.119309	0.116727	0.117053	0.002112	0.11417	0.113407	0.111305	0.1129607	0.0014837
go-go	0.10455	0.104691	0.104445	0.104562	0.0001234	0.104888	0.105708	0.105364	0.10532	0.0004118	0.104726	0.103691	0.104887	0.1044347	0.000649	0.107703	0.104078	0.104905	0.105562	0.0018997

Appendix 3

ANTHROPOLOGIC LANDMARKS OF THE SKULL

Glabella (g): Most projecting anterior median point on lower edge of the frontal bone, on the brow ridge, in between the superciliary arches and above the nasal root. In adults, glabella usually represents the most anterior point of the frontal bone.

Opisthocranion (op): Most posterior median point of the occipital bone, instrumentally determined as the greatest chord length from g. Usually above the external occipital protuberance.

Condylion laterale (cdl): Most lateral point on the mandibular condyle.

Euryon (eu): Instrumentally determined as the most lateral point of the cranial vault, on the parietal bone.

Frontotemporale (ft): Most anterior and medial point of the inferior temporal line, on the zygomatic process of the frontal bone

Ectoconchion (ec): Lateral point on the orbit at a line that bisects the orbit transversely.

Maxillofrontale (mf): Intersection of the anterior lacrimal crest with the frontomaxillary suture.

Dacryon (d): The point on the medial border of the orbit where the lacrimomaxillary suture meets the frontal bone. There is often a small foramen at this point.

Zygion (zy): Instrumentally determined as the most lateral point on the zygomatic arch.

Alare (al): Instrumentally determined as the most lateral point on the nasal aperture in a transverse plane.

Prosthion (pr): Median point between the central incisors on the anterior most margin of the maxillary alveolar rim.

Nasospinale (ns): The point where a line drawn between the inferior most points of the nasal aperture crosses the median plane. Note that this point is not necessarily at the tip of the nasal spine.

Nasion (n): Intersection of the nasofrontal sutures in the median plane.

Gnathion (gn): This is the midpoint on the lower border of the mandible in the midsagittal plane. It is not uncommon to find that gnathion is not the most inferiorly located point of the mandible, as the more laterally placed elements of the mandible may be extending far more inferiorly. This is especially the case in mandibles with broad and square chin development.

Gonion (go): Point on the rounded margin of the angle of the mandible, bisecting two lines one following vertical margin of ramus and one following horizontal margin of corpus of mandible.

[Adapted from Caple & Stephan [38]]

Appendix 4

I. African American female skull 3D reconstruct

A total of 105 photos and 34,674 points were used in the reconstruction of the African American female skull.

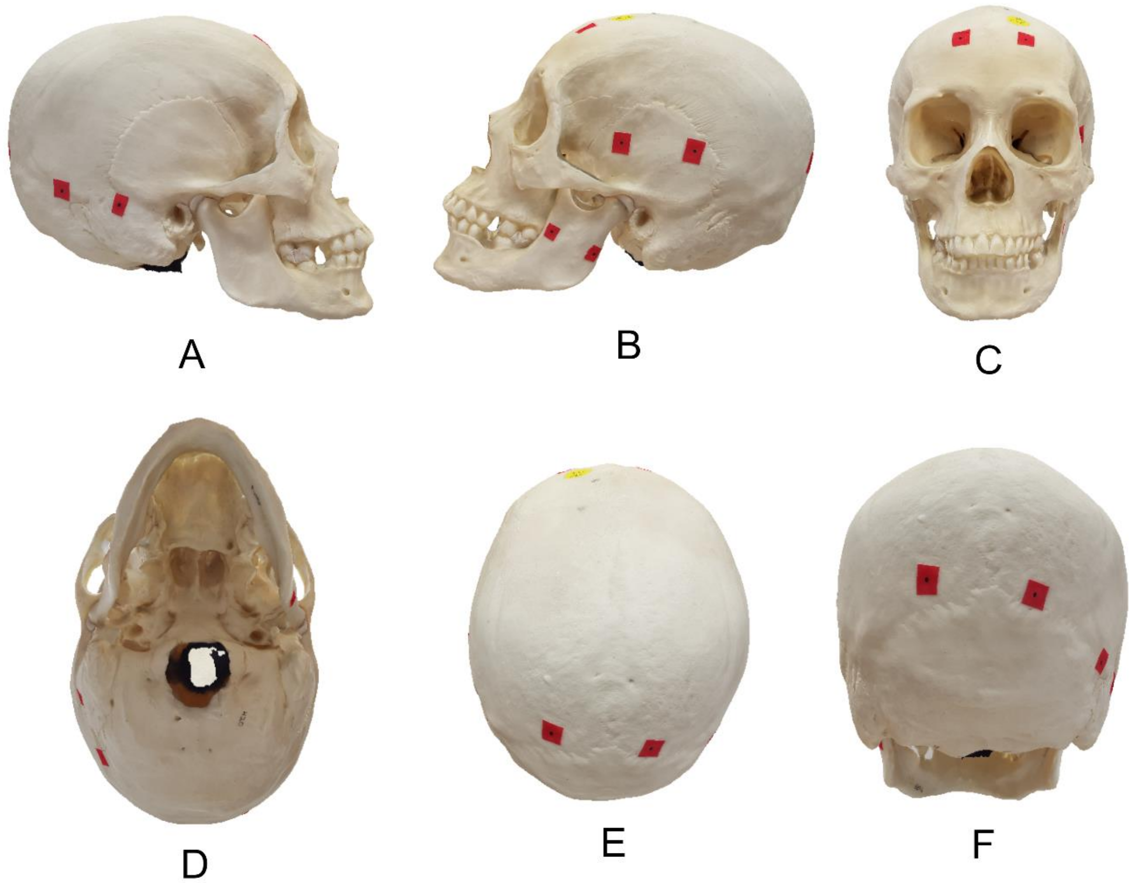

A&B- Norma lateralis; C- Norma frontalis; D- Norma basalis; E- Norma verticalis; and F- Norma occipitalis

Caucasian male skull 3D reconstruct

A total of 73 photos and 18,245 points were used in the reconstruction of the Caucasian male skull.

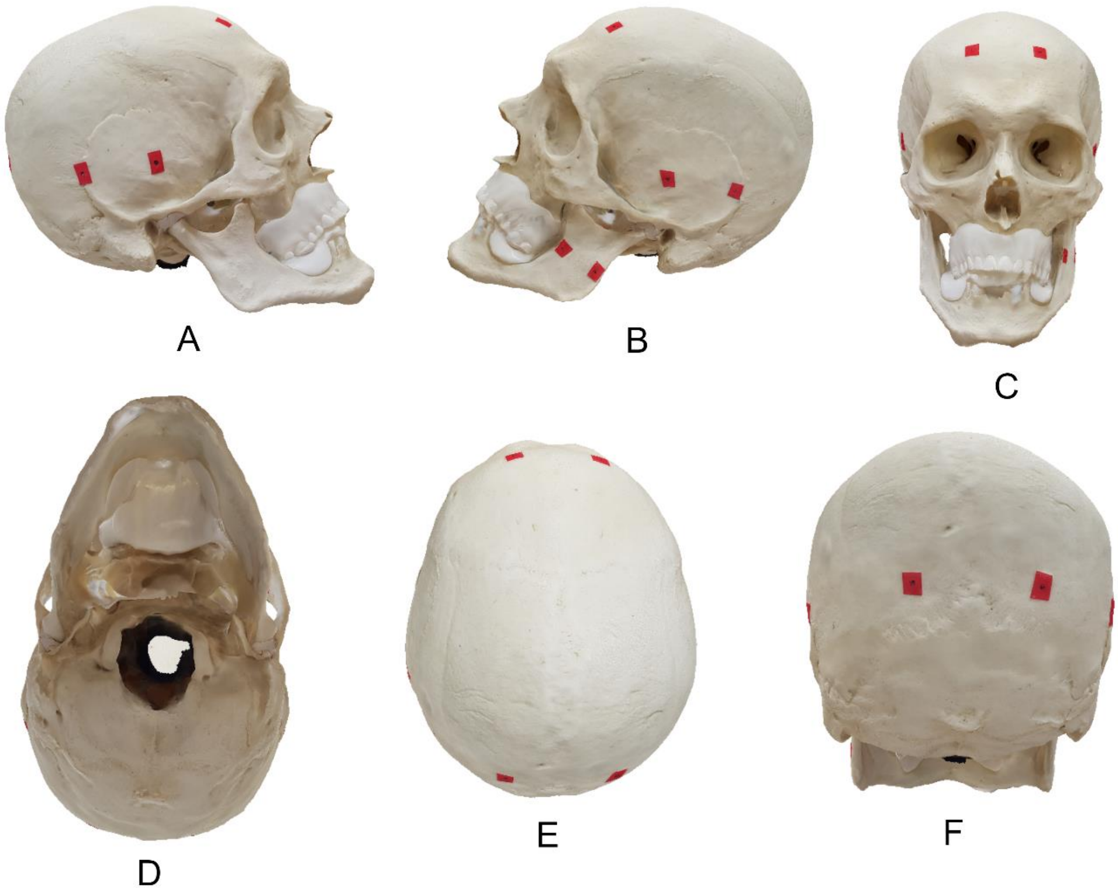

A&B- Norma lateralis; C- Norma frontalis; D- Norma basalis; E- Norma verticalis; and F- Norma occipitalis

II. CT scan 3D reconstruction

(i) 3D reconstruction view

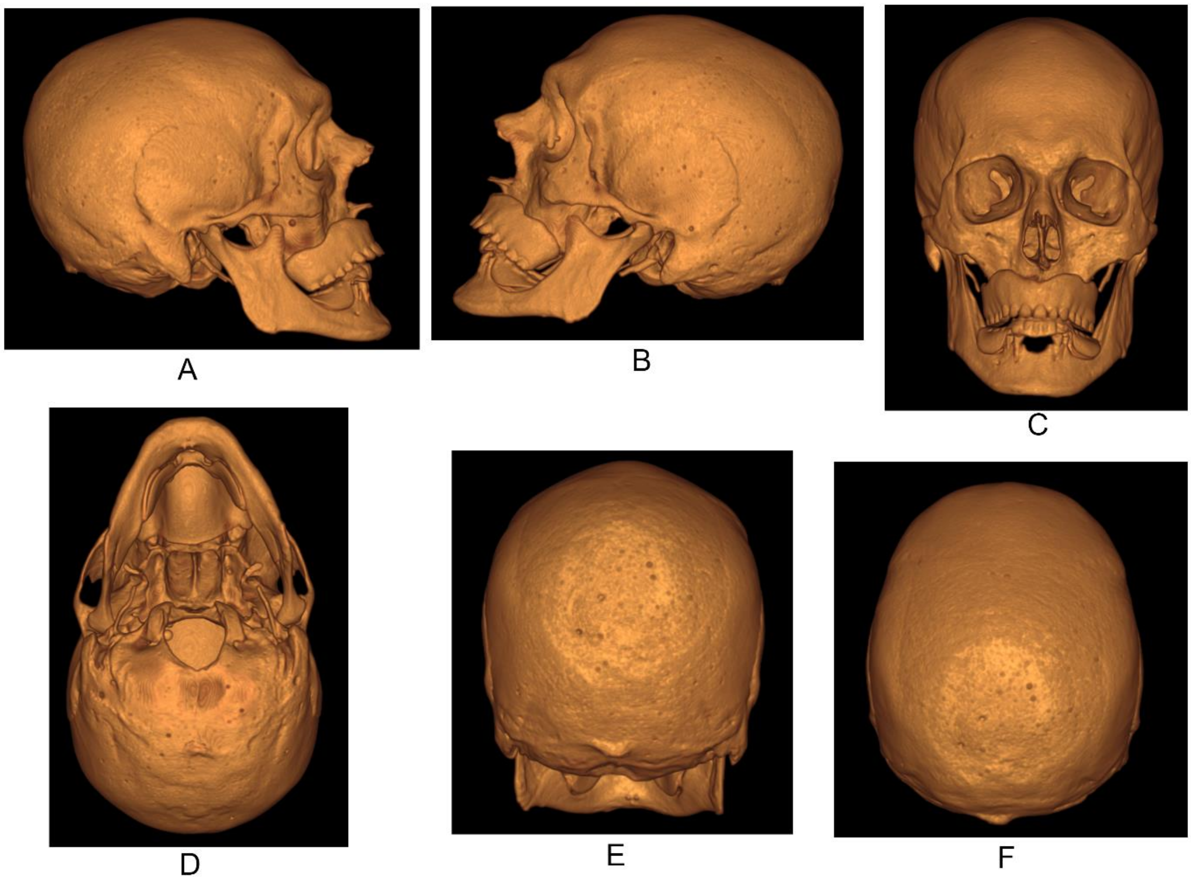

One of the three skulls (Caucasian Male) as seen in the 3D reconstruction view of the RadiAnt DICOM viewer software. A&B- Norma lateralis; C- Norma frontalis; D- Norma basalis; E- Norma occipitalis; and F- Norma verticalis

(ii) MPR View – Asian Male

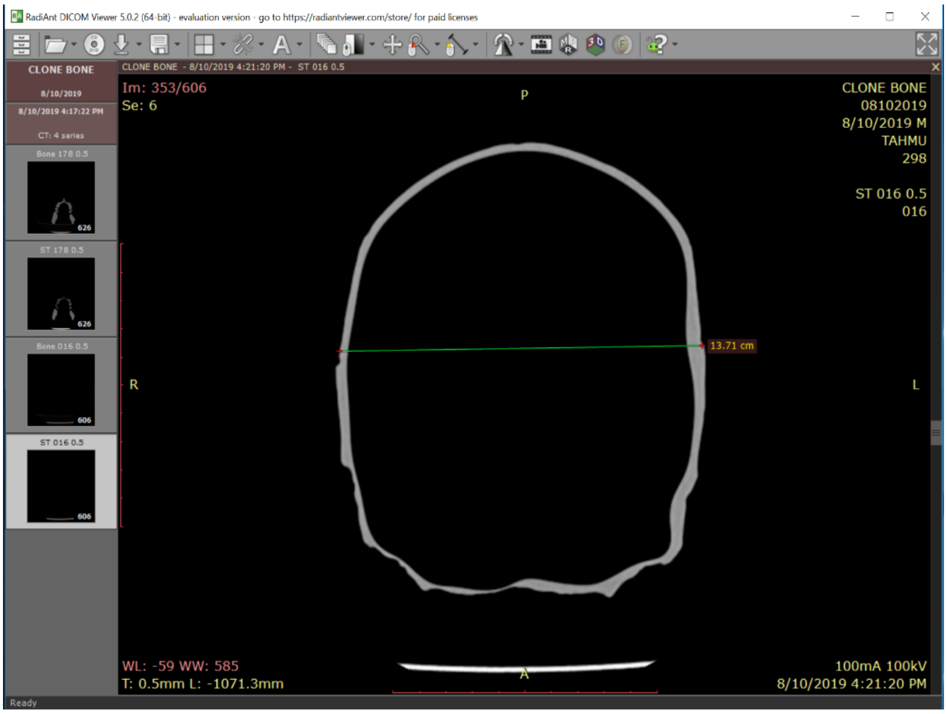

Axial view of the MPR of the Asian male showing the eu-eu measurement

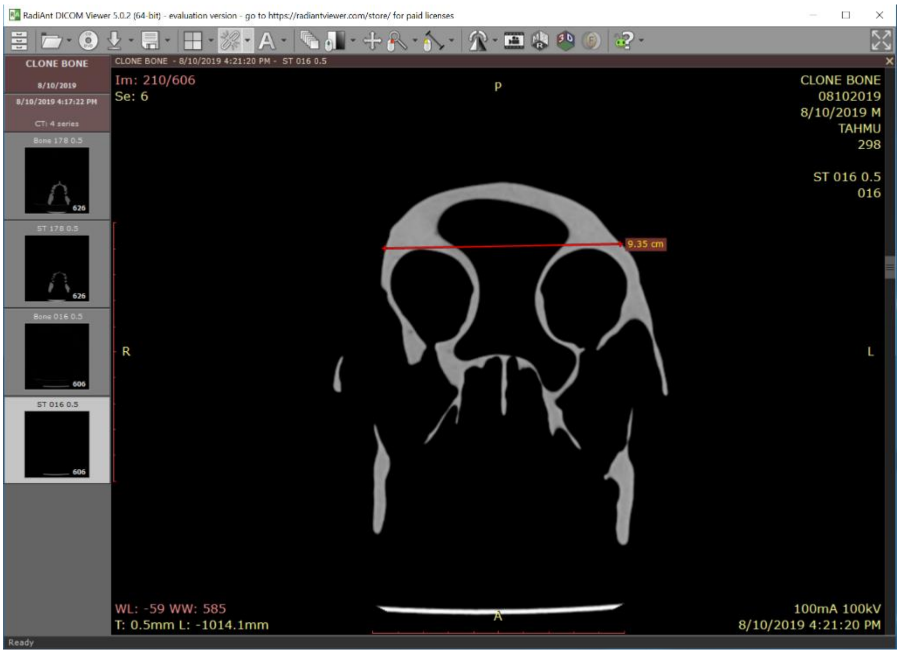

Axial view of the MPR of the Asian male showing the ft-ft measurement

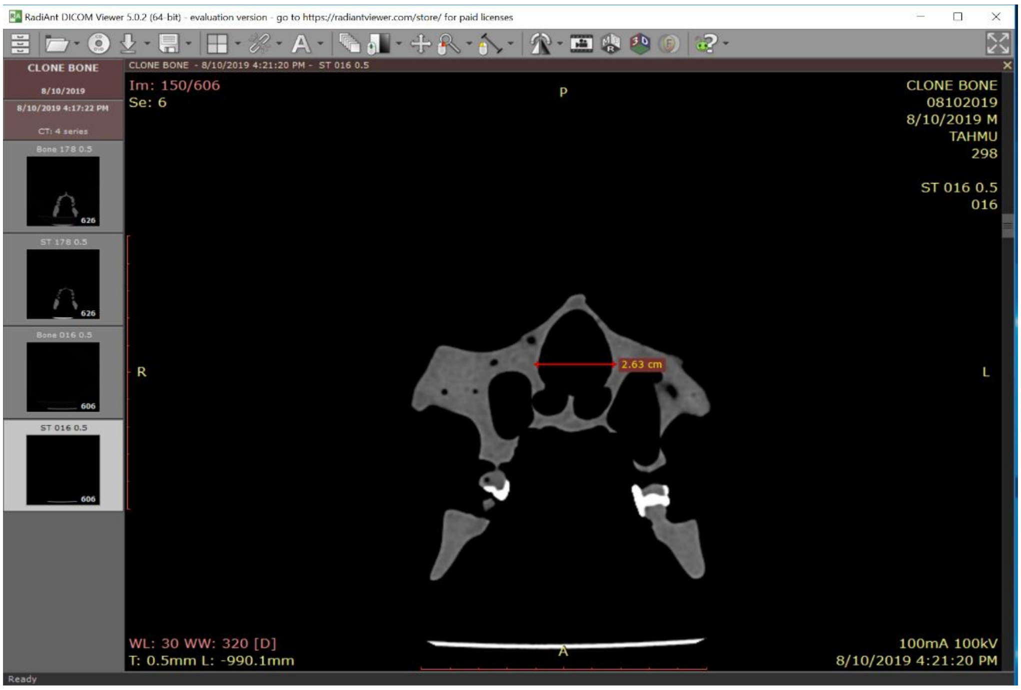

Axial view of the MPR of the Asian male showing the al-al measurement

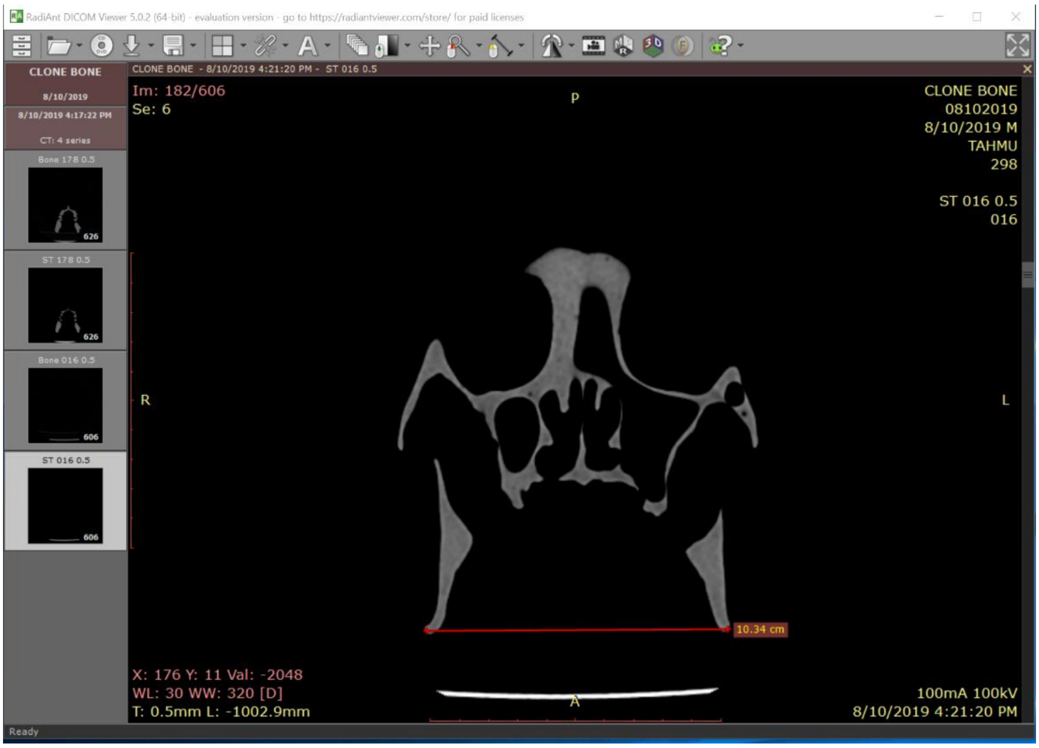

Axial view of the MPR of the Asian male showing the go-go measurement

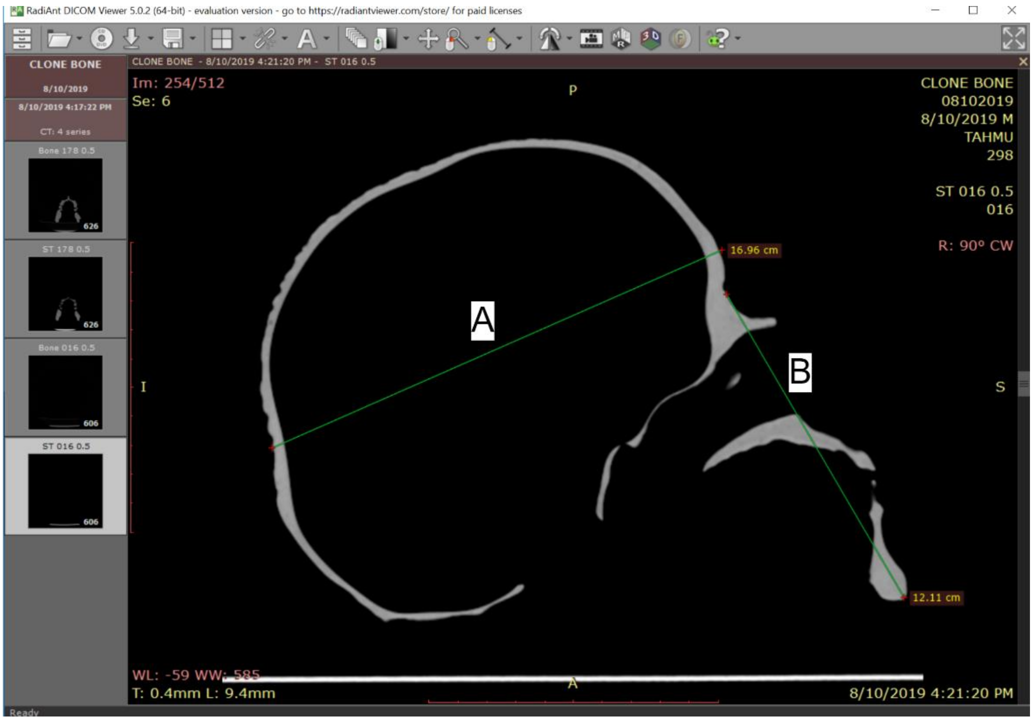

Sagittal view of the MPR of the Asian male showing A- g-op; and B- n-gn measurements